Laboratoire Génie Civil et géo-Environnement Lille Nord de France

Université de Lille 1 SCIENCES ET TECHNOLOGIES

Université Lille1

Sciences et Technologies

Laboratoire Génie Civil et Géo-environnement

Ecole doctorale Sciences Pour l'Ingénieur

Thèse

Pour obtenir le grade de Docteur de l'Université Lille1

Sciences et Technologies

Discipline : **Génie Civil**

Intitulée:

Exploration de matériaux avancés pour des applications en génie civil

Présentée et soutenue publiquement par

Amine BOUIBES

Le 24 Novembre 2014 devant le jury :

Rapporteur	**Rajeev AHUJA**, Professeur, Université d'Uppsala (Suède)
Rapporteur	**Anatoly BELONOSHKO**, Professeur, Royal Institute of Technology-KTH-(Suède)
Rapporteur	**Mohamed FERHAT**, Professeur, Université des sciences et de la Technologie d'Oran (Algérie)
Examinateur	**Isam SHAHROUR**, Professeur, Université Lille 1 (France)
Examinateur	**Yuanyuan ZHENG**, Maître de Conférences, Université Lille1 (France)
Directeur de Thèse	**Ali ZAOUI,** Professeur, Université Lille 1 (France)

A mes parents (Zahra & Ahmed),

A Mama Aicha,

A ma grande mère,

A toute ma famille, ...

Acknowledgments

It is so difficult to find the words to express my deepest gratitude to my supervisor Pr. Ali ZAOUI. He is genius professor who learned me many things, even beyond scientific research. His daily cheerfulness, patience, continuous encouragement, support and guidance from the beginning up to now enabled me to be firstly impassionate by research and to progress in my thesis work. He gave me the opportunity to discover and to learn this new and very interesting field of research.

It is an honor for me to thank Professor Isam SHAHROUR, for the good time and good atmosphere in our laboratory and for his continuous encouragement.

A special thank to Dr Yuanyuan ZHENG who given me support and encouragement during my thesis work.

I would like to thank my committee members, Professor Rajeev AHUJA from the University of Uppsala, Professor Anatoly BELONOSHKO from KTH Stockholm and Mohamed FERHAT from the University of Sciences and Technologies of Oran for their help and suggestions concerning my research work.

I would also to thank Professor Artem OGANOV from Stony Brooks University as well as Dr Daniel TUNEGA from BOKU of Vienna for their cooperation and help during the realization of this thesis.

I would like to take this opportunity to express my sincere gratitude to our group members: Wei YANG and Anna LUSHNIKOVA who have given me support and encouragement during my thesis work.

I also thank my friennds: Mohamed YASEEN, Mohamed MOKHTARI, Zouhair ABBADI, Faten RAFEH, Abdelhafid KASMI, Ahmed EL MOUMEN, ……., who have given me abundantly help and advices and accompany me during the hard period .

Finally, I wish to express my love and gratitude to my family, especially my parents who have sacrificed so much for me, Mama Aicha, grandmother, uncle Benaissa, uncle Mohamed and aunt Malika , uncle Abdellah and aunt Fatiha, my brother and my sister, Amina and Hamza, Asmae, sami, salma…… and all the rest of my family for their understanding, endless love, encouragement and support, through the duration of my studies.

Table of contents

List of Figures

List of Tables

General introduction

The civil engineering progress would not have been possible without new materials development. In fact, new materials with efficient properties allowed the construction of modern structures, taller building, longer bridges,…etc. Furthermore, it is essential for the progress continuity of this field in the future. Especially, in the smart construction approach we will need new materials with high-performance properties. Of this fact, civil engineering scientists delve increasingly into the field of materials science. The study of the properties of materials at the molecular level, to determine how those materials will function and react on a macro level. It is through the understanding of how materials react at a molecular level that we are able to understand their strengths under a large number of conditions.

In spite of the considerable evolution of civil engineering materials, there is still much development to do, which is true for many materials of various civil engineering specialties. Some materials, widely used in building and public works, can stabilize into different structures with different compositions. Meaning that, they can have different properties, which can be further useful. On the other hand, some geotechnical materials properties are still unknown even in Earth's surface, as well as their properties and behavior in different depths of the earth.

In this thesis, we focused on three types of materials. The first one is carbonates rocks, especially zinc carbonate, which is still unknown as geotechnical materials. The second one is Lime, which is widely used in building and public works; and the last one is zinc oxide which is an important material for steel construction.

Carbonates belong to the most abundant Earth materials. They have, for a long time, been considered as important means of carbon sequestration in deep Earth. Those carbonates contain about 60% of the world's oil reserves and previous studies have shown that carbonates rocks are potential geological reservoir for CO_2 storage. Besides their natural role, they could be used in many industries, including steel construction and oil (particularly oil drilling field). Smithsonite ($ZnCO_3$) is one of the carbon bearings phase within the interior of the Earth. However, the knowledge on this zinc carbonate remains still very weak or almost unknown so far despite the possible interesting properties that could be hidden in such mineral and the various possible applications equivalent to those of other carbonates. This carbonate could be likely different in other situations under normal conditions or under pressure.

Lime is one of the most important and largely used building materials. It is used in several ways in civil engineering. Uses include lime mortar, lime plaster, lime render, lime-ash floors, tabby concrete, whitewash, silicate mineral paint, limestone blocks, which may be of many types. The lime is also used in making roads or paths, usually in the form of quicklime. It can be used alone hydrated and also by mixing it with other civil engineering materials to perform their properties.

Zinc oxide is one of promising alkaline earth metals. It has various technological applications, for example, ceramics, piezoelectric, transducers, chemical sensors, catalysis, optical coating and photovoltaic. In civil engineering, it is used in steel construction, mainly in roofing and gutters.

Many scientists focused their research to answer this problematic. Therefore, many types of advanced techniques have been suggested to solve the problem of crystal structure prediction (CSP). Recently, the more advanced methods including simulated annealing, minima hopping, basin hopping, metadynamics, genetic algorithm, and random sampling method have been developed and applied, which allow a systematic search for the ground state structures based on the chemical composition and the external conditions. The simulated annealing, basin hopping, minima hopping and metadynamics focus on overcoming the energy barriers and are successful in many researches, particularly when the starting structure is close to the global minimum. The genetic algorithm starts to use a self-improving method and is thus able to correctly predict many structures. The random sampling method, as a simple and efficient method, is also successful in many applications.

Recently Universal structure prediction method (USPEX), based on physically motive forms of variation operators and local optimization, demonstrated to be a powerful approach in determining the crystal structure of materials. Universal structure prediction method has shown great success in numerous applications. This method has been used in the present work.

It is the purpose of the present thesis, to investigate in details the three different materials at various pressures by means of the universal structure prediction method based on *ab initio* tool. This thesis is organized in two parts. The first part is theory and the second one summarizes the results and discussions.

The theory part contains two chapters. The first one gives an overview on the studied materials. We present the carbonates minerals with a focus on zinc carbonates. Then details will be given about lime, and finally the general properties of zinc oxide ceramic will be presented. The second chapter describes the methods employed here, i.e. the density functional theory (DFT) and the universal structure predictor method (USPEX).

In the second part we present the complete details of our results. This part contains four chapters. In the first chapter (chapter 3), we spread out in details the various fundamental state properties of smithsonite rock ($ZnCO_3$) for which the most intrinsic quantities remain still unknown.

In chapter 4, we investigate the high-pressure behavior of smithsonite using universal structure prediction method together with the density functional theory. We will focus on the best structures that $ZnCO_3$ may adopt, as well as the three phases below 150 GPa. The two pressures induced phase transition, as well as their properties at high pressure, will be presented.

In chapter 5, lime system CaO, which is known as thermodynamically stable, will be investigated in order to explore all its possible phases under pressure. To this end, we used a variable-composition *ab initio* evolutionary algorithm. At ambient pressure we will predict, in addition to CaO, CaO_2 as thermodynamically stable compound. At increasing pressure, CaO_3 becomes thermodynamically stable at high pressure above 65 GPa.

In the last chapter, the high-pressure stability of zinc oxide will be investigated using a variable composition *ab initio* evolutionary algorithm. In addition to the well-known ZnO, we will predict a new stable compound ZnO_2, which is thermodynamically stable only above 120 GPa.

Finally, a summary of the thesis will be given at the end of the manuscript.

PART I : Theory

Chapter 1 :

Overview on studied materials

1.1. Carbonates

1.1.1 Carbonate minerals

The carbonates are minerals largely represented on the surface of the sphere. Carbonates belong to the most abundant Earth materials after silicates. The crystal structure of many carbonates minerals reflects the trigonal symmetry of the carbonate ion (CO_3^{2-}), which is composed of a carbon atom centrally located in an equilateral triangle of oxygen atoms (Fig.1.1).

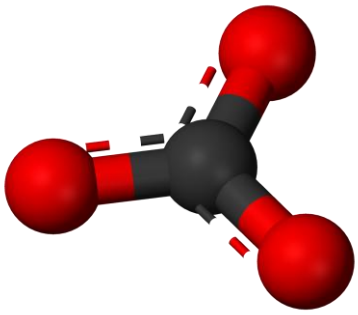

Fig.1.1 : CO_3^{2-} ion

This anion group usually occurs in combination with calcium, sodium, uranium, iron, aluminum, manganese, barium, zinc, copper, lead, or the rare-earth elements. The most known of them are presented in Fig.1.2.

H_2CO_3																	He
$LiCO_3$	$BeCO_3$											B	C	$(NH_4)_2CO_3$, NH_4HCO_3	O	F	Ne
Na_2CO_3, $NaHCO_3$, $Na_3H(CO_3)_2$	$MgCO_3$, $Mg(HCO_3)_2$											$Al_2(CO_3)_3$	Si	P	S	Cl	Ar
K_2CO_3, $KHCO_3$	$CaCO_3$, $Ca(HCO_3)_2$	Sc	Ti	V	Cr	$MnCO_3$	$FeCO_3$	$CoCO_3$	$NiCO_3$	$CuCO_3$	$ZnCO_3$	Ga	Ge	As	Se	Br	Kr
Rb_2CO_3	$SrCO_3$	Y	Zr	Nb	Mo	Tc	Ru	Rh	Pd	Ag_2CO_3	$CdCO_3$	In	Sn	Sb	Te	I	Xe
Cs_2CO_3, $CsHCO_3$	$BaCO_3$		Hf	Ta	W	Re	Os	Ir	Pt	Au	Hg	Tl_2CO_3	$PbCO_3$	$(BiO)_2CO_3$	Po	At	Rn
Fr	Ra		Rf	Db	Sg	Bh	Hs	Mt	Ds	Rg	Cn	Uut	Fl	Uup	Lv	Uus	Uuo
		↓															
		$La_2(CO_3)_3$	Ce	Pr	Nd	Pm	Sm	Eu	Gd	Tb	Dy	Ho	Er	Tm	Yb	Lu	
		Ac	Th	Pa	UO_2CO_3	Np	Pu	Am	Cm	Bk	Cf	Es	Fm	Md	No	Lr	

Fig.1.2: Carbonates minerals

The principal carbonates are classified in three groups: Calcite group, dolomite group and aragonite group. The three groups are presented in Table 1.1. Calcite and dolomite group have the same structure, which is rhombohedral. The dolomite group contains anhydrous carbonates, which are composed of more than one cation in combination with carbonate ion. The most known mineral of this group is dolomite which is composed of calcium magnesium carbonate $CaMg(CO_3)_2$. It occurs in a few restricted modern environments, particularly in certain supratidal environments and freshwater lakes, but it is much less abundant in modern carbonate environments than aragonite and calcite. In the other hand, Aragonite is metastable polymorph (having the same chemical composition but different crystal structure) of $CaCO_3$ and it is converted fairly rapidly under aqueous conditions to calcite.

Calcie Group		***Dolomite Group***		***Aragonite Group***	
Rhombohedral		*Rhombohedral*		*Orthorhombic*	
Mineral	**Formula**	**Mineral**	**Formula**	**Mineral**	**Formula**
Calcite	$CaCO_3$	Dolomite	$CaMg(CO_3)_2$	Aragonite	$CaCO_3$
Magnesite	$MgCO_3$	Ankerite	$Ca(Mg,Fe)(CO_3)_2$	Witherite	$BaCO_3$
Siderite	$FeCO_3$	Kutnohorite	$CaMn(CO_3)_2$	Strontianite	$SrCO_3$
Rhodochrosite	$MnCO_3$			Cerussite	$PbCO_3$
Smithsonite	$ZnCO_3$				

Table1.1 : carbonate groups

In fact, the most abundant and known are calcite, aragonite, and dolomite. Other sedimentary carbonates of non-negligible importance are magnesite (magnesium carbonate) and siderite (ferrous iron carbonate). Dolomites containing some percentage of Fe^{2+} are called ferroan dolomite. The middle member of the range between dolomite and hypothetical $(Fe, Ca)(CO_3)_2$ is called ankerite.

Fig.1.3 is a composition triangle showing the range of carbonate minerals stable at the low temperatures at or near the Earth's surface. It is in terms of the three divalent positive ions, Ca^{2+}, Mg^{2+}, and Fe^{2+}.

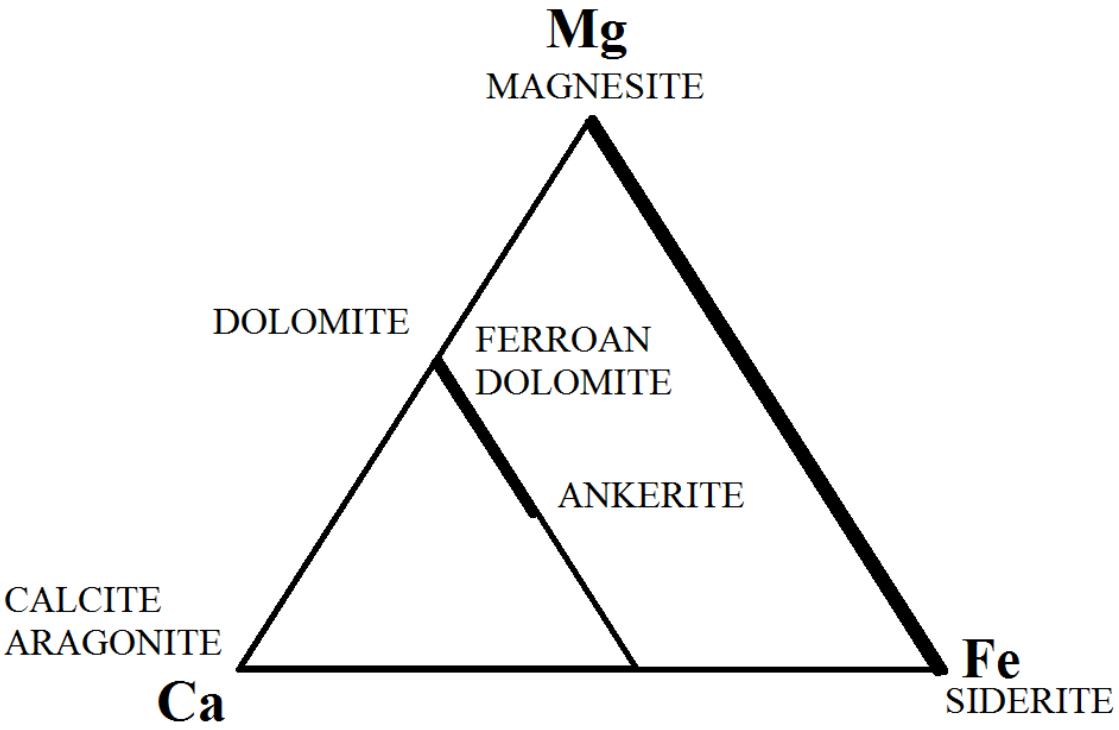

Fig.1.3 : Composition triangle of carbonate minerals stable at Earth-surface.

1.1.2 Role of carbonates and their uses

The carbonates can be found in several earth layers under different structures. Carbonates play an important role in the Earth's carbon cycle (Fig.1.4) [1]. They have for a long time been considered as important means of carbon sequestration in deep Earth. High-pressure phases of carbonates are probably among the host minerals for carbon that are present deeply in the mantle. For these reasons, phase transitions and physical properties of high-pressure phases related to carbonates have been subject of intense investigations [1-6]. Therefore, those carbonates contain about 60% of the world's oil reserves and previous studies have shown that carbonates rocks are potential geological reservoir for CO_2 storage.

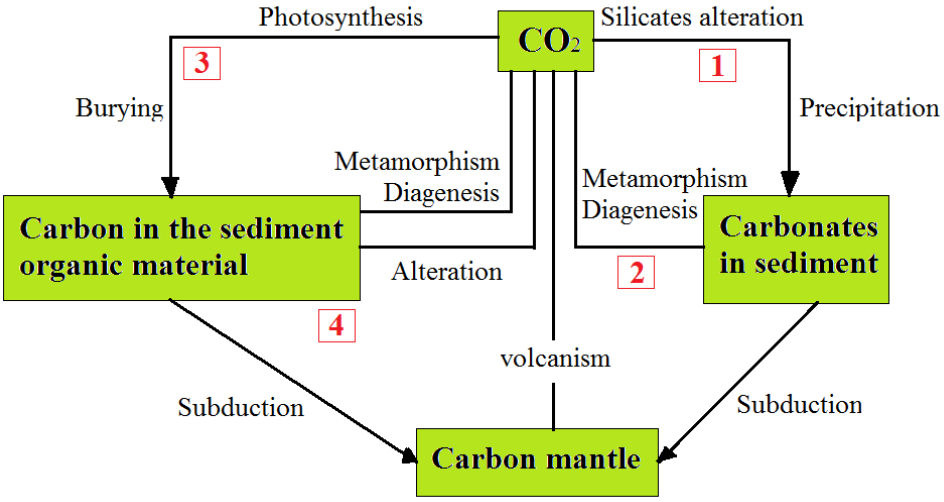

Fig.1.4: Carbon cycle

On the other hand, besides their natural role, they could be used in many industries such as construction, steel industries, oil, agriculture and pharmaceutical industries... For example, many carbonates are used in construction field. One can cite calcite; it was used like limestone and marble. These rocks are used as large stone or as mortar. Those materials are easily mixed, transported and formed into a paste, which hardens into a durable building material. Furthermore, we can cite smithsonite, zinc carbonates, It was used in steel construction mainly in roofing and gutters (Fig.1.5); also, oil particularly oil drilling field.

Fig.1.5: Zinc carbonates applications in civil engineering.

1.1.3 Zinc carbonate

Smithsonite ($ZnCO_3$) is one of the carbon bearing phase within the interior of the Earth. However, the knowledge on this zinc carbonate remains still very weak or almost unknown so far despite the possible interesting properties that could be hidden in such mineral and the various possible applications equivalent to those of other carbonates. These applications could be likely different in other situations under normal conditions or under pressure. Zinc carbonate ($ZnCO_3$) belongs to the calcite group and crystallizes in the trigonal system (rhombohedral carbonate) in normal conditions of temperature and pressure. This mineral is isomorphic with calcite ($CaCO_3$) and dolomite ($MgCO_3$) [1, 3].

Only few experimental studies of smithsonite have been reported in the literature [7-8]. Graf [7] has presented and defined the structure of $ZnCO_3$. Zhang and Reeder [8] performed experimentally the structural properties of smithsonite and they have also determined the bulk modulus. Even if there is no clear study indicating the direct importance of zinc carbonate on interior earth, this mineral belongs to group II of carbonates such as $MgCO_3$, $MnCO_3$, $FeCO_3$[9]. Group II contains the most solid minerals needing a high pressure to crystallize. Several studies were performed on $FeCO_3$ and $MgCO_3$ because of their importance for earth science at high pressure. On the other hand, further study shows that high CO_2 (g) partial pressure results in zinc carbonate being stable and potentially limit zinc mobility [10].

1.2. Civil engineering materials

1.2.1 Revolutionary materials

The modern buildings were a result of the civil engineering materials revolution. Indeed, there are two areas of construction type. This can take us to define two main material types: Natural materials used directly in their pure states and the revolutionary materials created from a composition or mixture of materials.

The ancient structures were built principally by natural stone, clay and timber. The main rocks used in construction are granite, limestone, sandstone, millstone, marl, slate and marble. However, their properties for a natural use are very limited. This led to making new materials by mixing and composition. The most known composite that has been used in construction is reinforced concrete. Concrete is extremely strong under compression, but weak under tension. This inherent weakness in concrete is solved by adding structural steel rods into the wet

concrete. The rebar have ridges on the outside, permitting a strong metal to stone bond. Since steel is strong both under compression and tension, it reinforces the concrete under tension, preventing it from breaking. Until today, scientists still try to perform this material. One way to perform its properties is to mix it with lime.

1.2.2 Lime

Lime is one of the most important and largely used building materials. It is broadly classified as pure, hydraulic, and poor lime; can be natural or artificial; and may be also identified by its magnesium content such as dolomitic or magnesium lime. Lime can be used as lime mortar, lime plaster, lime render, lime-ash floors, tabby concrete, whitewash, silicate mineral paint, limestone blocks which may be of many types. One can find lime in other ways in civil engineering as road.

Fig.1.6: the use of lime in Civil Engineering

Lime is basically known thermodynamically stable as a calcium oxide (CaO). Therefore, it is usually made by the decomposition of materials that contain calcium carbonate by decomposition reaction: $CaCO_3 = CaO + CO_2$. As the case of all metal oxides, they come from carbonate rocks.

Calcium oxide, CaO, is next most abundant phases in planetary mantles after MgO, SiO_2 and FeO, which are considered as the building blocks of the mantle minerals [11]. A number of experimental and theoretical investigations of high-pressure structure and phase stability of CaO have been done, resulting that, CaO crystallizes in the NaCl-type structure (B1) and transforms into CsCl-type structure (B2) about 62 GPa pressure. All its properties (Structural, mechanical and optical properties) have been calculated in previous experiment and theoretical studies [11-13].

1.3. Oxides

1.3.2 Zinc oxide

High pressures materials happen at the centers of planets and in both natural and man-made explosions. Alkaline earth metals are abundant in planetary mantles, and understanding its high-pressure behavior is essential for construction models of the Earth's and planetary interiors. Zinc oxide is one of promising alkaline earth metals. It occurs naturally as a mineral and it can have several phases under high-pressure. These phases may be geologically important as a component of the lower mantle. For these reasons, it has been the subject of several experimental and theoretical studies, in ground state and under pressures [14-17]. At ambient conditions; ZnO is thermodynamically stable in wurtzite phase. The zinc-blende ZnO structure can be stabilized only by growth on cubic substrates, and the rock-salt (NaCl) structure may be obtained at relatively high pressures [15]. Two pressures induced phase transitions were reported. The first one occurs about 10.45 GPa and the second one about 352 GPa [15]. As it was previously reported, the most stable ZnO at ambient condition corresponds to the B4 structure with P63mc space group. Then, the B1 structure with Fm-3m space group becomes stable between 10.45 GPa and 352 GPa. Above 352 GPa, B2 structure with Pm3m space group becomes the most stable structure of ZnO [15]. Furthermore, it has been identified as a potential green precursor to obtain ZnO [18], because its thermal decomposition into ZnO, in addition to smithsonite rock ($ZnCO_3$).

1.3.2 Civil engineering uses

Zinc oxide has various technological applications. Many applications exploit the reactivity of the oxide as a precursor to other zinc compounds. Zinc oxide has high refractive index, high thermal conductivity, binding, antibacterial and UV-protection properties. Therefore, it is

added into materials and products including ceramics, glass, cement, rubber, lubricants, paints, adhesive, sealants, concrete manufacturing, and pigments [19-20].

Zinc oxide can also be found in steel construction. It is recommended for construction because Zinc is safe for the environment and it has a durability and life span that are highly desirable. Consequently, it is mainly used for building environmentally sound structures.

References

[1] Bakri, Z., and Zaoui, A. Structural and mechanical properties of dolomite rock under high pressure conditions: A first-principles study. *Phys. Status Solidi B*, **248**, 1894-1900 (2011).

[2] Ono, S. Synergy Between First-Principles Computation and Experiment in Study of Earth Science. In *Some Applications of Quantum Mechanics* (ed Pahlavani, M.R.) 91-108 (Vienna-Austria, 2012).

[3] Sekkal, W., Taleb, N., Zaoui, A., & Shahrour, I. A lattice dynamical study of the aragonite and post-aragonite phases of calcium carbonate rock. *Am. Mineral.* **93**, 1608-1612 (2008).

[4] Sekkal, W., and Zaoui, A. Nanoscale analysis of the morphology and surface stability of calcium carbonate polymorphs. *Sci. Rep.* **3**, 1587 (2013).

[5] Zaoui, A., and Shahrour, I. Molecular dynamics study of high-pressure polymorphs of $BaCO_3$. *Philos.* Mag. Lett. 90, 689-697 (2010).

[6] Bouibes, A., and A. Zaoui. High-pressure polymorphs of $ZnCO_3$: Evolutionary crystal structure prediction. *Sci. Rep.* 4 (2014).

[7] Graf, D. L. Crystallographic tables for the rhombohedral carbonates. *Am. Mineral.* **46**, 1283-1316 (1961).

[8] Zhang, J., & Reeder, R. J. Comparative compressibilities of calcite-structure carbonates: Deviations from empirical relations. *Am. Mineral.* **84**, 861-870 (1999).

[9] Goldin, D. M., & Kulikova, G. V. On the dissociation mechanism of carbonates and their isomorphous mixture. *J. Therm. Anal.* **29**, 139-145 (1984).

[10] McPhail, D. C., Summerhayes, E., Welch, S., & Brugger, J. The geochemistry and mobility of zinc in the regolith. *Adv. Regolith*, 287-291 (2003).

[11] Deng, Ye, et al. Phase transition and elastic constants of CaO from first-principle calculations. *Physica B: Condens. Matter* **392**. 229-232 (2007).

[12] Richer, P., et al. Static compression and equation of state of CaO to 1.35 Mbar, *J. Geophys. Res.* **93**, 279-288 (1988)

[13] Ghebouli, B., et al. First-principles calculations of structural, elastic, electronic and optical properties of XO (X= Ca, Sr and Ba) compounds under pressure effect. Mater. *Sci. Semicond. Process.* **13**. 92-101 (2010).

[14] Ahuja, R., et al. Elastic and high pressure properties of ZnO. *J. Appl. Phys.* **83**, 8065-8067 (1998).

[15] Zaoui, A., and W. Sekkal. Pressure-induced softening of shear modes in wurtzite ZnO: A theoretical study. *Phys. Rev.B* **66**, 174106 (2002).

[16] Zaoui, A., Energetic stabilities and the bonding mechanism of ZnO {0001}/Pd (111) interfaces. *Phys. Rev.B* **69**, 115403 (2004).

[17] Desgreniers, S. High-density phases of ZnO: Structural and compressive parameters. *Phys. Rev. B* **58**, 14102 (1998).

[18] Escobedo-Morales, A., et al. Structural and vibrational properties of hydrothermally grown ZnO_2 nanoparticles. J. Cryst. Growth 316, 37-41 (2011).

[19] Sanchez-Pescador, R. et al. The nucleotide sequence of the tetracycline resistance determinant tetM from Ureaplasma urealyticum. *Nucleic Acids Research* **16** (3): 1216 (1988).

[20] Hernandezbattez, A et al. CuO, ZrO_2 and ZnO nanoparticles as antiwear additive in oil lubricants. *Wear* **265** (3–4): 422. (2008).

Chapter 2:

Computational techniques

2.1 Density functional theory

The most advanced theoretical formalism that we will use for local optimization is density functional theory (DFT). A short description of this theory is given in the following.

2.1.1 Problematic

The material study at the quantum level consists to solve the Schrödinger equation describing a periodic crystalline system, composed of nuclei (n) in mutual interaction and electron spin (σ_i) positioned at R= (R_I; I=1,…,N_n) and at r=((r_i, σ_i); i=1,…,N_e) respectively.

$$H*\Psi(R,r) = E*\Psi(R,r) \qquad (2.1)$$

Where H is the Hamiltonian. It comprises at five words, the kinetic energy of the electrons and nuclei, and interactions between them.

$$H= T_n + T_e + U_{n-n} + U_{e-e} + U_{n-e} \qquad (2.2)$$

Solving this problem was impossible given the large number of unknown and given the limited memory of the computer tools. However, it is possible to reformulate the problem by using appropriate theorems and approximations.

2.1.2 Principle of theory

The resolution of the stationary equation remains very difficult due to its complexity, when it is applied to real systems including more atoms and electrons. However in most cases, the treatments based on the simplified mean-field theory are adequate to give answer to the problem.

The theory of density functional is the most common approach used now. The main goal of density functional theory is to replace the multi-electronic wave function by the electron density as a amount of basis for the calculations. While the wave function depends on multi-electronic variables 3N (where N is the total number of particles in the system), the density is only a function of three variables; it is therefore a quantity easier to treat both mathematically and conceptually. The principle of DFT is a reformulation of quantum problem of many-body in a single-body problem (or, at two-body considering the problems of spin) with the parameter of electron density. The central idea of DFT is that the only electron density of the ground state of the system completely determines the mean values of observables, such as energy.

2.1.3 Hohenberg-Kohn theorem

Hohenberg and Kohn proved in 1964 [1] that electron density could play a decisive role in electronic calculations, with two theorems, and thus provided a sound foundation for the designation of electron density as the key player in the DFT. These theorems changed DFT in exact science for many-body system and they consequently completed the links between electron density, external energy, Hamiltonian, and wave function.

The two Hohenberg-Kohn theorems are as follows:

Theorem I: *For any system of interacting particles in an external potential $V_{ext}(r)$, the density is uniquely determined (in other words, the external potential is a unique functional of the density).*

Theorem II*: A universal functional for the energy E[ρ] can be defined in terms of the density. The exact ground state is the global minimum value of this functional.*

The founding principle of the DFT can be summarized in these two theorems, which affirm that there is a one to one correspondence between external potential $V_{ext}(r_i)$ and density.

2.1.4 Kohn-Sham approach

DFT is the most widely used method today for electronic structure calculation because of the approach proposed by Kohn and Sham [2]. This approach aims to replace the original many-body problem by an auxiliary independent-particle problem.

The Kohn-Sham approach converts the many-body system of the interacting electrons, $\Psi(r_1,r_2,\ldots)$, into a whole of non-interacting one-body wave functions, $\{\Upsilon_i(r)\}$, and with the same density, $r = \sum |\Upsilon_i(r)|^2$. The ground state energy of the interacting system E[ρ] is then the same as the ground state energy of the non-interacting system $E_{KS}[\rho]$, which can be expressed as:

$$E_{KS}[r] = E_{kinetic} + \int d^3r [V_{ext}(r) r(r)] + E_{Hartree}[r] + E_{xc}[r] \qquad (2.3)$$

The first term is the kinetic energy of the non-interacting electrons and the second term is the potential energy of electrons due to the external field. $E_{Hartree}[r]$ is the direct

Coulomb interaction between electrons. The fourth term is the exchange-correlation energy, which is the only unknown term so far. The KS approach involves independent particles but an interacting density. Thus, all the difficult many-body terms are incorporated into the exchange-correlation functional of the density. If the solution of $E_{xc}[r]$ is available, the KS equation can be solved by self-consistent iteration, which would lead to the exact energy. However, there is no way to obtain the exact form $E_{xc}[r]$. Instead, we have to reasonably approximate it.

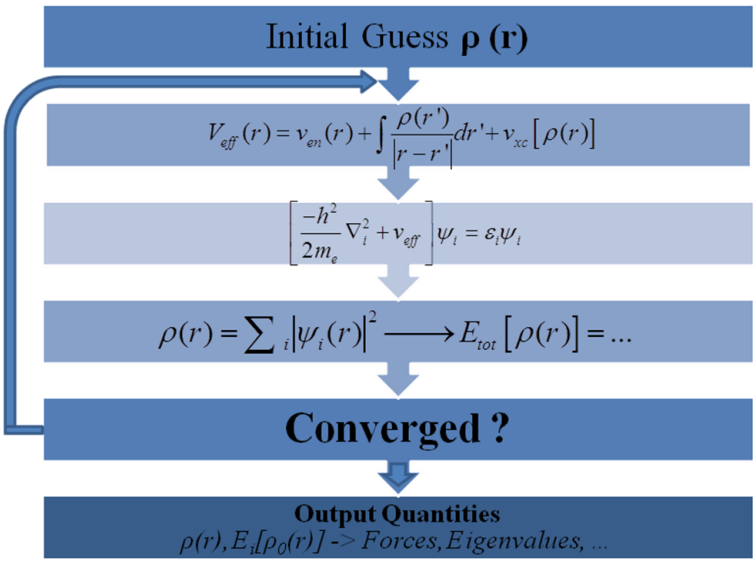

Fig. 2.1: Representation of the self-consistent loop for solution of KS equation.

2.1.5 Exchange-correlation functional

The main problem with the Kohn-Sham approach is the introduction of the unknown exchange-correlation functional. As long as there is no expression for this term, it is impossible the solve Kohn-Sham equation. To solve the latter, various exchange-correlation functional have therefore been considered. Let us define the most popular and used of them in the following.

2.1.5.1 Local Density Approximation (LDA)

When considering approximations for the exchange-correlation energy, one simple way of accounting for the varying electron densities in a system is by assuming that electrons see the overall landscape in the same way as they see locally. Each system can be transformed into many pieces of uniform electron density with different values. It is now possible to calculate the exchange-correlation energy for each electron with the electron density that is assumed to be constant in that piece. The energies associated with these local elements can be summed up to equal the total exchange-correlation energy. This is the local density approximation (LDA) [2].

The LDA becomes exact only in the limit of homogeneous electron gas or very slowly varying densities. In practical calculations, however, the known numerical results from the above quantum Monte Carlo calculations are interpolated, and the values of $\varepsilon_{xc}^{hom}<\rho(r)>$ per volume of constant ρ for all densities are parameterized. Then the exchange-correlation energy of the LDA can be calculated by multiplying $\varepsilon_{xc}^{hom}<\rho(r)>$ by the local electron density and integrating it over the space:

$$E_{xc}^{LDA}[r(r)] = \int r(r) e_{xc}^{hom}[r(r)]\,dr \qquad (2.4)$$

At first sight, it would seem that LDA is not very accurate since the density of any real system is far from homogeneous, but in practice it seems to work surprisingly well.

2.1.5.2 Generalized Gradient Approximation (GGA)

Real systems are evidently not homogeneous and have varying density landscape around electrons. To generate more accurate exchange-correlation functional, the generalized gradient approximation (GGA) [3] captures both the local and semi-local information: the electron density and its gradient at a given point. The general formula of energy with density gradient as an additional variable:

$$E_{xc}^{GGA}[r(r)] = \int r(r) e_{xc}^{GGA}[r(r), \nabla r(r)]\,dr \qquad (2.5)$$

Therefore, the general form of GGA in practice is expressed based on the LDA with an additional enhancement factor $F_{xc}(s)$ that directly modifies the LDA energy:

$$E_{xc}^{GGA}[\rho(r),s]=\int \varepsilon_{xc}^{LDA}[\rho(r)]\rho(r)F_{xc}(s)dr \qquad (2.6)$$

Here, the s depends on both electron density and its gradient:

$$s=\frac{|\nabla\rho(r)|}{2k_F\rho} \qquad (2.7)$$

Where $k_F=(3\pi^2\rho)^{1/3}$ is the Fermi wave vectore of the electron gas of density ρ.

Many different forms of F_{xc} have been proposed. In this thesis, we have used PW91 [4], PBE [3], PBEsol [5] and AM05 [6]:

A) Perdew-Wang'91 (PW91)

Perdew-Wang'91 has been very popular in applications for a wide range of materials due to its reasonable accuracy and general applicability.

- PW91 exchange functional:

$$\varepsilon x=\varepsilon_x^{LDA}\left(\frac{1+a_1 s\sinh^{-1}(a_2 s)+(a_3+a_4e^{-100s^2})s^2}{1+a_1 s\sinh^{-1}(a_2 s)+a_5 s^4}\right) \qquad (2.8)$$

Where a_1= 0.19645, a_2= 7.7956, a_3= 0.2743, a_4= - 0.1508 and a_5=0.004.

- PW91 correlation functional:

$$\varepsilon_c=\varepsilon_c^{LDA}+\rho H[\rho,s,t] \qquad (2.9)$$

With: $$H[\rho,s,t]=\frac{\beta}{2\alpha}\ln\left(1+\frac{2\alpha}{\beta}\frac{t^2+At^4}{1+At^2+A^2t^4}\right)+C_{c0}\left[C_c(\rho)-C_{c1}\right]t^2e^{-100s^2} \qquad (2.10)$$

And $$A=\frac{2\alpha}{\beta}\left[e^{-2\alpha\varepsilon_C[\rho]/\beta^2}-1\right]^{-1} \qquad (2.11)$$

Where α=0.09, β=0.06672, C_{C0}=15.7559, C_{C1}=0.003521,

$$t=|\nabla\rho(r)|/(2k_s\rho) \qquad (2.13)$$

For $$k_s=(4k_F/\pi)^{1/2} \qquad (2.14)$$

and $$\rho\varepsilon_C[\rho]=\varepsilon_C^{LDA}[\rho] \qquad (2.15)$$

B) Perdew-Burke-Ernzerhof (PBE&PBEsol)

Based on PW91, PBE presents a simplified and improved GGA version with no empirical elements. It includes features such as local electron density and its gradient and second-order gradient and second-order gradient in the enhancement factors, F(x) and F(c). Recently, PBEsol was optimized against the jellium-surface exchange-correlation energies, and this, in conjunction with changing another parameter to restore the first-principles gradient expansion for exchange, was sufficient to yield accurate lattice constants of solids.

The exchange energy for GGA has the following form:

$$E_x^{GGA}\left[\rho(r),s\right]=\int \varepsilon_x^{LDA}\left[\rho(r)\right]\rho(r)F_x(s)dr \qquad (2.16)$$

F_x(s) is the exchange enhancement factor, which in $s\to 0$ limit can be written as :

$$F_x(s)=1+\mu s^2+...(s\to 0) \qquad (2.17)$$

For slowly varying electron densities the gradient expansion has $\mu_{GE}=10/81=0.1235$.

The gradient expansion for GGA correlation functional for uniform gas is:

$$E_c\left[\rho\right]=\int \rho(r)\left\{\varepsilon_c^{LDA}(\rho)+\beta t^2(r)+...\right\}dr \qquad (2.18)$$

Where β is a coefficient, and :

$$t=\frac{|\nabla\rho|}{2k_{TF}\rho} \qquad (2.19)$$

$$k_{TF}=\sqrt{\frac{4k_F}{\pi}} \qquad (2.20)$$

Is the appropriate reduced density gradient for correlation (fixed by Thomas-Fermi screening wave vector). For slowly varying high densities $\beta_{GE}=0.0667$.

For PBE $\beta=\beta_{GE}=0.0667$ and $\mu\approx 2\mu_{GE}$

And For PBEsol $\beta=0.0375$ and $\mu=\mu_{GE}$.

C) Armiento and Mattson (AM05)

AM05, recent density functional, performs exceptionally well for solids and surfaces. AM05 is of a regular semilocal generalized gradient approximation form. The performance of AM05 is on average found to be superior to selecting the best of local density approximation and PBE for each solid.

The AM05 surface exchange functional is a parameterization of the Airy electron gas data. The Local Airy Approximation (LAA) parametrization used in AM05 is given by:

$$\varepsilon_x^{LAA}(r,\rho) = \varepsilon_x^{LDA}(\rho(r))\left[X + (1-X)F_x^{LAA}(s)\right] \quad (2.21)$$

And the correlation functional:

$$\varepsilon_c(r,\rho) = \varepsilon_c^{LDA}(\rho(r))\left[X + (1-X)\gamma\right] \quad (2.22)$$

Where $$X = 1 - \frac{\alpha s^2}{1+\alpha s^2} \quad (2.23)$$

And the refinement function $$F_x^{LAA}(s) = \frac{cs^2+1}{\frac{cs^2}{F_x^b}+1} \quad (2.24)$$

Where c=0.7168, α_{LAA}=2.804, γ_{LAA}=0.8098 and F_x^b is constructed as an analytical interpolation between two known limits of the Airy refinement function.

2.2 Pseudo-potentials

There is two regions of electrons; core and valence regions. The core electrons are usually chemically inert, and only valence electrons contribute to bonding. Therefore, pseudopotential can be constructed to frozen the core electrons while only consider the chemically active valence electrons. A good pseudopotential should satisfy the following rules:

1) The pseudo wave functions should be identical to the all-electron wave functions outside the cut-off radius (r_c), as shown in Fig.2.2.

$$\Psi^{AE}(r) = \Psi^{PP}(r), \qquad r>r_c \quad (2.25)$$

2) The eigenvalues should be conserved.

$$\varepsilon_i^{AE}(r) = \varepsilon_i^{PP} \qquad (2.26)$$

3) The total charge of each pseudo wave function should equal the charge of the all-electron wave function.

$$\int_0^{r_c} \left|\psi_i^{AE}(r)\right|^2 dr = \int_0^{r_c} \left|\psi_i^{PP}(r)\right|^2 dr \qquad (2.27)$$

4) The scattering properties of the pseudopotential should be conserved.

According to norm-conserving condition, the pseudopotential $V_i(r)$ can be split into a local part, long-ranged and behaving like $-Z_v e^2/r$ for $r \to \infty$, and a short-ranged semilocal term:

$$V^{PP}(r) = V_{loc} + V_{SL} \qquad (2.28)$$

Where $V_{loc}(r)$ is a radial function, and the semi-local part is the deviation from the all-electron potential inside the core region,

The pseudopotential reproduces the true potential outside the core region, but is much smoother inside the core. The oscillations of the electron wave function inside the core region are eliminated by the pseudopotential. This is a great advantage for numerical calculations. A further approximation, the ultrasoft pseudo-potential [7], uses more than one projector for each momentum, and further makes smooth the electron wave function.

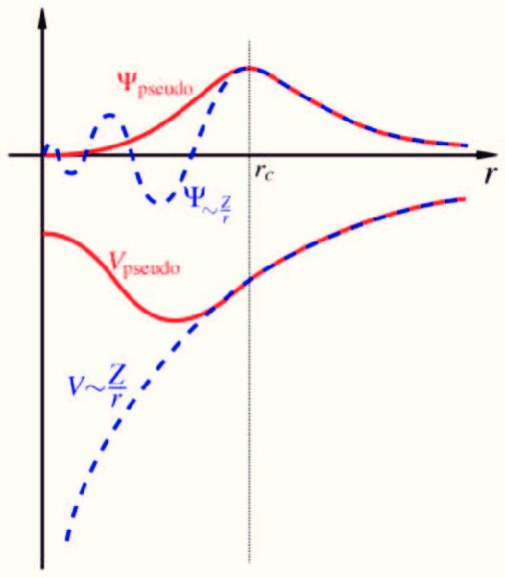

Fig. 2.2: Comparison of a wave function in the Coulomb potential of the nucleus (blue) to the one in the pseudopotential

2.3 Solving techniques

When the exchange-correlation functional is known, it is theoretically possible to solve Kohn-Sham equations. However, the resolution of a system consisting of an infinite number of electrons is very difficult. Therefore, it is essential to use complex numerical methods.

2.3.1 Bloch theorems

Bloch's theorem is founded on this idea of translational invariance among the different atomic sites and/or primitive cells of the crystal, considering only one of those repeating units, thus tremendously simplifying the problem to be tackled.

Let's now consider a real three-dimensional crystal. For simplicity, we will consider the nuclei to be static, and the electrons to be non-interacting particles moving in a static potential V(r). The perfect crystal constitutes a periodic array of lattice vectors $\{R\}$. The potential is periodic and invariant under translation, so that we always have:

$$V(r + \mathbf{R}) = V(r) \qquad (2.29)$$

and hence the Hamiltonian operator should be periodic, i.e.:

$$H(r + \mathbf{R}) = H(r) \qquad (2.30)$$

The game would then be to find a translation operator T_R for each lattice vector **R** which could act on any function $f(r)$ so that:

$$T_R f(r) = f(r + \mathbf{R}) \qquad (2.31)$$

One can show that such an operator acting onto the wavefunction would yield the following identity relation:

$$T_R \psi(r) = \psi(r + \mathbf{R}) = \exp(ik \cdot \mathbf{R}) \psi(r) \qquad (2.32)$$

If we now consider the function $u(r) = \exp(-ik \cdot r) \psi(r)$, we can see that

$$\begin{aligned} u(r + R) &= \exp(-ik \cdot [r + \mathbf{R}]) \psi(r + \mathbf{R}) \\ &= \exp(-ik \cdot r) \exp(-ik \cdot R) \exp(ik \cdot R) \psi(r) \\ &= \exp(-ik \cdot r) \psi(r) \end{aligned} \qquad (2.33)$$

thus the function $u(r)$ also has the periodicity of the lattice and is cell-periodic since we saw that $u(r + \mathbf{R}) = u(r)$, and it makes it possible to express the eigenstates of the full Hamiltonian as:

$$\psi_{nk}(r) = u_{nk}(r)\, e^{ik.r} \qquad (2.34)$$

Since now we have taken care of the translational invariance, Bloch's theorem allows us to simplify the problem: instead of having to solve for the entire infinite space, we are only left with solving for the wavefunction within a single cell (in fact the first Brillouin zone), but at an infinite number of k-points. Outside of this cell, the values of the wavefunctions are identical by translational symmetry so that:

$$\begin{cases} \psi_{n,k+G}(r) = \psi_{n,k}(r) \\ \varepsilon_{n,k+G} = \varepsilon_{n,k} \end{cases} \qquad (2.35)$$

2.3.2 Brillouin zone

In order to construct the density, the occupied Hamiltonian eigenstates must be calculated. In fact, all possible eigenstates are characterized by the wave-vector k into primitive cell in the periodic reciprocal space. Therefore, the question which arises: is there a more appropriate choice of this cell? *The first Brillouin zone* (FBZ), that volume of reciprocal-space enclosing the origin which is bounded by the planes which perpendicularly bisect lines from the origin to surrounding lattice points.

Thus, to obtain properties such as total energy, charge density, etc. We must integrate k-points in the Brillouin zone. The volume of the Brillouin zone Ω_{BZ} is related to the volume of the supercell Ω_{cell} by :

$$\Omega_{BZ} = \frac{(2\pi)^3}{\Omega_{cell}} \qquad (2.36)$$

so that for large systems, the Brillouin zone volume is very small and only a few k-points need to be considered to describe the variation across the Brillouin zone accurately. It is possible to transform this integration to the addition of the selected sample.

Many election procedures exist for these k-points. These include, in particular those of Baldereschi [8], Chadi and Kohen [9] and Monkhorst and Pack [10] as the most frequently used.

2.4 Universal Structure Predictor: Evolutionary Xtalloraphy (USPEX)

2.4.1 Global Optimization Methods

Several global optimization algorithms are conceived for crystal structure prediction. Among the most known and used, we find simulated annealing [11-12], metadynamics [13], genetic algorithms [14], evolutionary algorithms [15-16], random sampling [17], basin hopping [18], minima hopping [19], and data mining [20].

Universal structure predictor is based on evolutionary algorithm, which uses a "self-improving" method that locates, step by step, the best structures. The strength of evolutionary simulations is that they do not necessarily require any system-specific knowledge except chemical composition, and are self-improving, i.e., in subsequent generations increasingly good structures are found and used to generate new structures.

2.4.2 Evolutionary Algorithm

The evolutionary algorithm employs variation operators as genetic heredity, mutations and permutation. The procedure is as shown in Fig.2.3:

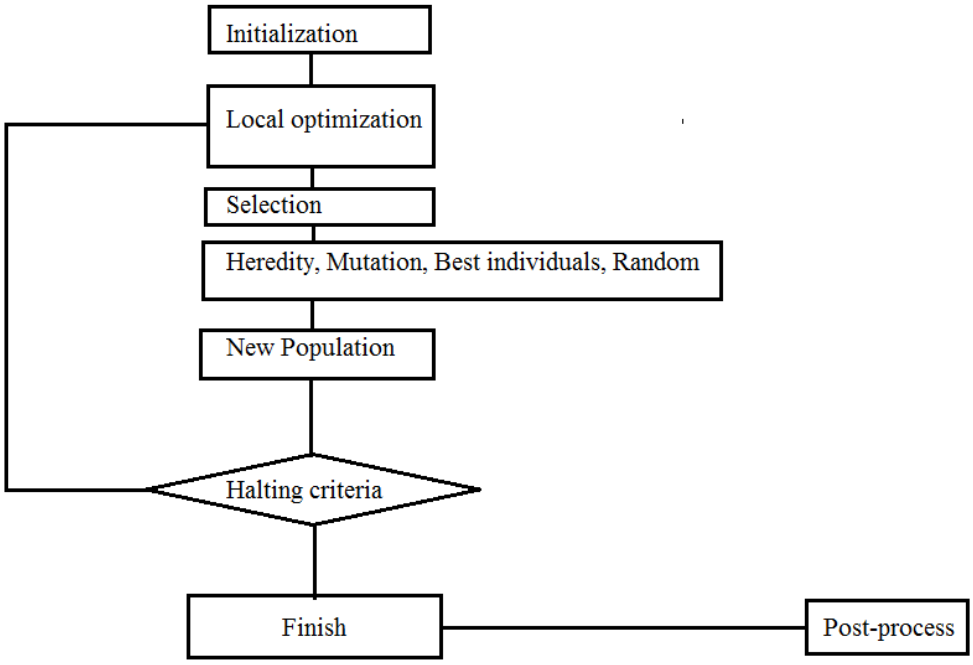

Fig.2.3 : Illustration of the evolutionary algorithm for crystal structure prediction.

(1) Initialization of the first generation, that is, a set of structures satisfying the hard constraints are randomly generated;

(2) Determination of the quality for each member of the population using the so-called fitness question;

(3) Selection of the best members from the current generation as parents from which the structures of the new population are created by applying specially designed variation operators.

(4) Evaluation of the quality for each new member of the population.

(5) Repeat steps 3-4 till the halting criteria is achieved.

The above algorithm has been implemented in the USPEX (Universal Structure Predictor: Evolutionary Xtallography) code [17,25-27].

2.4.3 Variation Operators

USPEX features three different variation operators: heredity, mutation and permutation. These operators are described in details below.

2.4.3.1 Heredity

Two structures, called parent structures, are selected and used to produce one new candidate structure. This is achieved by taking a fraction of each structure parent and combining them. However, the fraction of each parent structure should contain as much information of the structure as possible. The main information within crystal structures is the relative position of the nearby atoms. Thus, to conserve information, the fraction of a structure is selected by taking a spatially coherent slab. The two slabs, one of each parent, are fitted together and the result thereafter made feasible by adjusting the number of atoms of each type to the requirements. An example for heredity can be found in Fig. 2.4.

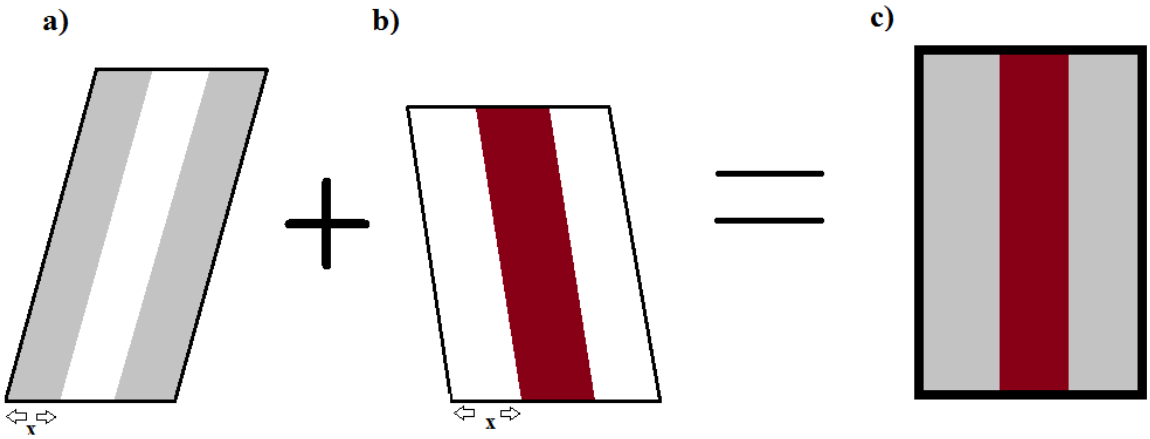

Fig. 2.4: Heredity. (a) Parent 1, (b) parent 2, (c) hereditary structure.

2.4.3.2 Mutation

One individual is selected and used to produce one new candidate. The lattice vectors $\vec{a}$ are transformed to new vectors $\vec{a}'$ by applying a strain matrix:

$$\vec{a}' = \left[I + \varepsilon_{ij} \right] \vec{a} \qquad (2.37)$$

where I is the unit matrix and ε_{ij} is the symmetric strain matrix, such that:

$$\left[I + e_{ij} \right] = \begin{pmatrix} 1+e_{11} & \frac{e_{12}}{2} & \frac{e_{13}}{2} \\ \frac{e_{12}}{2} & 1+e_{22} & \frac{e_{23}}{2} \\ \frac{e_{13}}{2} & \frac{e_{23}}{2} & 1+e_{33} \end{pmatrix} \qquad (2.38)$$

An example for mutation can be found in Fig. 2.5.

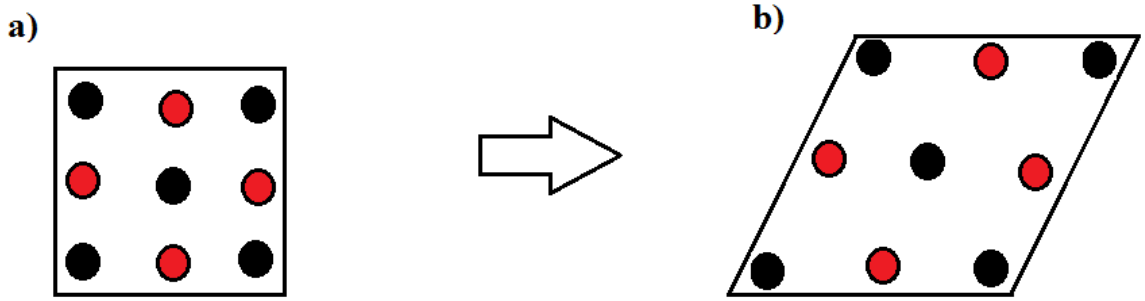

Fig. 2.5: Example of a mutation. (a) Initial structure, (b) mutated structure.

2.4.3.3 Permutation

One individual is selected and used to produce one new candidate. Two atoms of different types are exchanged, a variable number of times. Permutation facilitates finding the correct atomic ordering. Obviously, permutation is possible only for systems with different types of atoms. An example for permutation can be found in Fig. 2.6. [28].

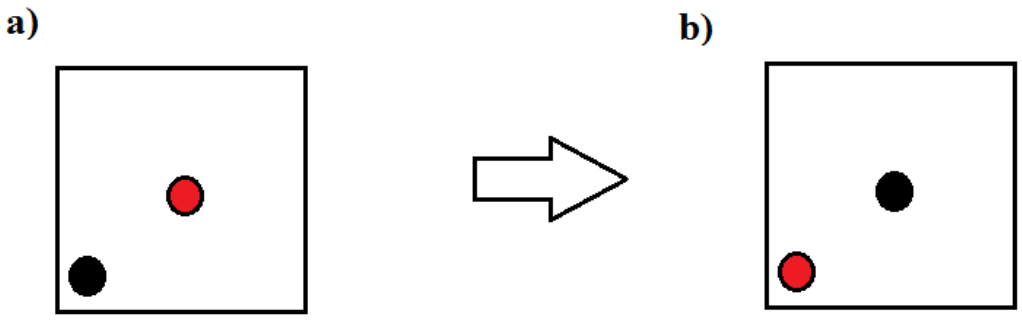

Fig.2.6 : Example of a permutation. (a) Initial structure, (b) permutated structure

2.4.4 Variable composition method

Universal structure predictor method can also predict stable chemical composition and corresponding crystal structures. Variable composition prediction was performed here by convex hull construction.

Indeed, the stability of compounds with different stoichiometries can be evaluated by the formation energy towards the decomposition into mixtures of other compounds.

For example for a system AB, the energy of formation can described as follows:

$$E_{formation} = E_{AB} - E_A - E_B \qquad (2.39)$$

Where E_A and E_B are the energy of the elements A and B respectively.

Stable compounds have negative energy of formation, which a necessary condition but not sufficient for thermodynamically stable systems. A sufficient condition is that a compound is stable to decomposition into any other compounds or elements.

A variable composition algorithm employs the same variable operators in addition to the chemical transmutation operators. The transmutation operator selects one individual to produce one new candidate. One type of atom is changed by another one (Fig.2.7). This operator turns out to be quite efficient for driving the system from a known minimum to another 'good' minimum in a different area of compositional space.

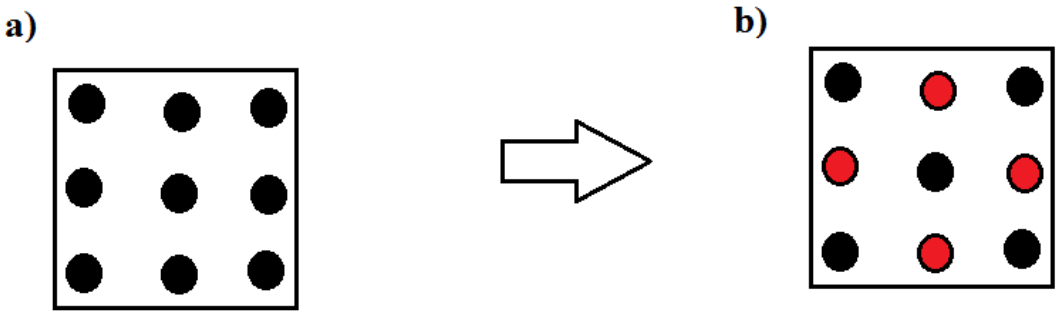

Fig.2.7: Example of a transmutation: (a) initial structure, (b) transmuted structure.

The new variation composition algorithm is shown in Fig.2.8 below indicating the most important steps until the convergence is achieved.

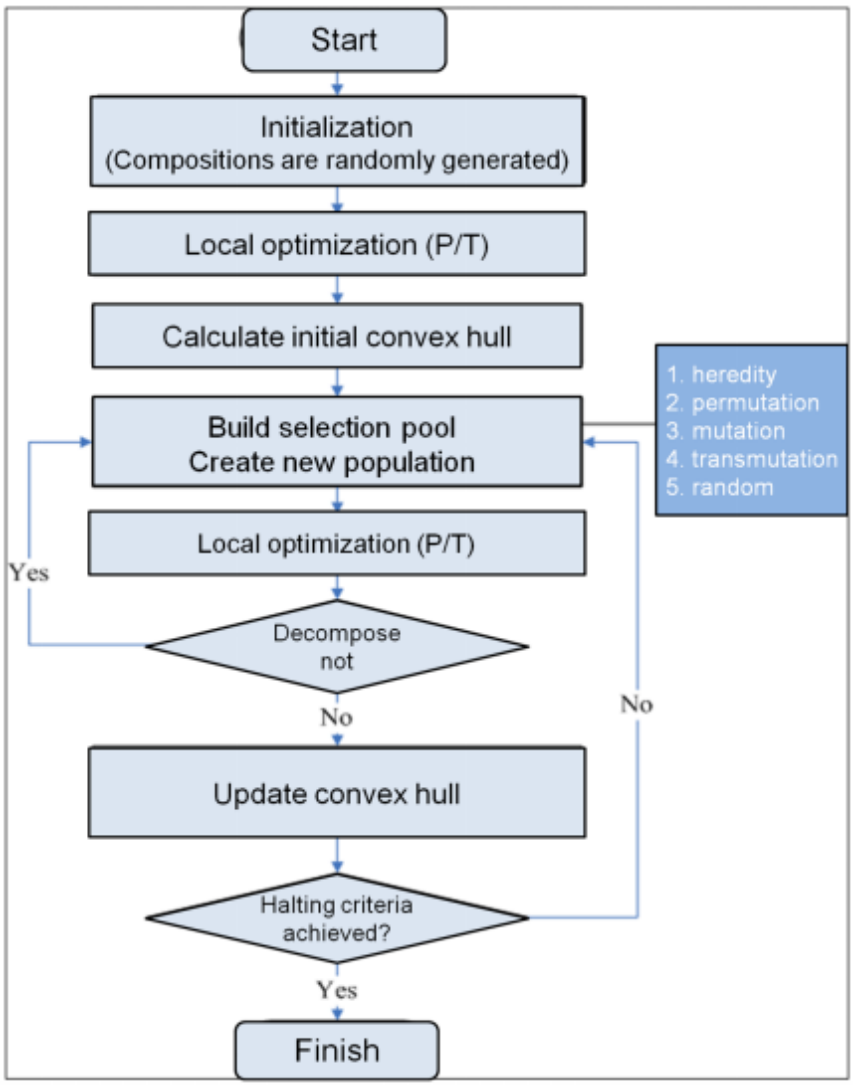

Fig 2.8: Variable composition algorithm

References:

[1] Hohenberg, P. and Kohn, W. Inhomogeneous electron gas. *Phys. Rev.*, **136**: B864–B871 (1964).

[2] Kohn, W. and L. J. Sham. Self-consistent equations including exchange and correlation effects. *Phys. Rev.*, **140**:A1133–A1138, (1965).

[3] Perdew, J.P., Burke K., and Ernzerhof M., Generalized gradient approximation made simple." *Phys. rev. lett.* **77**: 3865 (1996).

[4] Perdew J.P., and Wang Y., Pair-distribution function and its coupling-constant average for the spin-polarized electron gas. *Phys. Rev. B* **45** 13244 (1992).

[5] Perdew J.P., et al., Restoring the density-gradient expansion for exchange in solids and surfaces. *Phys. Rev. Lett.* **100** 136406 (2008).

[6] Mattsson, A.E., et al., The AM05 density functional applied to solids. J. chem. Phys. **128** 084714 (2008).

[7] Vanderbilt, D. Soft self-consistent pseudopotentials in a generalized eigenvalue formalism. *Phys. Rev. B*, **41**:7892–7895, (1990).

[8] Baldereschi, A., Mean-value point in the Brillouin zone. *Phys. Rev. B* **7**: 5212, 1972.

[9] D. J. Chadi and M. L. Cohen, *Phys. Rev. B* **8**: 5747, 1973.

[10] Monkhorst, H. J. and Pack, J. D. Special points for Brillouin-zone integrations. *Phys. Rev. B***13**: 5188, 1976.

[11] Pannetier J. , et al. Prediction of crystal structures from crystal chemistry rules by simulated annealing. *Nature*, **346**:343–345 (1990).

[12] Schon, J. C. and Jansen, M., First step towards planning of syntheses in solid-state chemistry: Determination of promising structure candidates by global optimization. Angew. *Chem. Int. Ed. Engl.*, **35**:1286–1304 (1996).

[13] Martoňák, R., Laio, A. , and M. Parrinello. Predicting crystal structures: The parrinello-rahman method revisited. *Phys. Rev. Lett.*, **90**:075503, (2003).

[14] Woodley, M. S. et al . The prediction of inorganic crystal structures using a genetic algorithm and energy minimisation. *Phys. Chem. Chem. Phys.*, **1**:2535–2542 (1999).

[15] Oganov, A. R. and Glass, C. G. Crystal structure prediction using evolutionary algorithms: principles and applications. *J. Chem. Phys.*, **124**:244704 (2006).

[16] Oganov, A. R., Lyakhov, A. O. and Valle, M. . How evolutionary crystal structure prediction works - and why. *Acc. Chem. Res.*, **44**: 227–237 (2011).

[17] Freeman, C. M. et al. Inorganic crystal structure prediction using simplified potentials and experimental unit cells: application to the polymorphs of titanium dioxide. *J. Mater. Chem.*, **3**:531–535 (1993).

[18] Wales, D. J. and Doye, J. P. K.. Global optimization by basin-hopping and the lowest energy structures of lennard-jones clusters containing up to 110 atoms. *J. Phys. Chem. A,* **101**:5111–5116 (1997).

[19] Goedecker, S . Minima hopping: Searching for the global minimum of the potential energy surface of complex molecular systems without invoking thermodynamics. *J. Chem. Phys.,* **120**: 9911–9917, (2004).

[20] S. Curtarolo et al. Crystal structures with data mining of quantum calculations. *Phys. Rev. Lett.*, **91**:135503, (2003).

[21] S. Curtarolo et al. Crystal structures with data mining of quantum calculations. Phys. Rev. Lett., 91:135503, (2003).

[22] Yang, K. et al. A search model for topological insulators with high-throughput robustness descriptors. *Nat. Mater.*, **5**:623–626, (2006).

[23] Glass, C. W., Oganov, A. R., and Hansen, N. Uspex evolutionary crystal structure prediction. *Comput. Phys. Comm.*, **175**:713–720, (2006).

[24] Oganov, A. R. and Glass, C. W., Evolutionary crystal structure prediction as a tool in materials design. *J. Phys.: Cond. Matter*, **20**:064210, (2008).

[25] Kresse, G. Furthmuller, J. Efficient iterative schemes for ab initio total-energy calculations using a plane wave basis set". *Phys. Rev. B*, **54** (1996), pp. 11169–11186

[26] Michalewicz, Z. Fogel, D.B. How to Solve It: Modern Heuristics. *Springer, Berlin* (2004).

[27] Zhu Q., Oganov A.R., and Zhou X.F. Crystal structure prediction and its application in Earth and Materials Sciences. *Topics in Current Chemistry*, (2014).

[28] Glass C.W., Oganov A.R., and Hansen N. USPEX – evolutionary crystal structure prediction. *Comp. Phys. Comm.* **175**, 713-720 (2006).

PART II: Results

Chapter 3:

Bonds, bands and elasticity of $ZnCO_3$

3.1. Abstract

The objective here is to spread out in detail the various fundamental state properties of smithsonite rock ($ZnCO_3$) for which the most intrinsic quantities remain still unknown. First-principles electronic structure calculations based on the density functional theory with the pseudopotential method were performed using divers functionals. A number of mechanical quantities were evaluated such as bulk modulus, elastic constants, Young and shear moduli, and transversal and longitudinal sound velocities (V_S and V_P). Fitting the compression data of smithsonite to the third-order Birch-Murnaghan equation of state gives a bulk modulus of 124.17 GPa, which reflects an important rigidity compared to the other carbonates. The analysis of the band structure reveals a band-gap energy of 3.36 eV that is close enough to some semiconductors rather than insulators. Finally the chemical bonding was analyzed through the electronic charge density of the total contributions of the valence bands. A pronounced charge transfer was observed towards the carbonate ion, indicating thereby the ionic character of $ZnCO_3$.

3.2 Introduction

Carbonates belong to the most abundant Earth materials after silicates and play an important role in the Earth's carbon cycle [1, 2]. They have for a long time been considered as important means of carbon sequestration in deep Earth. Those carbonates contain about 60% of the world's oil reserves and previous studies have shown that carbonates rocks are potential geological reservoir for CO_2 storage. Besides their natural role, they could be used in many industries such as steel construction mainly in roofing and gutters, oil particularly oil drilling field or pharmaceutical industries.

Moreover, the content of carbon in the exosphere is small compared to the total amount of carbon that our planet might contain and this implies that most of carbon might be present in the Earth's mantle. $ZnCO_3$ is one of the carbon bearing phase within the interior of the Earth. However, the knowledge on this zinc carbonate remains still very weak or almost unknown so far despite the possible interesting properties that could be hidden in such mineral and the various possible applications equivalent to those of other carbonates, which could be likely different in other situations under normal conditions or under pressure. It is the purpose of the present study to shed light on the overall ground state properties of smithsonite in order to subsequently account for all intrinsic properties of the system what can be eventually linked to possible applications related to CO_2 storage as well as industrial applications.

Zinc carbonate ($ZnCO_3$) belongs to the calcite group and crystallizes in the trigonal system (rhombohedral carbonate) in normal conditions of temperature and pressure having *R*-3c space group. This mineral is isomorphic with calcite ($CaCO_3$) and dolomite ($MgCO_3$)[1, 2]. Only few experimental studies of smithsonite have been reported in literature. Graf [3] has defined the structure and calculated its dimensions. Zhang and Reeder [2] have performed experimentally the dimensions of smithsonite structure and they have also determined the bulk modulus. Apart from smithsonite, there are numerous theoretical studies of other, more common carbonates such as calcite or dolomite[1, 4].

In this paper, we aim to investigate the overall ground state properties of smithsonite including mechanical quantities, band structure, and bonding. For this purpose density functional theory (DFT) was applied using the pseudopotential method and several DFT functionals. The rest of the paper is organized as follows. In Sec. II we briefly describe the

computational details. In Sec. III, we present the obtained results and discussions. Sec. IV is the conclusion.

3.3 Computational details

The total energy calculations have been performed here by means of the projector-augmented wave (PAW) [5] potential method to solve the Kohn–Sham equations, as implemented in the Vienna *ab initio* simulation package (VASP) [6, 7]. The exchange and correlation function is treated within density functional theory (DFT) by using the local density approximation (LDA)[8] and the generalized gradient approximation (GGA). Among the available GGA functionals[9], we selected two frequently used and popular standard functionals PW91 [10] and PBE [9], respectively. Additionally, two other functionals, PBEsol [11] and AM05 [12], were used as well. These functionals were developed specially for calculations on solids and solid surfaces.

We have optimized the kinetic energy cut-off and the k-points mesh by carrying out self-consistent calculations and testing the unit cell parameters. An energy cutoff of 600 eV was found to be enough for the convergence with an accuracy of less than 10^{-5} eV/atom. A well converged mesh of 3 × 3 × 1 k-points grid of 30 atoms in hexagonal cell was used within the Monkhorst–Pack method [13] to take the reciprocal space integration of Brillouin zone. The geometry relaxation of atomic positions and the volume shape optimization were performed using a conjugate-gradient algorithm with a stopping criterion of 10^{-5} eV for the total energy and of 0.01 eV/Å for the root-mean-squared (rms) residual forces acting on each atom.

3.4 Results and discussions

3.4.1 Structural properties

The initial structure of smithsonite for the structural relaxation was taken from the experimental data derived by Graf [3]. The structure was completely relaxed (including cell parameters) for each DFT functional. Bulk modulus and its pressure derivative of $ZnCO_3$ have been deduced by fitting the data of total energy to a third order Birch–Murnaghan equation of states (BM EoS), where the total energy is a function of the volume [14, 15]:

$$E(V) = E_0 + \frac{9V_0B_0}{16}\left\{\left[\left(\frac{V_0}{V}\right)^{\frac{2}{3}} - 1\right]^3 B_0^{'} + \left[\left(\frac{V0}{V}\right)^{\frac{2}{3}} - 1\right]^2 \left[6 - 4\left(\frac{V0}{V}\right)^{\frac{2}{3}}\right]\right\} \quad (3.1)$$

E_0 is the total energy, V_0 is the equilibrium volume, B_0 is the bulk modulus at zero pressure, and B_0' is the first derivative of the bulk modulus with respect to pressure. To obtain B_0 and B_0' from the Birch–Murnaghan equation of states (BM EoS) , several isostatically compressed structures were relaxed. Elastic constants were computed from the stress-strain relation as implemented in the VASP code.

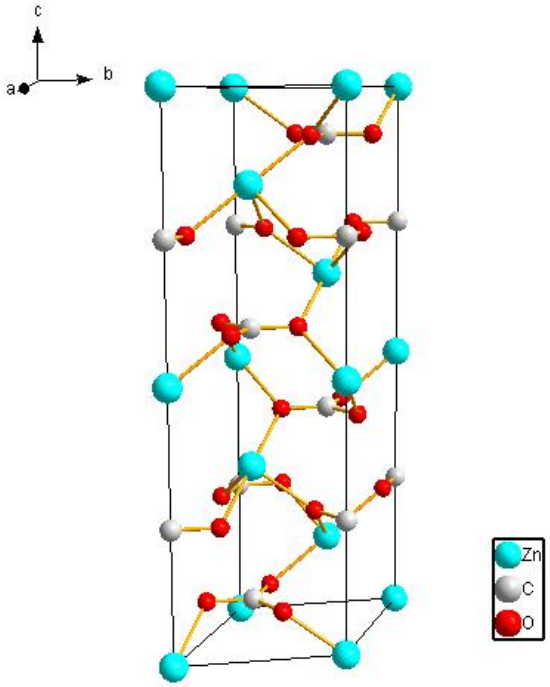

Fig. 3.1: Optimized structure of $ZnCO_3$.

The corresponding optimized cell parameters, unit cell volume, and distances between atoms in the smithsonite structure computed with various functionals are reported in Table 3.1. The $ZnCO_3$ relaxed structure, with PBEsol functional, is displayed in Fig. 3.1. The obtained results are favorably compared to the available experimental data [2, 3]. Very good agreement (within ~1% deviation) between experimental and calculated lattice parameters is noticed for the three functionals: AM05, PBEsol, and PW91. In case of the PBE functional, a certain overestimation (~0.2 Å) is observed, specifically for the *c* vector. All calculated bond distances show an excellent agreement with the experimental values (again with a small overestimation by PBE functional).

	Experimental		This work				
	exp 1	**exp2**	**LDA**	**PW91**	**PBE**	**AM05**	**PBEsol**
volume (Å ^{3})	283.27	281.69	290.64	281.69	293.64	282.42	285.79
a (Å)	4.66	4.65	4.71	4.68	4.72	4.67	4.67
c (Å)	15.08	15.03	15.15	14.88	15.22	14.96	15.06
d(Zn-O) (Å)	2.12	2.11	2.13	2.11	2.14	2.11	2.12
d(Zn..C) (Å)	2.97	2.96	3.00	2.97	3.01	2.97	2.98
d(Zn..Zn) (Å)	3.68	3.67	3.71	3.67	3.72	3.67	3.69
d(C-O) (Å)	1.29	1.29	1.30	1.29	1.30	1.29	1.30
d(C..C) (Å)	3.68	3.67	3.71	3.67	3.72	3.67	3.69

Exp1: J. Zhang and R. J. Reeder, American Mineralogist, Volume 84, pages 861–870 (1999).
Exp 2: D. L. Graf, American Mineralogist. 46. (1961)

Table 3.1: Calculated structural parameters of Smithsonite compared with available experimental Data.

Further, we evaluated structural changes as a function of the pressure. Fig. 3.2 and Fig. 3.3 show the evolution of lattice vector of smithsonite structure according to the pressure. We note that both lattice vectors (a and c) grow proportionally with the applied pressure.

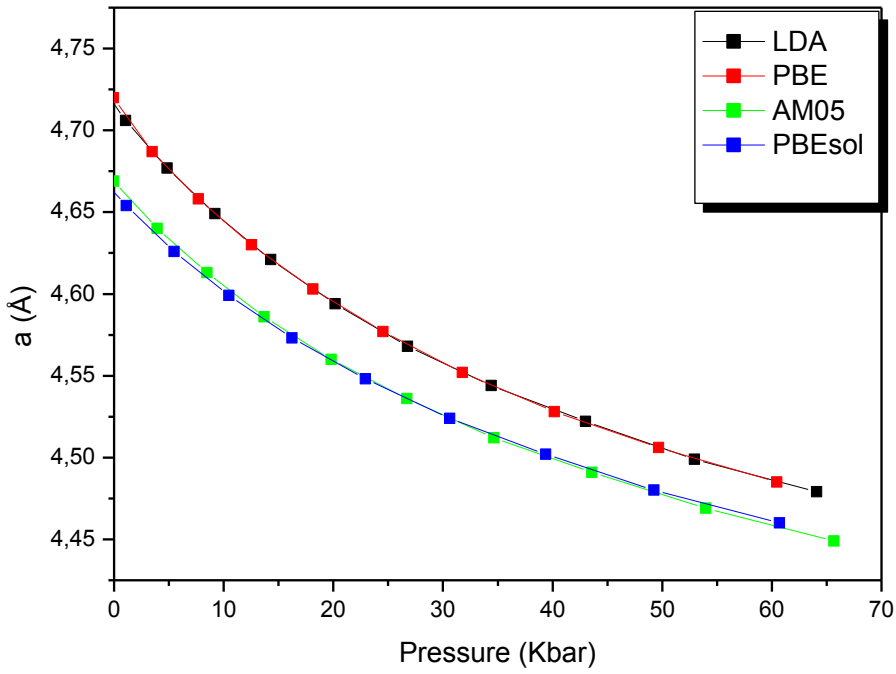

Fig. 3.2: Lattice parameter a of Smithsonite as function of pressure.

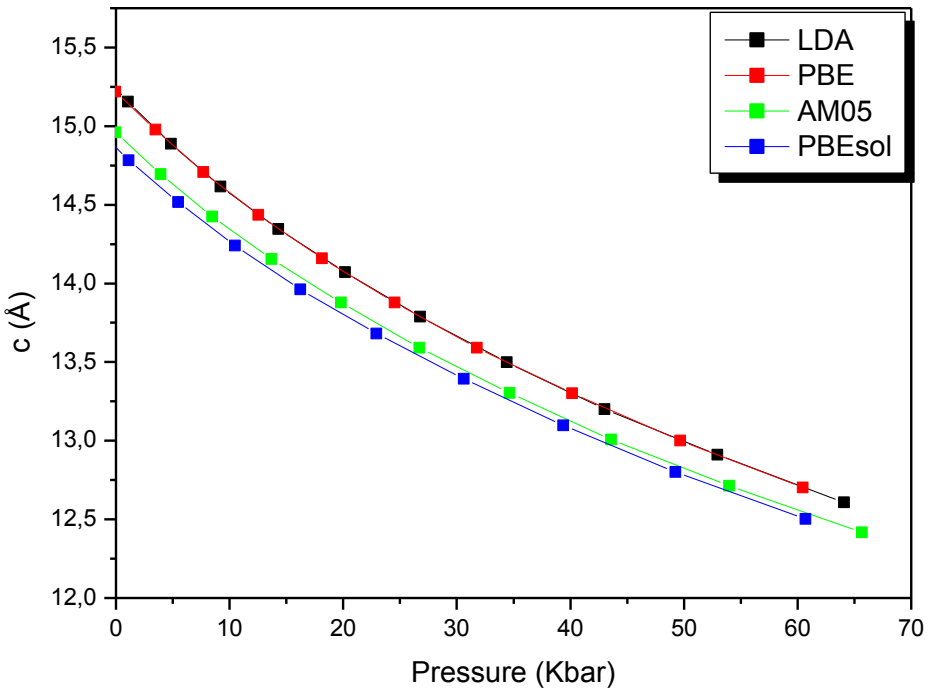

Fig. 3.3: Structural parameter c of Smithsonite as function of pressure.

3.4.2 Mechanical properties

As mentioned above the calculated structural parameters were fitted to the Birch-Murnaghan equation of state (BM EoS) [14] to obtain the bulk modulus of $ZnCO_3$ (Table 3.2). We found a bulk modulus value of 124.19 GPa with a pressure derivative of 3.99. A very good agreement is noticed between the obtained bulk modulus and the experimental one (B= 124 GPa [2]).

	Smithsonite						**Calcite**
	Experimental	**This work**					
C_{ij} (GPa)	**Exp**	**LDA**	**PW91**	**PBE**	**AM05**	**PBESol**	
C_{11}		230.45	227.84	223.02	243.51	233.48	152.3[b]
C_{22}		228.22	219.06	222.49	240.24	228.74	
C_{33}		131.91	115.62	126.96	145.36	129.58	87.77[b]
C_{44}		62.13	61.87	60.62	69.34	63.99	36.00[b]
C_{55}		40.40	38.39	36.50	41.31	33.61	
C_{66}		38.39	37.87	35.90	41.62	37.77	
C_{12}		104.86	99.47	103.12	103.75	102.68	57.05[b]
C_{13}		67.45	57.99	63.32	71.13	62.90	54.83[b]
C_{23}		65.40	53.55	61.97	68.58	60.00	
B	124[a]	115[c] 119.14[d]	114.6[c] 111.35[d]	114.04[c] 114.72[d]	124.19[c] 124.93[d]	128.29[c] 117.05[d]	80.64[b] 75.27[b]
B'		3.98	4	4.03	3.99	4.07	3.73[b]
A		0.99	0.96	1.01	0.99	0.98	38.96[b]
G		52.33	53.76	51.40	44.39	54.01	
E		136.32	139.48	134.07	118.98	142.08	100.68[e]
ν		0.30	0.30	0.30	0.34	0.32	0.26[e]
Vs		3.44	3.48	3.41	3.17	3.49	3.91[b]
Vp		6.46	6.48	6.42	6.43	6.72	7.1[b]

[a] *Zhang and Reeder, American Mineralogist 84. 861–870 (1999).*
[b] *Ayoub, Zaoui, Berghout. Computational Materials Science 50. 852–857(2011).*
[c] *This work according to the Birch–Murnaghan equation of state.*
[d] *This work according to Voigt formula*
[e] *Calculated from the data of Ayoub, Zaoui, Berghout. Computational Materials Science 50. 852–857(2011).*

Table3.2: Calculated elastic constants, Zener anisotropy factor (A), Poisson's ratio (v), Young modulus (E), and isotropic shear modulus (G) of Smithsonite and the comparison with calcite's mechanical properties.

The second-order elastic constants calculated from the stress-strain relation of all considered functionals are presented in Table 3.2.

The comparison between C_{11}, C_{22}, and C_{33} constants show the anisotropic character of the smithsonite structure with a weaker hardness in the *c* direction. We have evaluated the anisotropy of smithsonite from the anisotropy Zener factor *A*, according to the following relation :

$$A = \frac{2C_{44}}{C_{11} - C_{12}} \qquad (3.2)$$

The Zener anisotropy factor *A* is a measure of the degree of elastic anisotropy in solids. The *A* takes the value of 1 for a fully isotropic material. If the value of *A* is smaller or greater than 1, it will show the degree of elastic anisotropy. The calculated Zener anisotropy factors for $ZnCO_3$ are lower than 1 (Table 3.2), which indicates that these compounds are anisotropic materials.

From the volume compression, we have also calculated a dependence of the elastic constants as a function of the pressure variation from 0 to 60 GPa. Fig. 3.4–a shows that the variation curve of C_{11} and C_{22} is considerably higher than C_{33}, what means that the structure is more compressible along the direction perpendicular to the layers parallel to (0 0 1) plane. Fig. 3.4-b shows that the static elastic constant of C_{12} is greater than C_{13} and C_{23}, which reflects that $ZnCO_3$ structure can be more resistant to the torsion along the (1 0 0) plane. From Fig. 3.4-c, we may notice that the C_{44} variation is higher than C_{55} and C_{66}, what clearly indicates that the structure is more resistant to the shear constraint along the (1 0 0) direction.

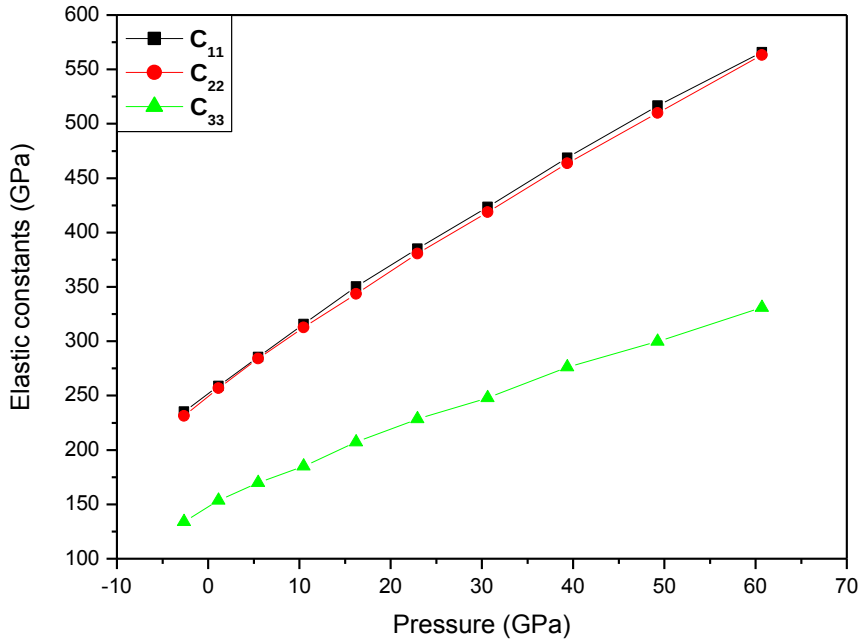

(a)

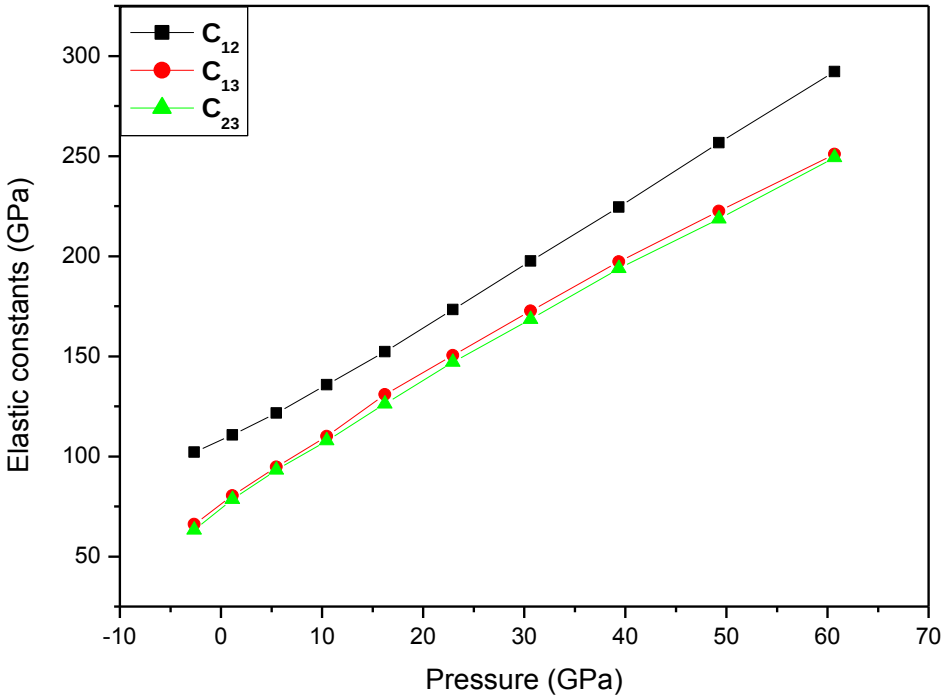

(b)

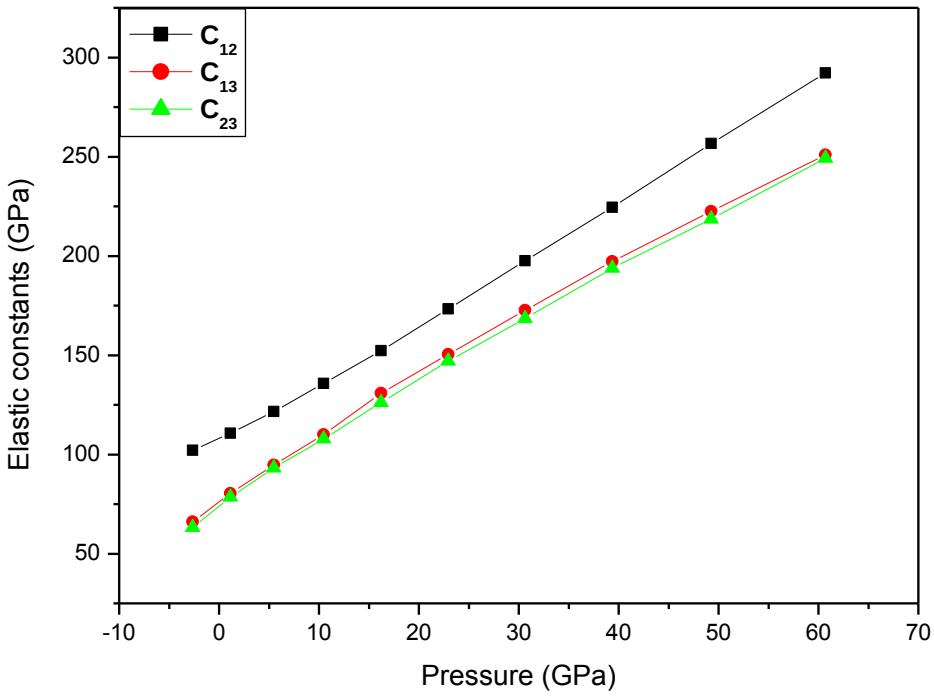

(c)

Fig. 3.4: Elastic constants C_{11}. C_{22} and C_{33} (a); C_{44}. C_{55} and C_{66} (b); and C_{12} . C_{13} and C_{23} (c) vs pressure for $ZnCO_3$.

From the elastic constants, we can deduce further mechanical properties of smithsonite. In particular, the most important elastic moduli reflecting rigidity and hardness of the system, bulk (B) and shear (G) modulus, formally derived from elastic constants by the Voigt and Reuss formula[16]. These quantities show the response of the system to various kinds of deformation. Bulk and shear modulus can be derived from elastic constants values according to the following Voigt relation:

$$B = \frac{1}{9}\left[2\left(C_{11}+C_{12}\right)+4C_{13}+C_{33}\right] \tag{3.3}$$

Similarly, the shear modulus is given as:

$$G = \frac{1}{5}\left(G_{eff}^{v}+2C_{44}+2C_{66}\right) \tag{3.4}$$

Where,

$$G_{eff}^{v} = \frac{1}{3}\left(C_{11}+C_{33}-2C_{13}-C_{66}\right) \tag{3.5}$$

The resulting bulk and shear moduli of smithsonite are listed in Table 3.2 and compared to that of calcite ($CaCO_3$) in Table 3.2.

We can notice that the value of bulk and shear moduli of $ZnCO_3$ are clearly higher than those of $CaCO_3$. Smithsonite rock is then definitely more resistant to the compressibility and shear than calcite.

The knowledge of Young modulus, E, and Poisson ratio, ν, are very important properties for industrial applications. The Young modulus, E, is the ratio of the tensile stress to the corresponding tensile strain, which is required to provide information about the measure of the stiffness of the solids. The lower limit and upper limit of Poisson ratio, ν, correspond to 0.25 and 0.5 for central forces in solids, respectively [17]. Besides, this quantity is small for covalent materials (ν = 0.1) and increases essentially for ionic materials [18]. We have calculated the Poisson ratio (ν), and Young modulus (E) according to the following relations [19, 20]:

$$\nu = \frac{1}{2}\left[\frac{\left(B-(2/3)G\right)}{\left(B+(1/3)G\right)}\right] \tag{3.6}$$

And,

$$E = \frac{9GB}{G+3B} \tag{3.7}$$

The obtained Poisson ratio ν and Young modulus E of smithsonite are presented in Table 3.2. Calculated Poisson's ratio value is equal to 0.34 which shows that the interatomic forces in the $ZnCO_3$ are predominantly central forces. The present Young modulus value of smithsonite (E=118.98 GPa) is higher than the calcite one (E=110.68 GPa) , which implies that $ZnCO_3$ is stiffer than $CaCO_3$.

The acoustic velocities can be a real key in the interpretation of seismic data. The polycrystalline averages of these acoustic velocities in a solid can be derived from the bulk and shear modulus of the material, as well as the density (ρ). Two types of acoustic velocities are present, longitudinal (V_p) and transversal (V_s) wave velocities, which can be given as:

$$V_S = \sqrt{\frac{G}{\rho}}, \tag{3.8}$$

$$V_P = \sqrt{\frac{4G+3B}{3\rho}} \tag{3.9}$$

The obtained acoustic velocities values of smithsonite are given in Table 3.2. Fig. 3.5 shows the variation of elastic wave velocities with respect to the pressure. We note an increasing of the wave velocity with pressure, which means that under pressure the system became more rigid. This increasing is more pronounced for longitudinal wave velocity than transversal one.

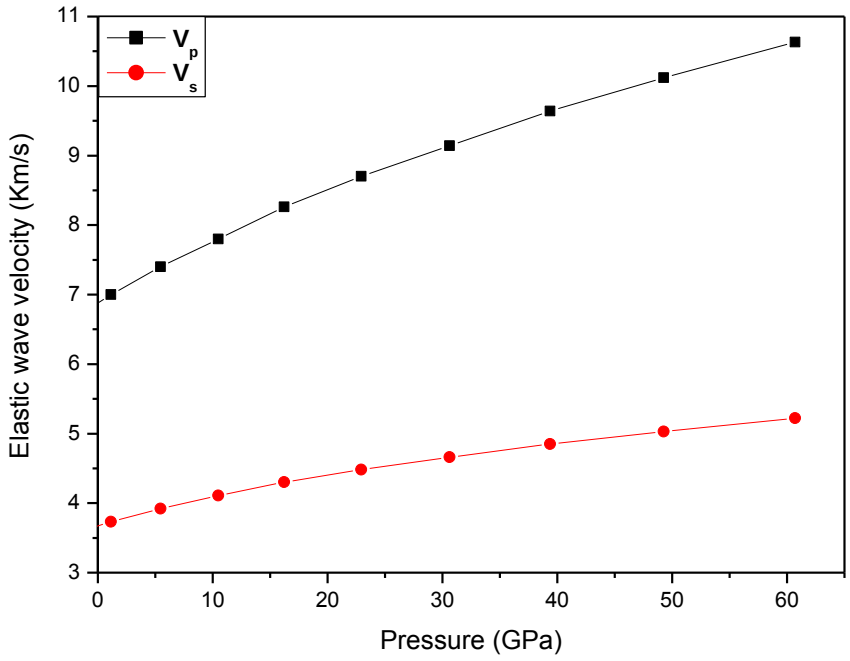

Fig. 3.5: Variation of transversal V_s and longitudinal V_P wave velocities with pressure.

3.4.3 Electronic and bonding properties

Fig. 3.6 shows the density of states (DOS) of zinc. One main valence region can be identified: concerning the two very small peaks the contribution is rather insignificant, we can say that the first and single peak lies between -10.84 eV and 0.00 eV. It is a large region where we remark several peaks coming essentially from d orbital. The conduction bands originate mainly from s orbital and p orbital.

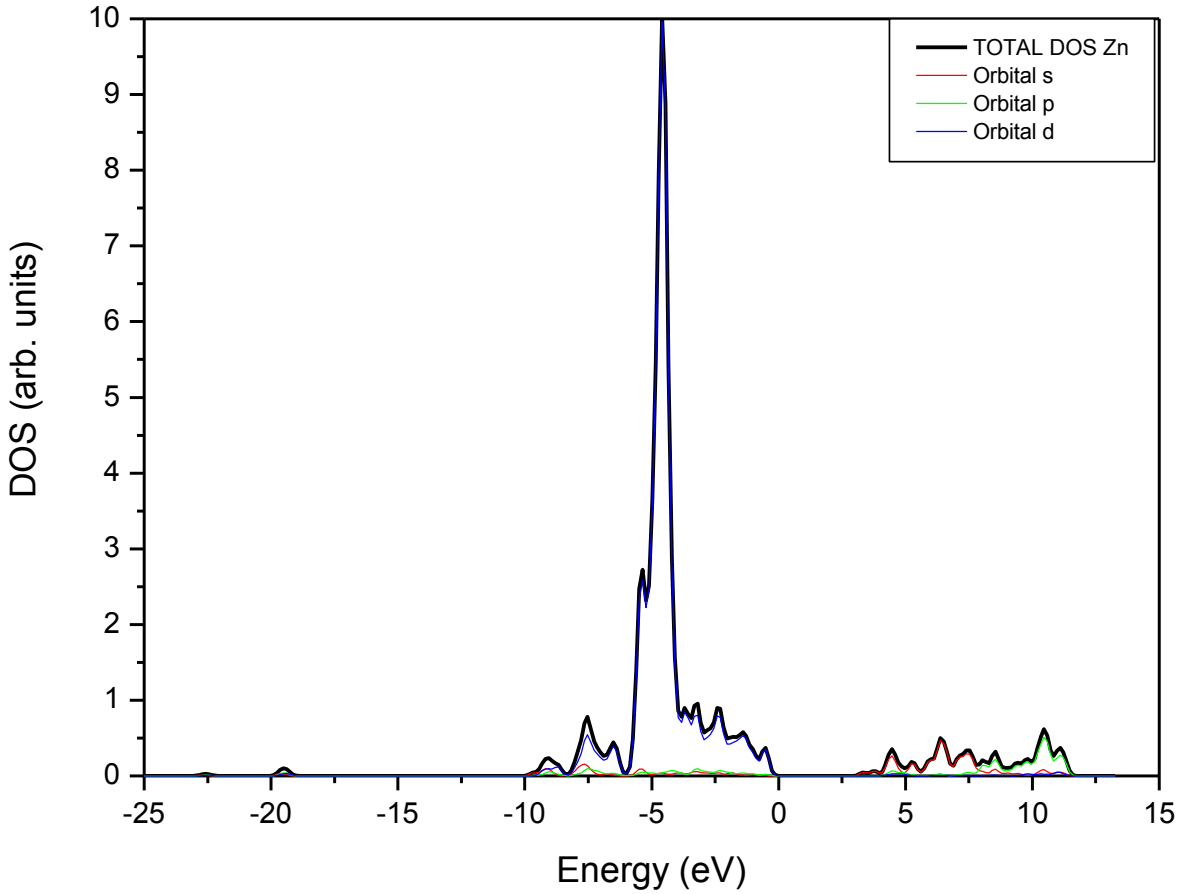

Fig. 3.6: DOS of Zn atom with orbital contributions.

The partial DOS of carbone is presented in Fig. 3.7. The latter shows that the valence band of C atom consists of three regions. The first one is a peak situated between -23.98 eV and -21.05 eV, the main one comes from s orbital. The second peak lies between -20.66 eV and -17.98 eV, which comes principally from p orbital. The third region lies between -10.71 eV and 0.0 eV, where we notice a contribution of both orbitals s and p. The conduction bands originate from p orbital, with low contribution of s orbital between 8.02 eV and 11.86 eV.

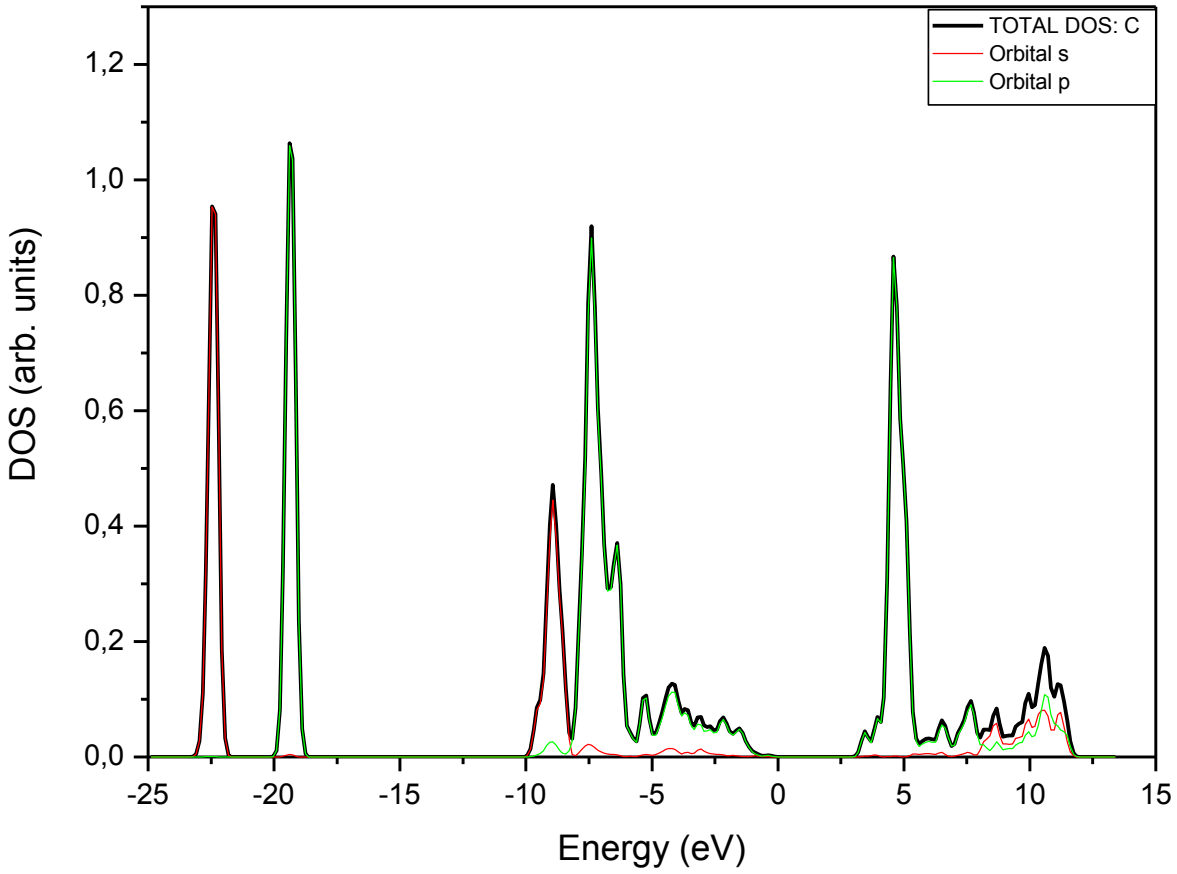

Fig. 3.7: DOS of C atom with orbital contributions.

Fig. 3.8 shows the partial DOS of oxygen. We may remark that the first two peaks come mainly from the s orbital contribution. The fist one lies between -24.11 eV and -21.17 eV, the second one is between -20.79 eV and -18.11 eV. After a gap of 7.27 eV the third valence region appears, it lies between -10.84 eV and 0.00 eV. We notice here many peaks originate from the p orbital. The conduction band is located between 2.93 eV and 11.99 eV and originates essentially from the p contribution.

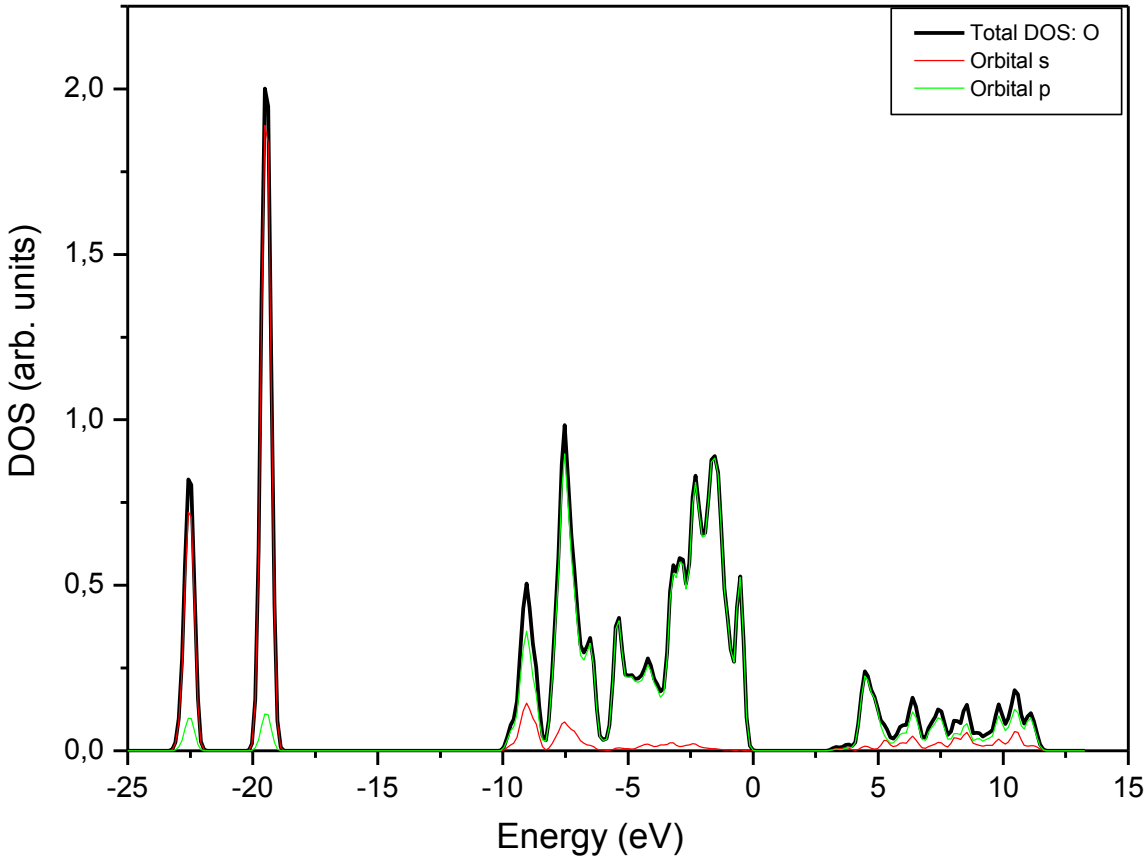

Fig. 3.8: DOS of O atom with orbital contributions.

Fig. 3.9 shows the atomic contribution of each constituent atom as well as the total DOS. We can observe the main atomic contribution that comes from zinc and oxygen. Indeed, we can remark three peaks regions from valence band. The first one is located between -24.11 eV and -21.17 eV; C and O atoms contribute together to this peak. The second peak originates essentially from oxygen atom with contribution of carbone atom and very low contribution of zinc.It lies between -21.79 eV and -18.11 eV. As for the case of the third valence region we may remark a dominant contribution of the zinc atom, with contribution of oxygen atom, the carbone atom contributes from -10.84 eV to -6.01eV and very lowely for the rest of the third region. Conduction band is constituted by contribution of all atoms. Between 3.36 eV and

5.22 eV we can remark that the carbon atom contributes mainly than other atoms. The rest of the region we can remark the greater contribution of zinc atom..

The main electronic band gap corresponds to 3.36 eV. We can underline here that the band gap of smithsonite is much closer to some semiconductors such as ZnO (Eg =3.2 eV [21]) than carbonates, such as $CaCO_3$ (Table 3.4), which are rather considered as insulators [22].

	$ZnCO_3$ (PBESol)
q(Zn) (lel)	1.49
q(CO_3) (lel)	-1.4

Table 3.3: Bader atomic charges of Smithsonite.

Band-gap of Structures / Functionals	Δ_g **($ZnCO_3$)**	Δ_g **($CaCO_3$)**	Δ_g **(ZnO)**
LDA	3.31	4.95[a]	
PW91	3.48		
PBE	3.47	5.07[a]	0.74[c]
PBESol	3.43		
AM05	3.36		
PBE0			3.18[c]
Experiment		6.00[b]	3.44[c]

[a] *Medeiros et al., J. Phys. D: Appl. Phys. 40. 5747–5752 (2007).*
[b] *Baer and Blanchard Appl. Surf. Sci (1993).*
[c] *Oba. Togo and Tanaka. Physical Review B 77. 245202 (2008).*

Table3.4: Band-gap (Δ_g) of Smithsonite calculated from several functionnals and compared with those of other carbonates.

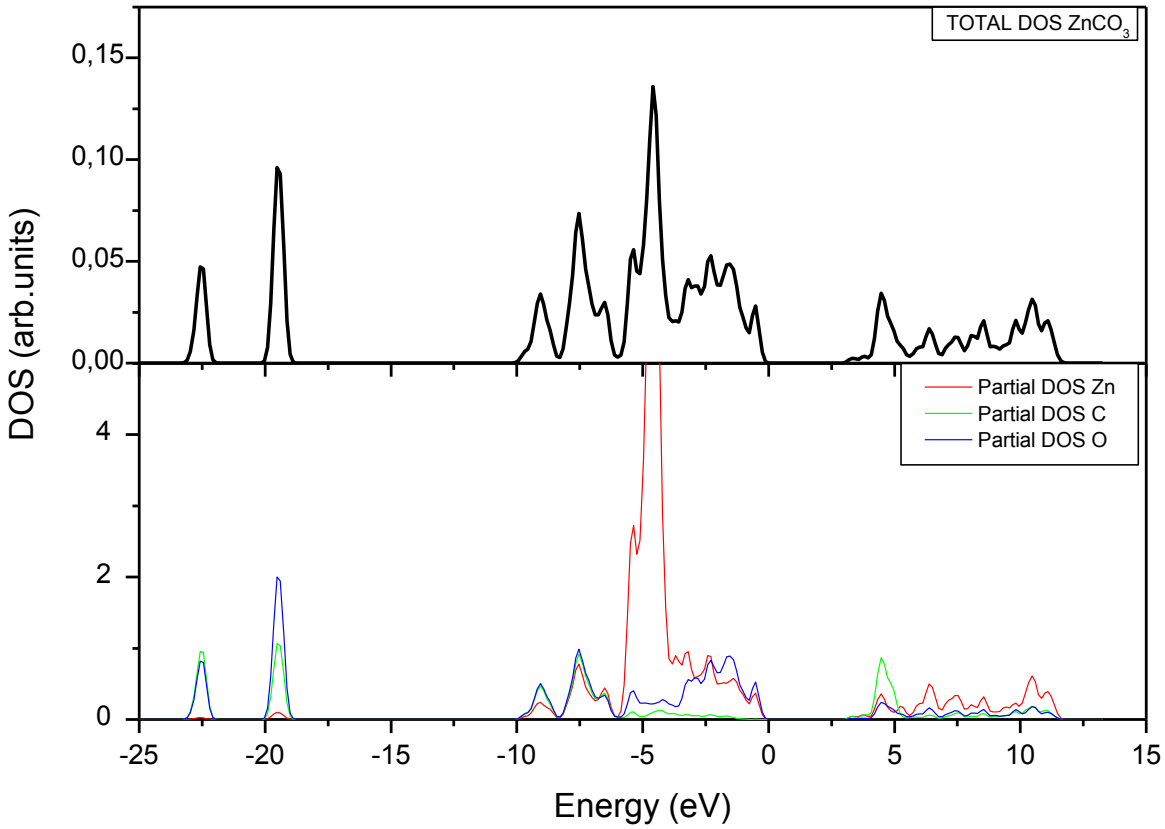

Fig. 3.9: Total DOS of $ZnCO_3$ with orbital contributions.

Finally, Fig. 3.10 shows the electronic charge density in the plane (1/2 0 2), which crosses a maximum of three kinds of atoms in $ZnCO_3$. In this plane we see the important ionic character of this mineral. The charge distribution is more clear in Fig. 3.11 where we notice a maximum of charge transfer between zinc and oxygen also between oxygen and carbon.. This charge transfer reflects a strong ionic bonding in the lattice structure of smithsonite, confirming thereby a well marked ionicity factor.

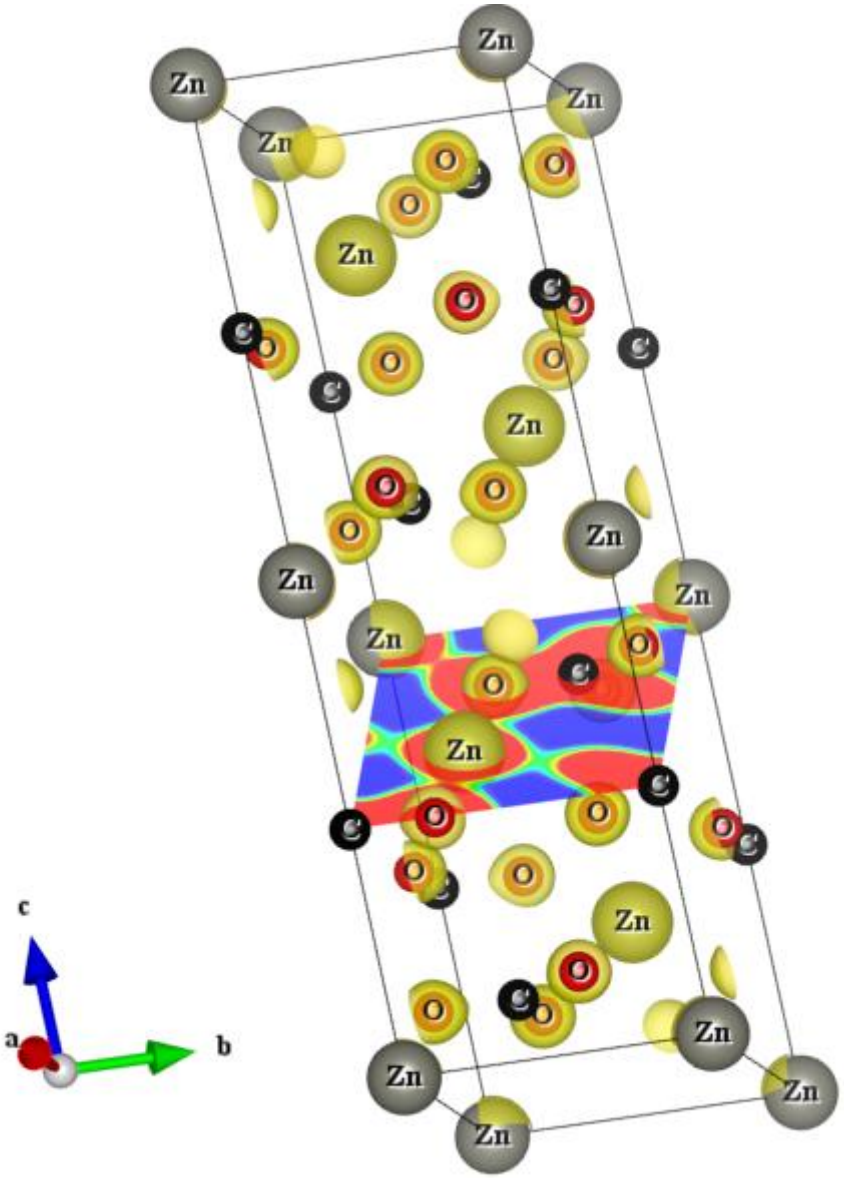

Fig. 3.10: Valence charge density of $ZnCO_3$.

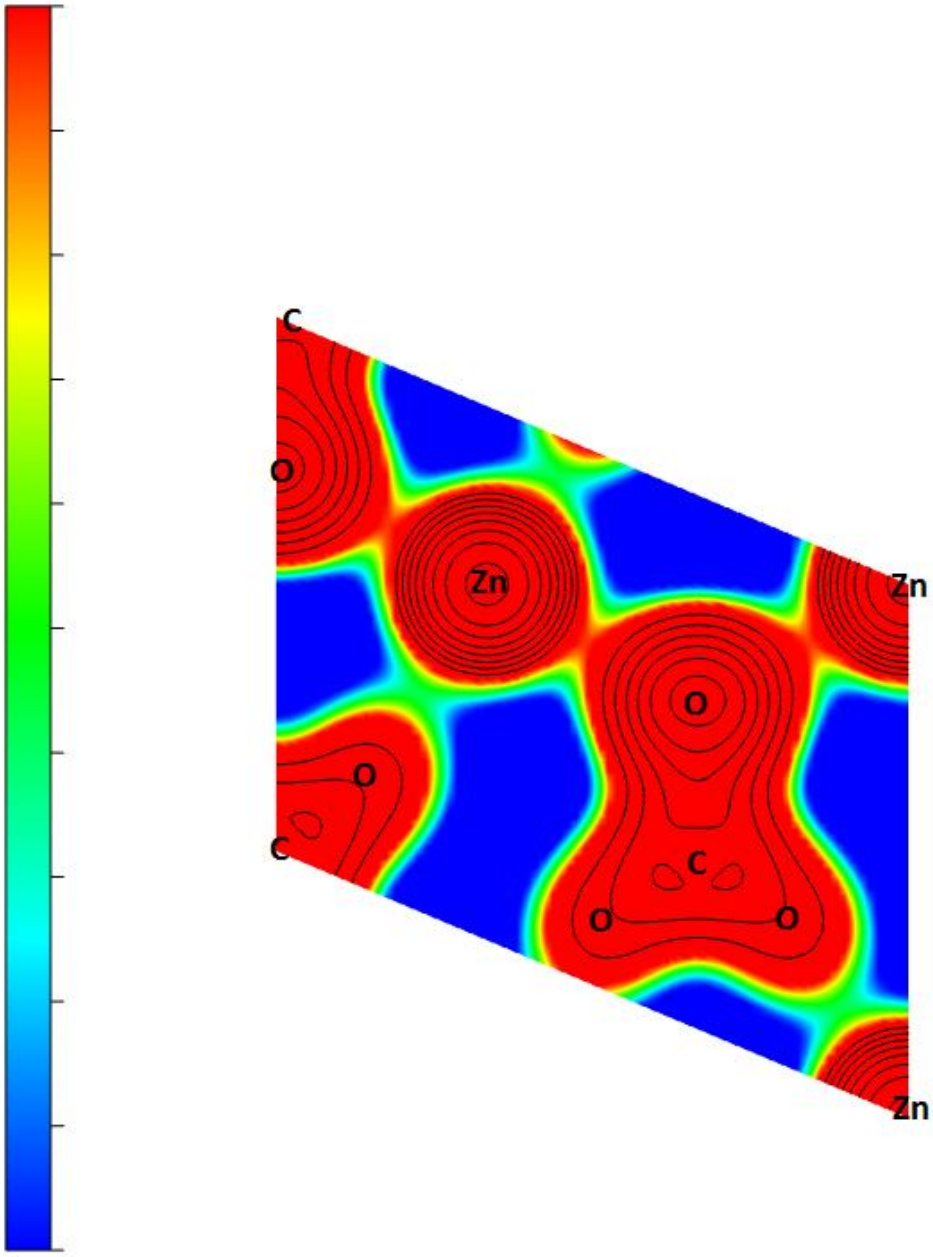

Fig. 3.11: Valence density of $ZnCO_3$ along the (1 0 1) plane.

3.5 Conclusion

In conclusion, we have performed first-principles calculations in order to study the ground state properties of smithsonite rock. Good agreement was noticed between our obtained values of structural and mechanical properties and available experimental data. The analysis of the band structure and charge density gives a band-gap closer to semiconductors and reveals an important ionic character in the charge transfer of this rock system.

References

[1] Bakri Z., and Zaoui A., Structural and mechanical properties of dolomite rock under high pressure conditions: A first-principles study. *Physica status solidi (b)* **248** : 1894 (2011).

[2] Zhang J., and Reeder R.J., Comparative compressibilities of calcite-structure carbonates: Deviations from empirical relations. *American Mineralogist* **84:** 861 (1999).

[3] Graf D., Crystallographic tables for the rhombohedral carbonates. *American Mineralogist,* **46:** 1283 (1961).

[4] Ayoub A., Zaoui A., and Berghout A., High-pressure structural phase transitions and mechanical properties of calcite rock. *Computational Materials Science*, **50** 852 (2011).

[5] Blöchl P.E., Projector augmented-wave method. *Physical Review B* **50** 17953 (1994).

[6] Kresse G., and Hafner J., Ab initio molecular dynamics for liquid metals. *Physical Review B* **47:** 558 (1993).

[7] Kresse, G., and J. Hafner. Norm-conserving and ultrasoft pseudopotentials for first-row and transition elements. *Journal of Physics: Condensed Matter* **6** : 8245 (1994).

[8] Kohn W., and Sham L.J., Self-consistent equations including exchange and correlation effects. *Phys. Rev* **140** : A1133 (1965).

[9] Perdew J.P., Burke K., and Ernzerhof M., Generalized gradient approximation made simple. *Physical review letters* **77:** 3865 (1996).

[10] Perdew, John P., and Yue Wang. Accurate and simple analytic representation of the electron-gas correlation energy. *Physical Review B* **45**.23: 13244 (1992).

[11] Perdew J.P., et al., Restoring the density-gradient expansion for exchange in solids and surfaces. *Physical Review Letters* **100:** 136406 (2008).

[12] Mattsson A.E., , et al., The AM05 density functional applied to solids. *The Journal of chemical physics* **128**: 084714(2008).

[13] Monkhorst H.J., and Pack J.D., Special points for Brillouin-zone integrations. *Physical Review B* **13** 5188 (1976).

[14] Birch F., Finite elastic strain of cubic crystals. *Physical Review* **71:** 809 (1947).

[15] Birch F., Finite strain isotherm and velocities for single-crystal and polycrystalline NaCl at high pressures and 300° K. *Journal of Geophysical Research* **83:** 1257 (1978).

[16] Le Page Y., Saxe P., and Rodgers J., Ab initio stiffness for low quartz and calcite. *Physica status solidi (b),* **229** : 1155 (2002).

[17] Fu H., et al., Ab initio calculations of elastic constants and thermodynamic properties of NiAl under high pressures. *Computational Materials Science,* **44** :774 (2008).

[18] Haines J., Leger J., and Bocquillon G., Synthesis and design of superhard materials. *Annual review of materials research* **31** : 1(2001).

[19] Zener C., Elasticity and anelasticity of metals. University of Chicago press (1948).

[20] Mayer B., et al., Ab-initio calculation of the elastic constants and thermal expansion coefficients of Laves phases. *Intermetallics* **11** : 23 (2003).

[21] Oba F., et al. Defect energetics in ZnO: A hybrid Hartree-Fock density functional study . *Physical Review B* **77 :** 245202 (2008).

[22] Medeiros, S., et al., Electronic and optical properties of $CaCO_3$ calcite, and excitons in Si@ $CaCO_3$ and $CaCO_3$@ SiO_2 core-shell quantum dots. J*ournal of Physics D: Applied Physics* **40** : 5747 (2007).

Chapter 4:

High-pressure polymorphs of $ZnCO_3$: Evolutionary crystal structure prediction

4.1 Abstract

The high-pressure behavior of zinc carbonate $ZnCO_3$ has been investigated using universal structure prediction method together with the density functional theory. In order to explore all possible structures under pressure, separate calculations at high pressure are done here with increasing number of formula units in the unit cell. Two pressures induced phase transitions were considered. The first one occurs at 78 GPa and the second one at 121 GPa. The most stable $ZnCO_3$ at ambient condition corresponds to the space group R-3c (phase I), which is in favorable agreement with experiment. The structure with C2/m space group (phase II) becomes stable between 78 GPa and 121 GPa. Finally, the structure with the space group $P2_12_12_1$ (phase III) becomes the most stable when the pressure achieves 121GPa. Some mechanical properties of R-3c structure were –additionally- calculated and compared with the experimental and previous theoretical data. The resulting behaviors support our findings and confirm the obtained phase transition. Besides, from the analysis of the electronic charge density it comes that at 78 GPa, new bond between oxygen and zinc is formed, what is likely the main cause behind the phase transition.

4.2 Introduction

High-pressure polymorphs of carbon-bearing minerals are important to understand the circulation of carbon in the Earth's interior. Carbonates have been, for a long time, considered as important reservoirs of carbon in deep Earth. High-pressure phases of carbonates are probably among the host minerals for carbon that are present deeply in the mantle. For these reasons, phase transitions and physical properties of high-pressure phases related to carbonates have been subject of intense investigations[1-5]. Interesting crystal chemical changes that occur in carbonates under pressure, such as increase of coordination numbers and polymerization of carbonate-ions, may result on new useful materials.

Previous theoretical and experimental studies have focus on common carbonates such as magnesite ($MgCO_3$)[6-9] and calcite ($CaCO_3$)[10-13]. For instance, it has been proved that the magnesite is stable at pressure up to 80 GPa[6] and the calcite up to 3.3 GPa[10]. Magnesite goes through two phases transition, from magnesite phase I to magnesite phase II; and from phase II to phase III at 82 and 138 GPa respectively as reported by Oganov et al.[7]. In another work of Oganov et al.[11], calcite was found to go through three phase transitions at pressures up to 150 GPa from calcite to aragonite at 4 GPa; from aragonite to post-aragonite at 42 GPa, and then to the $C222_1$ phase at 137 GPa[7].

$ZnCO_3$ is one of carbon-bearing phases known at the surface at the Earth. This mineral has the same structure type as calcite. However, the knowledge of this zinc carbonate at high pressure remains still very limited. Only few experimental studies of smithsonite have been reported in the literature [14,15]. Graf [14] has presented and defined the structure of $ZnCO_3$. Zhang and Reeder [15] performed experimentally the structural properties of smithsonite and they have also determined the bulk modulus. Recently, Bouibes et al.[16] determined the ground state properties of smithsonite including structural, mechanical, electronic and bonding properties. Even if there is no clear study indicating the direct importance of zinc carbonate on interior earth, this mineral belongs to group II of carbonates such as $MgCO_3$, $MnCO_3$, $FeCO_3$[17]. Group II contains the most solid minerals needing a high pressure to crystallize. Several studies were performed on $FeCO_3$ and $MgCO_3$ because of their importance for earth science at high pressure. On the other hand, further study shows that high CO_2 (g) partial pressure results in zinc carbonate being stable and potentially limit zinc mobility [18].

The main goal here is to shed light on the structural evolution of $ZnCO_3$ at high-pressure. To this end, high-pressure phase transitions will be investigated using the USPEX method/code [19,20]. This method has shown great success in numerous applications, including carbonates [19].

4.3 Computational details

In order to find the stable high-pressure structures of $ZnCO_3$, an *ab initio* evolutionary algorithm (EA), as implemented in the "Universal Structure Predictor: Evolutionary Xtallography" (USPEX) code, is employed [19-21]. In this work, the structure prediction runs for $ZnCO_3$ were performed at 10 GPa, 20 GPa, 40 GPa, 60 GPa, 90 GPa and 120 GPa, all at zero Kelvin. In these variable-cell simulations, we consider the system with 10, 15 and 20 atoms in the unit cell. The population size is fixed between 20 and 35 number of structures. The first generation is then created randomly. However, in the calculations including 20 atoms/cell, we fix the first generation from the known structures among the other carbonate systems such as calcite, aragonite, post-aragonite, and other structures obtained during the simulations. Magnesite II and magnesite III with 30 atoms in unit cell were added to the resulting structures.

The underlying *ab initio* structure relaxations and enthalpy calculations were carried out using a plane-wave method and the local density approximation (LDA) for the exchange-correlation [22], as implemented in the Vienna *Ab-initio* Simulation Package (VASP) [23,24]. In addition, in order to investigate the fundamental properties of Smithsonite calculations, the exchange and correlation function was treated by means of generalized gradient approximation (GGA). Among the available GGA functional [28], we selected AM05 [29] functional, which is particularly appropriate for calculating the properties of $ZnCO_3$ [16]. The electron-ion interaction was described by the all-electron projector augmented wave (PAW) scheme [30] and the electron configurations $4s^2$, $2s^22p^2$ and $2s^22p^4$ were treated as valence for Zn, C, and O, respectively. During structural relaxation an energy cutoff of 500 eV was used for the plane wave basis sets, and a k-point resolution of 0.08 $Å^{-1}$ in the reciprocal space was used for all structures in order to minimize the error from the k-point meshes. The atomic positions, lattice parameters, and cell volume were fully relaxed until the force on each atom is less than 1 meV/Å, and stresses deviate from the desired hydrostatic pressure by less than 1 GPa.

4.4 Results

In Fig.4.1, we display some $ZnCO_3$ structures with lowest enthalpy. The obtained lattice parameters as well as bulk modulus and its pressure derivative for the most stable structure (R-3c) are summarized in Table.4.1.

Three structures corresponding to the space groups R-3c, P-31c and P3, contain triangular $(CO_3)^{2-}$ ions, which are flat and coplanar. However, two structures with C2/m and $P2_1$ space group (30 atoms in the primitive cell), are characterized by a three-membered ring $(C_3O_9)^{6-}$ of corner-sharing carbonate tetrahedra. These latter structures were previously found as magnesium carbonate $MgCO_3$ stable structure [7]. The structure with C2/m space group corresponds to $MgCO_3$ structure that is stable between 82 GPa and 138 GPa and it is called magnesite phase II. In addition, the structure with $P2_1$ space group, called magnesite phase III, is the structure of $MgCO_3$ above 138 GPa. The structure with space group Pnma is composed of a serial pentaedra carbonate. All the remaining structures contain carbonates $(CO_4)^{4-}$ tetrahedra.

Lattice parameters

a (Å)= 5.71;
α(°)=48.92;
V ($Å^3$)= 97.21

Atomic coordinates (space group R-3c)

Atom	X	Y	Z
Zn	0.00	0.00	0.00
C	0.25	0.25	0.25
O	0.97	0.52	0.25

Bond length (Å):

Zn--O = 2.14
C--O= 1.29

Third-order Birch–Murnaghan equation of state (fitted between 0 and 150 GPa)

B_0 (GPa) = 126.45 (± 1.6)
B'_0 = 4.00 (±0)
V_0 ($Å^3$)= 98.11 (±0.23)

Table 4.1: Stable $ZnCO_3$ structure (Phase I) between 0 GPa and 78 GPa.

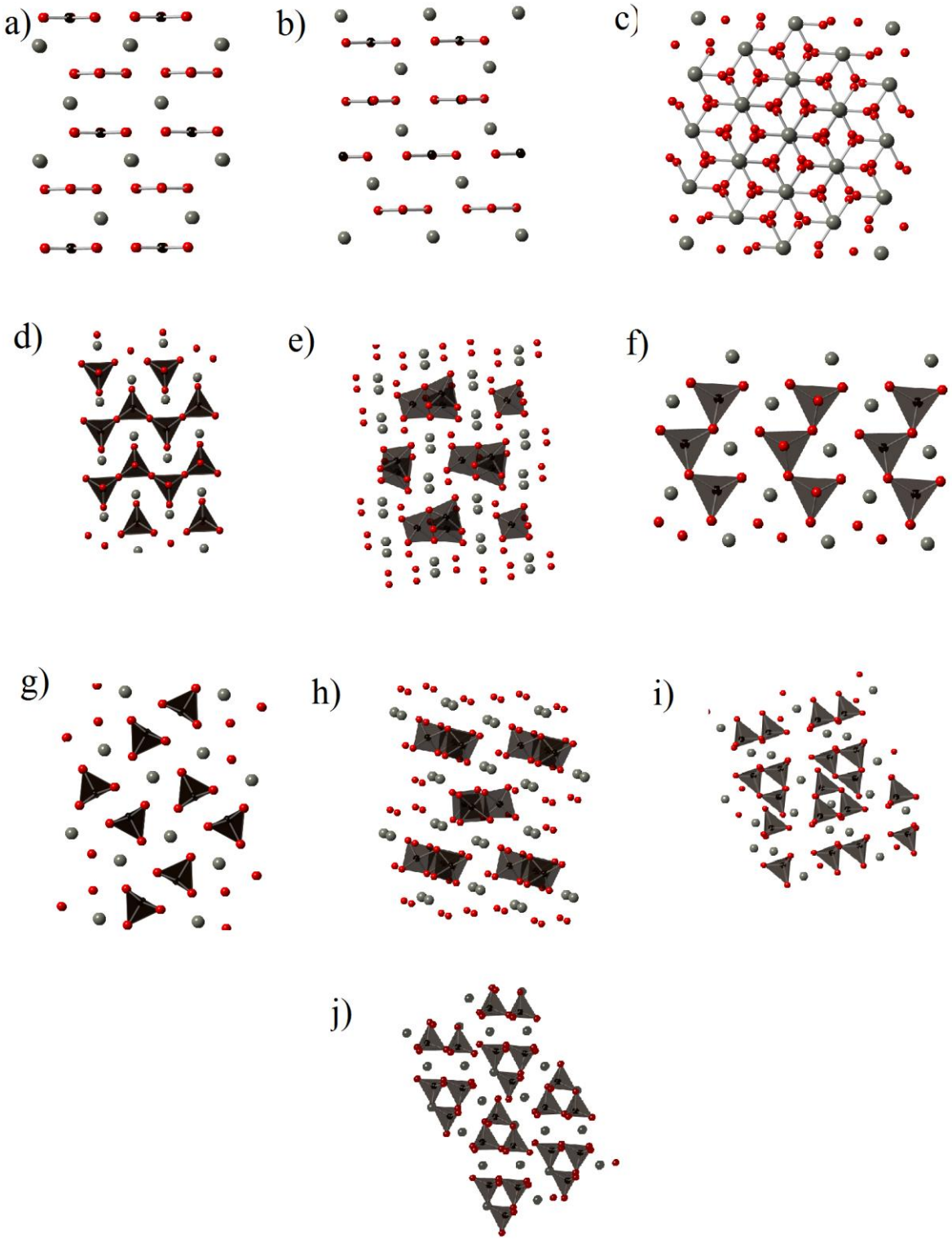

Fig. 4.1: Lowest-enthalpy structures for $ZnCO_3$: P-31C (a); P3 (b); R-3c (Phase I) (c); Pbcm (d); $P2_12_12_1$ (Phase III) (e); $Pca2_1$ (f); Pnma (g); $Pna2_1$ (h); C2/m (Phase II) (i); $P2_1$ (j).

Having determined the most promising structures, we optimized them with very strict computational conditions at pressures ranging from 0 GPa to 150 GPa. Fig.4.2 shows the enthalpy as a function of pressure. The most stable structure of $ZnCO_3$ at ambient conditions is the R-3c space group structure (calcite structure), which fits perfectly the experiment[15]. The first phase transition occurs at 78 GPa. Under increasing pressure, the second phase transition occurs at 121 GPa. Between 78 GPa and 121 GPa the most stable structure has a space group C2/m with 30 atoms in the primitive cell. This structure is detailed in Table.4.2. Above 121 GPa, the structure of $P2_12_12_1$ space group becomes more stable, as presented in Table.4.3.

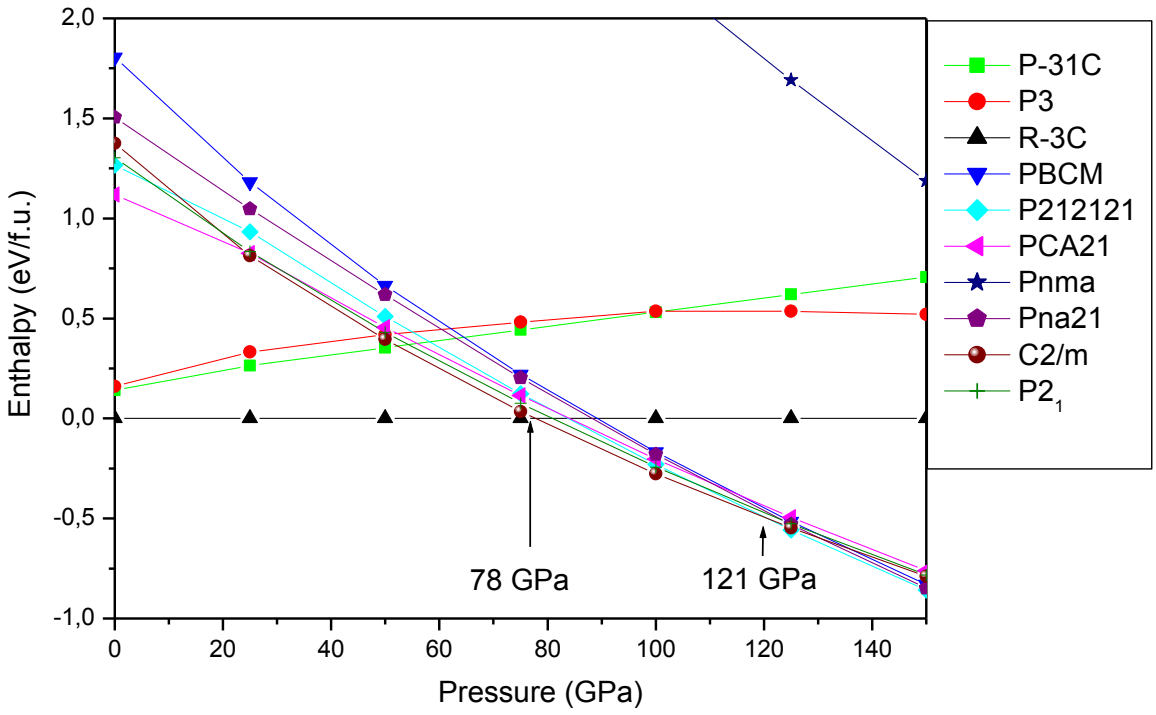

Fig. 4.2: Enthalpies of the best structures vs pressure at 78 GPa (C2/m: Phase II) and at 121 GPa ($P2_12_12_1$: Phase III).

Lattice parameters

a (Å)=9.27; b (Å)= 7.08; c (Å)= 8.17

β(°)=104.83;

V ($Å^3$)= 519.13

Atomic coordinates (space group C 2/m)

Atom	X	Y	Z
Zn1	0.53	0.00	0.19
Zn2	0.50	0.27	0.50
Zn3	0.34	0.50	0.14
C1	0.86	0.83	0.79
C2	0.74	0.00	0.53
O1	0.85	0.00	0.45
O2	0.85	0.00	0.88
O3	0.60	0.00	0.43
O4	0.74	0.84	0.64
O5	0.83	0.68	0.88
O6	0.99	0.80	0.76

Bond length (Å) :

Zn1--O1= 2.05; Zn1--O2= 2.04; Zn1--O5= 2.22; Zn1--O6= 2.22

Zn2--O1= 2.16; Zn2--O3= 2.07; Zn2--O4= 2.10; Zn2--O6= 2.04

Zn3--O2= 2.10; Zn3--O6=2.05

C1--O2=1.34; C1--O3=1.41; C1--O5=1.43; C1--O6=1.39

C2--O4=1.31

Third-order Birch–Murnaghan equation of state (fitted between 0 and 150 GPa)

B_0(GPa) = 180.8(±1.6)

B'_0= 3.94 (±0.05)

V_0 ($Å^3$)= 488.61 (±0.29)

Table 4.2: Stable $ZnCO_3$ structure (Phase II) between 78 GPa and 121 GPa.

Lattice parameters

a (Å)=8.67; b (Å)= 3.62; c (Å)= 5.63
α(°)=90.00; β(°)=90.00; γ(°)=90.00
V ($Å^3$)= 176.7

Atomic coordinates (space group $P2_12_12_1$)

Atom	X	Y	Z
Zn	0.15	0.66	0.19
C	0.03	0.54	0.61
O1	0.05	0.17	0.08
O2	0.34	0.60	0.02
O3	0.07	0.80	0.78

Bond length (Å):

Zn--O1=1.9; Zn--O2=2.03; Zn--O3=2.12
C--O1=1.35; C--O2=1.39; C--O3=1.42

Third-order Birch–Murnaghan equation of state (fitted between 0 and 150 GPa)

B_0 (GPa)=119.15 (±3.2)
B'_0 = 4.36 (± 0.07)
V_0 ($Å^3$)= 170.92 (±0.33)

Table 4.3: Stable $ZnCO_3$ structure (Phase III) above 121 GPa.

4.5 Discussions

Remarkably, the results found confirm that smithsonite belongs to the group of calcite, since calcite structure is the most stable structure that $ZnCO_3$ may adopt at ambient conditions. In order to assess the reliability of our simulation, the mechanical properties of $ZnCO_3$ structure-phase I (R-3c space group) are evaluated. The obtained data are fitted to the Birch-Murnaghan equation of state [25] in order to obtain the bulk modulus, which is in good agreement with the experimental [15] and previous theoretical results [16]. The set calculated data are listed in Table 4.4. The dependence of the elastic constants of $ZnCO_3$-phase I as a function of pressure variation is calculated from 0 to 90 GPa. Fig.4.3 shows that elastic constants increase proportionally with the applied pressure until 78 GPa where a clear discontinuity is noticed, especially for C_{11}, C_{22}, C_{33}, C_{12}, C_{13} and C_{23} curves. This continuity supports our prediction regarding the structural transition at this pressure.

	Experiment[a]	This work	Theory[b]
C_{11}		244.97	243.51
C_{22}		240.29	240.24
C_{33}		148.79	145.36
C_{44}		70.09	69.34
C_{55}		44.33	41.31
C_{66}		43.25	41.62
C_{12}		104.41	103.75
C_{13}		73.54	71.13
C_{23}		70.49	68.58
B	124	126.45[c]	124.19[c]
		126.86[d]	124.93[d]
B'		4.00	3.99
A		1.00	0.99
G		45.34	44.39
E		121.54	118.98
ν		0.34	0.34
V_s		3.20	3.17
V_p		6.50	6.43

[15] , b[16], c[25],d[16](Voigt formula)

Table 4.4: Mechanical properties of $ZnCO_3$ structure (Phase I), at ambient conditions.

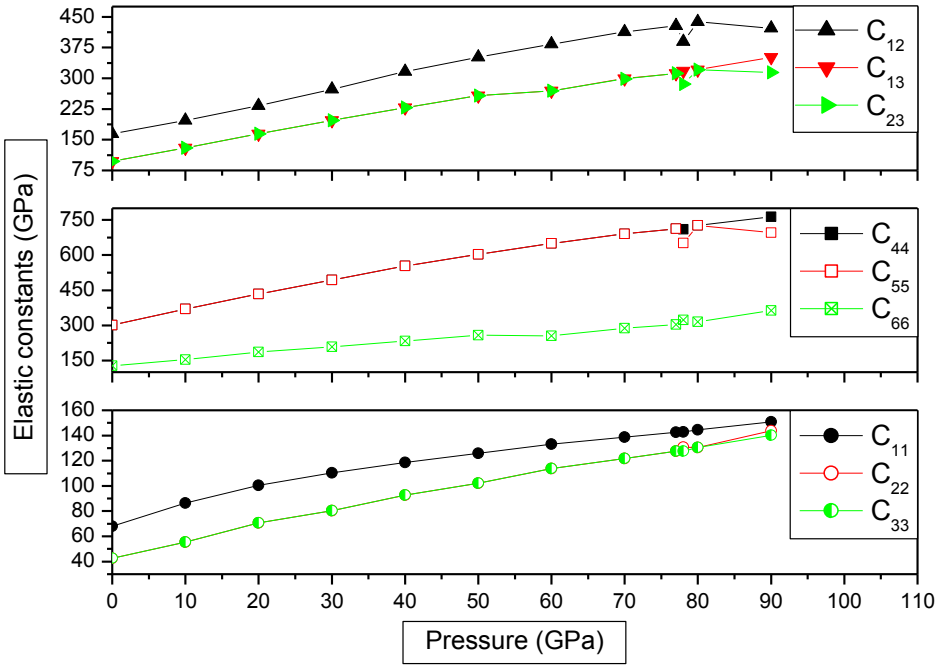

Fig. 4.3: Variation of the elastic constants C_{11}, C_{22} and C_{33}; C_{44}, C_{55} and C_{66}; and C_{12}, C_{13} and C_{23} vs pressure for $ZnCO_3$-Phase I.

In order to understand the main reasons for the first phase transition, we will analyze - in the following - the electronic charge density. Fig.4.4 represents the electronic charge density at 0 GPa (a), 78 GPa (b) and 90 GPa (c) in the (-3 2 1) plane, which includes the three constituents atoms of $ZnCO_3$. At zero pressure (Fig.4.4.a) there is a maximum of charge transfer between zinc and oxygen and also between oxygen and carbon. Fig.4.4.b shows the electronic charge density at 78 GPa, where a maximum of charge is transferred between oxygen and two zinc atoms as well as together between oxygen and carbon-zinc atoms. Consequently, a new bond between oxygen and zinc is formed at that pressure. However at 90 GPa (Fig.4.4.c), we notice only a slight new bond between oxygen and carbon.

On the other hand, a Bader charge analysis [26] of the obtained charge densities is carried out from the present first principles calculations. The charge at the atom is obtained by subtracting the Bader charge from the number of valence electrons considered for that particular atom in the density functional theory (DFT) calculations [27]. The charges at Zn, C and O atoms at different pressures are given in Table.4.5. Our Bader charge analysis shows that the positive charge at Zn and C decreases by ~0.035*e* and ~0.084*e* respectively, from 1.3839*e* at ambient pressure to 1.3489*e* at 90 GPa for Zn atoms and from 2.1478*e* at ambient pressure to 2.0632*e* at 90 GPa for C atoms. However, the negative charge of O atoms increases by 0.04*e* from -1.1773*e* at ambient pressure to -1.1373*e* at 90 GPa. Therefore, our Bader charge analysis shows a partial electronic charge transfer only from the Zn to O atoms and C to O atoms.

	Atomic charge (*e*) from Bader charge analysis		
Pressure (GPa)	**Zn**	**C**	**O**
0	1.3839	2.1478	-1.1773
50	1.3626	2.1184	-1.1603
70	1.3577	2.0656	-1.1411
78	1.3544	2.0639	-1.1394
90	1.3489	2.0632	-1.1373

Table 4.5: Atomic charge densities (e) from Bader charge analysis of Zn, C and O atoms at different pressures.

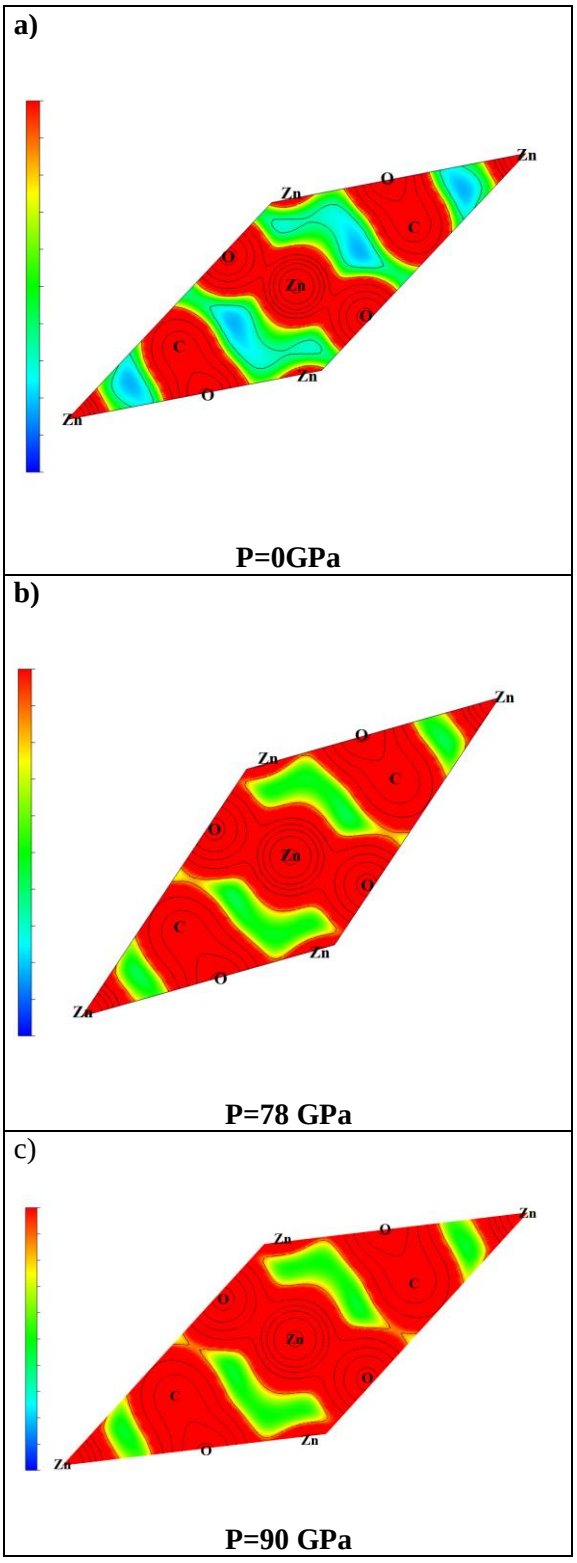

Fig. 4.4: Valence charge density of $ZnCO_3$-phase I along the (-3 2 1) plane at zero pressure (a), 78 GPa (b) and 90 GPa (c).

In order to complete the ground state properties of the obtained phases under pressure, we have – additionally – performed the total density of state for the three phases of $ZnCO_3$, as presented in Fig.4.5. The obtained band gap value of $ZnCO_3$-phase I corresponds to ~ 3.34 eV, which is slightly higher than the one of the ground state phase II (~ 2.64 eV), and than the one of the phase III (~ 1.45 eV). Bouibes et al.[16] found that the band gap value at the ground state of phase I is around 3.4 eV. The latter is in good agreement with the band gap value of phase I. However, it can be underlined here that the band gap of smithsonite remains closer to some semiconductors, such as ZnO (~3.4eV), than carbonates such as $CaCO_3$ (~6.0 eV), which is rather considered as insulator[7].

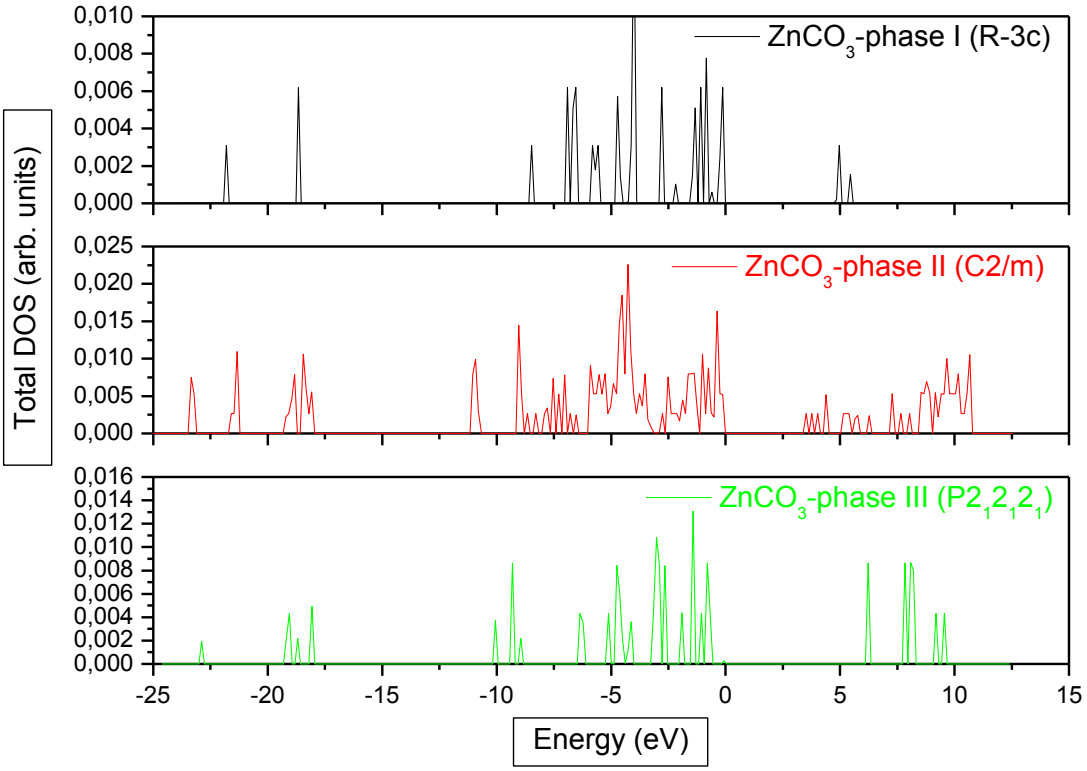

Fig. 4.5: Total DOS for each phase of $ZnCO_3$.

4.6 Conclusion

In summary, different phases of $ZnCO_3$ were predicted here by means of USPEX method together with DFT. We mainly conclude that below 78 GPa, $ZnCO_3$ stable structure has R-3c space group (calcite structure); and between 78 GPa and 121 GPa, $ZnCO_3$ takes up a more complex structure (magnesite phase II [7]) with C2/m space group and containing $(C_3O_9)^{6-}$ rings of carbonate. Above 121 GPa, the structure of $P2_12_12_1$ space group becomes more stable. The predicted structure is, remarkably, in perfect agreement with the experiment at ambient condition. In addition the computed mechanical quantities at the ground state of phase I agree well with experimental and previous theoretical data. Their behaviors under pressure support our prediction of structural transition of $ZnCO_3$ at 78 GPa. Finally, an analysis from electronic charge density and Bader charge was developed to explain the charge transfer that is behind the phase transition.

References:

[1] Ono, S. Synergy Between First-Principles Computation and Experiment in Study of Earth Science. In *Some Applications of Quantum Mechanics* (ed Pahlavani, M.R.) 91-108 (Vienna-Austria, 2012).

[2] Sekkal, W., Taleb, N., Zaoui, A., & Shahrour, I. A lattice dynamical study of the aragonite and post-aragonite phases of calcium carbonate rock. *Am. Mineral.* **93**, 1608-1612 (2008).

[3] Sekkal, W., & Zaoui, A. Nanoscale analysis of the morphology and surface stability of calcium carbonate polymorphs. *Sci. Rep.* **3**, 1587 (2013).

[4] Zaoui, A., & Shahrour, I. Molecular dynamics study of high-pressure polymorphs of BaCO3. *Philos. Mag. Lett.* **90**, 689-697 (2010).

[5] Bakri, Z., & Zaoui, A. Structural and mechanical properties of dolomite rock under high pressure conditions: A first-principles study. *Phys. Status Solidi B*, **248**, 1894-1900 (2011).

[6] Fiquet, G., Guyot, F., Kunz, M., Matas, J., Andrault, D., & Hanfland, M. Structural refinements of magnesite at very high pressure. *Am. Mineral.* 87, 1261-1265 (2002).

[7] Oganov, A. R., Ono, S., Ma, Y., Glass, C. W., & Garcia, A. Novel high-pressure structures of $MgCO_3$, $CaCO_3$ and CO_2 and their role in Earth's lower mantle. *Earth. Planet. Sci. Lett.* **273**, 38-47 (2008).

[8] Isshiki, M., *et al*. Stability of magnesite and its high-pressure form in the lowermost mantle. *Nature* **427**, 60-63 (2004).

[9] Boulard, E., *et al*. New host for carbon in the deep Earth. *Proc. Natl. Acad. Sci.* **108**, 5184-5187 (2011).

[10] Ayoub, A., Zaoui, A., & Berghout, A. High-pressure structural phase transitions and mechanical properties of calcite rock. *Comput. Mater. Sci.* **50**, 852-857 (2011).

[11] Oganov, A. R., Glass, C. W., & Ono, S. High-pressure phases of $CaCO_3$: Crystal structure prediction and experiment. *Earth. Planet. Sci. Lett.* **241**, 95-103 (2006).

[12] Ono, S., Kikegawa, T., Ohishi, Y., & Tsuchiya, J. Post-aragonite phase transformation in CaCO3 at 40 GPa. *Am. Mineral.* **90**, 667-671 (2005).

[13] Merlini, M., Hanfland, M., & Crichton, W. A. $CaCO_3$-III and $CaCO_3$-VI, high-pressure polymorphs of calcite: Possible host structures for carbon in the Earth's mantle. *Earth. Planet. Sci. Lett.* **333**, 265-271 (2012).

[14] Graf, D. L. Crystallographic tables for the rhombohedral carbonates. *Am. Mineral.* **46**, 1283-1316 (1961).

[15] Zhang, J., & Reeder, R. J. Comparative compressibilities of calcite-structure carbonates: Deviations from empirical relations. *Am. Mineral.* **84**, 861-870 (1999).

[16] Bouibes, A., Zaoui, A., & Tunega, D. Bonds, bands and elasticity of smithsonite rock. *Solid State Commun.* **166**, 76-82 (2013).

[17] Goldin, D. M., & Kulikova, G. V. On the dissociation mechanism of carbonates and their isomorphous mixture. *J. Therm. Anal.* **29**, 139-145 (1984).

[18] McPhail, D. C., Summerhayes, E., Welch, S., & Brugger, J. The geochemistry and mobility of zinc in the regolith. *Adv. Regolith*, 287-291 (2003).

[19] Glass, C. W., Oganov, A. R., & Hansen, N. USPEX—evolutionary crystal structure prediction. *Comput. Phys. Commun.* **175**, 713-720 (2006).

[20] Oganov, A. R., Lyakhov, A. O., & Valle, M. How Evolutionary Crystal Structure Prediction Works- and Why. *Acc. Chem. Res.* **44**, 227-237 (2011).

[21] Lyakhov, A. O., Oganov, A. R., Stokes, H. T., & Zhu, Q. New developments in evolutionary structure prediction algorithm USPEX. *Comput. Phys. Commun.* **184**, 1172-1182 (2013).

[22] Van Leeuwen, R., & Baerends, E. J. Exchange-correlation potential with correct asymptotic behavior. *Phys. Rev. A* **49**, 2421 (1994).

[23] Kresse, G., & Furthmüller, J. Software VASP, vienna (1999). *Phys. Rev. B* **54**, 169 (1996).

[24] Kresse, G., & Furthmüller, J. Efficient iterative schemes for ab initio total-energy calculations using a plane-wave basis set. *Phys. Rev. B* **54**, 11169 (1996).

[25] Birch, F. Finite elastic strain of cubic crystals. *Phys. Rev.* **71**, 809 (1947).

[26] Bader, R. F. *Atoms in molecules- A Quantum Theory* (Oxford Univ. Press, 1990).

[27] Pandey, K. K., Poswal, H. K., Kumar, R., & Sharma, S. M. High pressure iso-structural phase transition in BiMn2O5. *J. Phys.: Condens. Matter* **25**, 325401 (2013).

[28] Perdew, J. P., Burke, K., & Ernzerhof, M. Generalized gradient approximation made simple. *Phys. Rev. Lett.* **77**, 3865 (1996).

[29] Mattsson, A. E., Armiento, R., Paier, J., Kresse, G., Wills, J. M., & Mattsson, T. R. The AM05 density functional applied to solids. *J. Chem. Phys.* **128**, 084714 (2008).

[30] Kresse, G., & Joubert, D. From ultrasoft pseudopotentials to the projector augmented-wave method. *Phys. Rev. B* **59**, 1758 (1999).

Chapter 5:

Route for new civil engineering materials: the case of high pressure phases of lime

5.1 Abstract

Lime system has a chemical composition CaO, which is known as thermodynamically stable. The purpose here is to explore further possible phases under pressure. To this end, we use variable-composition *ab initio* evolutionary algorithm. The present investigation shows surprisingly new stable compounds of lime. At ambient pressure we predict, in addition to CaO, CaO_2 as new thermodynamically stable compound. The latter goes through a phase transition from C2/c space group structure to I4/mcm space group structure at 18.5GPa. Under increasing pressure, further compounds such as CaO_3 become the most stable and stabilize in P-42_1m space group structure above 65 GPa. For the necessary knowledge on the new predicted compounds, we have computed their mechanical and electronic properties to show and to explain the main reasons leading to transitions.

5.2 Introduction

Lime is one of the most important and largely used building materials. It is used in several ways in civil engineering. It can be used alone, hydrated and also by mixing it with other civil engineering materials to perform their properties. Lime is basically known thermodynamically stable as a calcium oxide (CaO). It is usually made by the decomposition of materials that contain calcium carbonate by decomposition reaction: $CaCO_3 = CaO + CO_2$. The stability and structural properties of the mineral parent (calcite) has been subject of intense investigations[1-5]. However, less is known about further possible phases of lime.

Number of recent studies was devoted to the prediction of new phases from initial composition for some systems such as Li-H [6], Na-H [7], K-H [8], Xe-O [9], Na-Cl [10] and Hf-C [11]. The goal of the present work is to investigate new thermodynamically stable compounds from lime system. New stable stoichiometries could have, indeed, important planetological and chemical implications.

Calcium oxide, CaO, is one of the most known thermodynamically stable compounds of Ca-O system at ambient conditions. This is one of the most abundant compounds in the planetary mantles after MgO, SiO_2 and FeO, which are considered as the building blocks of the mantle minerals [12]. Several experimental and theoretical investigations of high-pressure structure and phase stability of CaO have been done, resulting that, CaO crystallizes in the NaCl-type structure (B1) and transforms into CsCl-type structure (B2) around 62 GPa. The corresponding ground state properties have been widely investigated both experimentally and theoretically[12-14].

On the other hand, a recent theoretical study shown that calcium peroxide, CaO_2, is a thermodynamically stable composition in $Pna2_1$ space group structure at ambient conditions [15]. Mumtaz et al. performed experimentally the structural properties of calcium peroxides. They observed a tetragonal structure for CaO_2[16]. However, apart of this, much is still to be known about its fundamental properties as well as its behavior under pressure effect.

In the present study, we aim to investigate the new thermodynamically stable compounds based on Ca-O composition. To this end, we will explore all stable compositions from Ca-O system and their crystal structures at high pressures using the variable and fixe composition *ab initio* evolutionary algorithm [17]. Besides, we will discuss their different structures, phase transitions, elastic properties and chemical bonding. In Sec. II, we describe

the computational method. In sec. III, we present the results and discussions. Sec. IV is the conclusion.

5.3 Computational details

We use here the "Universal Structure Predictor: Evolutionary Xtallography" (USPEX) code [18-20]. The latter is based on approach features global optimization with real-space representation and physically motivated variation operators. For every candidate structure generated by USPEX, we use first-principles structural relaxation, based on density functional theory within the GGA functional [21] for solids as implemented in the Vienna *Ab-initio* Simulation Package (VASP) code [22,23].

We used the all-electron projector-augmented wave (PAW) [24] with Ca [$3s^2 3p^6 4s^2$] and O [$2s^2 2p^4$] cores (core radii 2.00 a.u. and 1.5 a.u., respectively). The plane-wave kinetic-energy cutoff is 600 eV, and the k-point mesh resolution in reciprocal space is 2 * 0.06 A^{-1}. These settings enable excellent convergences of the energy differences, stress tensors, and structural parameters. The predicted structure calculation was performed with USPEX fixed composition. The plane-wave kinetic-energy cutoff is also 600 eV, and the k-point mesh resolution in reciprocal space is 2 * 0.03 A^{-1}.

5.4 Results

To find all possible phases of lime and their corresponding structures, we used the *ab initio* evolutionary algorithm USPEX [17-19], which has a capability to simultaneously find stable stoichiometries and the corresponding structures in multicomponent systems. In our calculations, we allowed all possible compositions in our studied system with structures containing up to 10 atoms in the unit cell. The calculations were performed at zero Kelvin and pressures of 1 atm, 50 GPa, 70 GPa and 100 GPa. The initial generation consisted of 120 structures, and all subsequent generations have 40 structures. Stable structures and their compositions were determined using the convex hull construction. A compound is thermodynamically stable if the enthalpy of its decomposition into any other compound is positive [11].

The present investigation results a surprisingly new stable compounds of lime. While we reproduce stability of CaO in the whole pressure range investigated here, new stable compounds are predicted. In Fig. 5.1, we display the convex hull of Ca-O system at high

pressure. The enthalpies of formation of the predicted structures are shown as well. It can be clearly seen that in addition to CaO, CaO_2 is thermodynamically stable at high pressure.

At 70 GPa, convex hull diagram shows that a new compound, namely CaO_3, becomes thermodynamically stable. The latter remains thermodynamically stable up to 100 GPa (Fig. 5.1). The latter have never been reported before.

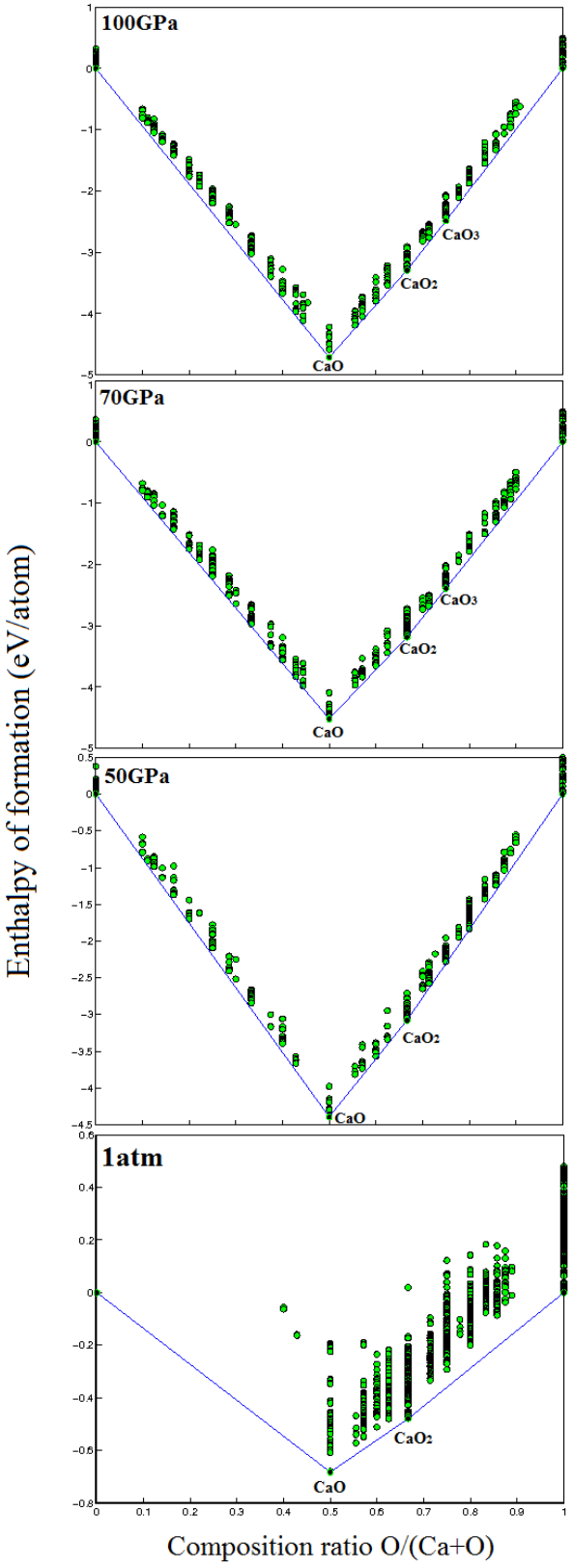

Fig. 5.1: Convex hull diagrams for the Ca – O system at different pressure: (a) 1atm; (b) 50 GPa, (c) 70 GPa and (d) 100 GPa.

Thereafter, we explore all our results of stable compounds for lime, using fixe composition evolution algorithm, in order to determine the possible phase change under pressure. The structure prediction runs for CaO and CaO_2 compound were performed at 1 atm, 20 GPa, 50 GPa, 70 GPa and 100 GPa, for CaO_3 at 70GPa and 100GPa, all at zero Kelvin. The phase diagram and crystal structures of the newly predicted compounds are remarkable. The pressure-composition phase diagram is shown in Fig 5.2. We may see that CaO phase transition occurs at around 65 GPa. It is stable below 65 GPa in Fm-3m space group structure. Above 65GPa, the structure of Pm3m space group becomes more stable. This is in good agreement with both experimental and theoretical data [12,14]. On the other hand, calcium peroxide, CaO_2, stabilize in C2/c space group structure (Fig 5.3.a) at ambient conditions. Under increasing pressure and above 18.5 GPa, a new I4/mcm structure (Fig 5.3.b) is predicted to be stable. CaO_3 stabilizes in P-42_1m space group structure above 65 GPa. CaO_3 is shown in Fig 5.4. The structural properties for all these compounds are reported in Table 5.1.

Structure	Space group	Entropy	Lattice Parameters (Å		X	Y	Z
CaO-Phase1	Fm-3m	0.0000	a=4.8	Ca	0.00	0.00	0.00
				O	0.50	0.00	0.00
CaO-Phase2	Pm3m	0.0000	a=2.56	Ca	0.00	0.00	0.00
				O	0.50	0.50	0.50
CaO_2-Phase1	C2/c	0.0003	a=6.82	Ca	0.5	0.14	0.75
			b=3.68	O	0.75	0.64	0.91
			c=7.04				
			β=117.9°				
CaO_2-Phase2	I4/mcm	0.0003	a=4.78	Ca	0.00	0.00	0.75
			c=6.15	O	0.11	0.39	0.50
CaO_3	P-42_1m	0.1128	a=4.68	Ca	0.00	0.00	0.00
			c=2.84	O1	0.00	0.50	0.79
				O2	0.82	0.32	0.51

Table 5.1: Structural properties and entropy of stable phases of lime.

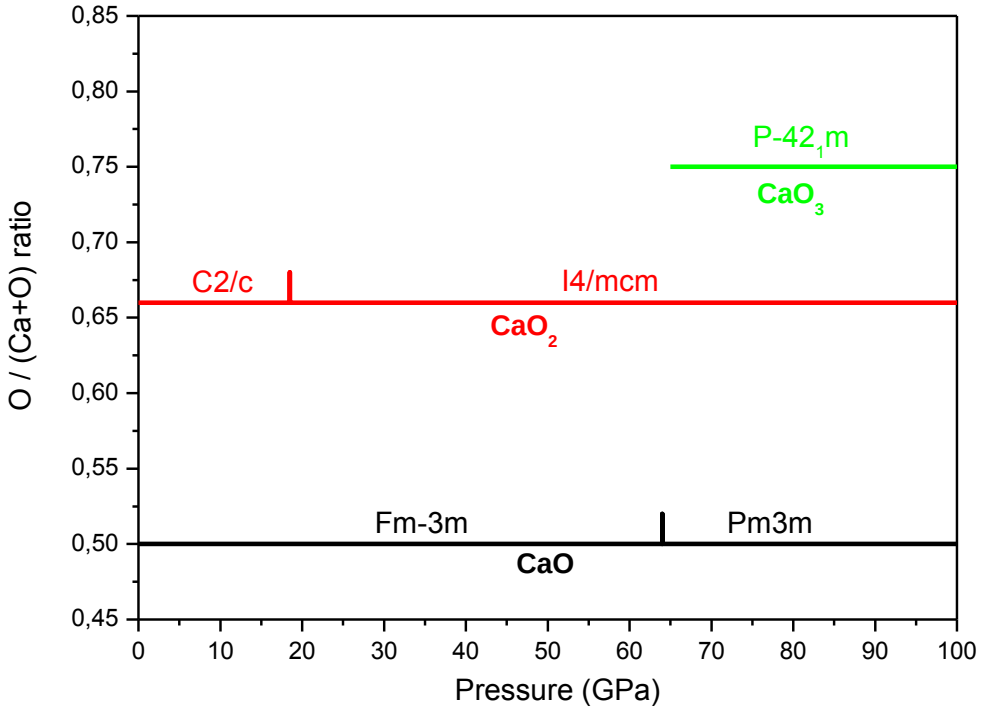

Fig. 5.2: Pressure composition phase diagram of Ca-O system.

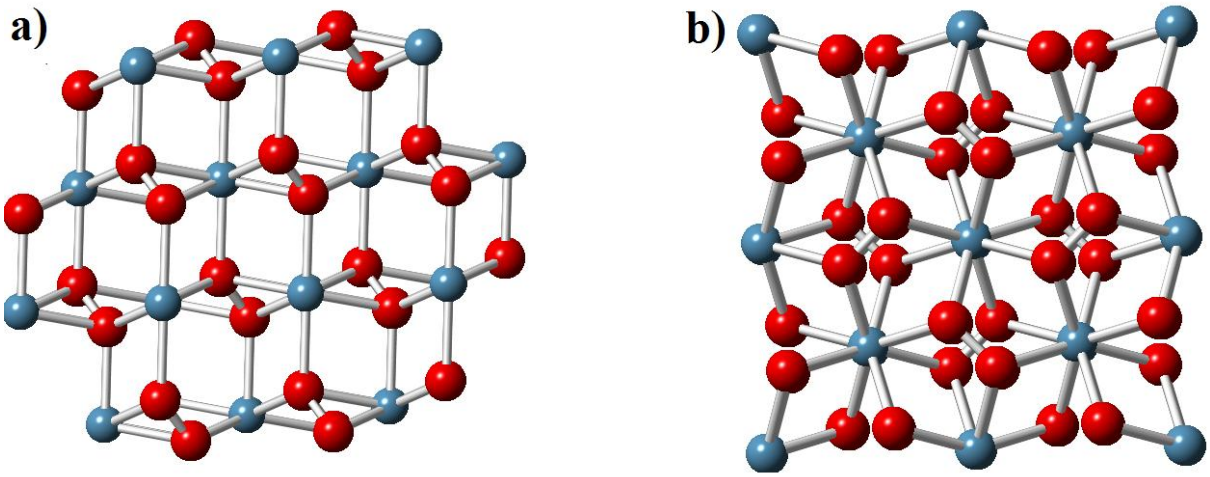

Fig. 5.3: CaO_2 structures: (a) CaO_2- C2/c (b) CaO_2 – I4/mcm. Large blue spheres –Ca atoms, small red spheres – O atoms.

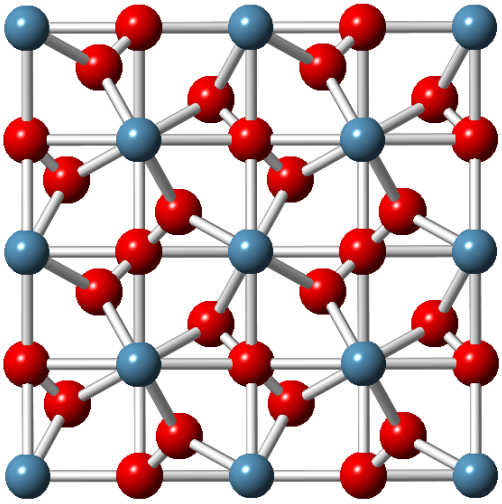

Fig. 5.4: Crystal structure CaO_3. Large blue spheres –Ca atoms, small red spheres – O atoms.

5.5 Discussions

In order to confirm the stability of the obtained structures at different pressures, we list in Table 5.2 the enthalpies per formula unit of each compound with the one of oxygen. A compound is thermodynamically stable if the enthalpy of its decomposition into any other compounds is positive. Indeed at 1atm, we obtain E (CaO)= -12.95 eV per f.u. and E(O_2)= -9.94 per molecule. The decomposition energy ΔE of the CaO_3 is -0.69 eV, indicating that it is not stable at ambient pressure.

Mechanically, the elastic constants of a material describe its response to an applied stress or, conversely, the stress required to maintain a given deformation. These properties are obviously directly related to the mechanical stability of a given system. The criteria of the mechanical stability of a monoclinic crystal are as follows [25]:

$$K_2=\det(C_{ij}),\ i,j<5,\quad K_2>0,\qquad C_{44}C_{66}-C_{46}^2>0 \qquad (5.1)$$

and of tetragonal crystal are [25]:

$$C_{44}>0,\ C_{66}>0,\ C_{11}-C_{12}>0,\ (C_{11}+C_{12})C_{33}-2C_{13}^2>0 \qquad (5.2)$$

	$E(O_2)$	**E(CaO)**	**$E(CaO_2)$**	**$E(CaO_3)$**
1atm	-9.94	-12.95	-17.96	-22.20
50GPa	-4.52	-5.38	-8.09	-10.52
70GPa	-2.85	-2.83	-4.78	-6.46
100GPa	-0.51	0.48	-0.12	-0.81

Table 5.2: Enthalpy of formation (eV) of lime phases at various pressure.

	CaO		**CaO_2**	**CaO_3**
	Fm-3m	***Theory-Experiment***	***C2c***	***P-42$_1$m***
C_{11}	204.92	200[a]-221.89[b]	151.38	442.31
C_{22}	206.51	--	136.95	442.90
C_{33}	206.49	--	133.35	454.63
C_{44}	74.68	66[a]-80.59[b]	38.83	226.16
C_{55}	74.78	--	58.73	176.29
C_{66}	74.78	--	53.49	174.29
C_{12}	54.07	50[a]-57.81[b]	56.80	219.08
C_{13}	53.91	--	69.89	177.54
C_{23}	54.86	--	54.53	177.91
C_{46}	-0.003		0.35	0.11
B	104.46	102[a]-110[b]	92.14	276.40
G	75.04	71[a]-80.59[b]	43.03	184.68
***k*=G/B**	0.71		0.46	0.67
H	13.75		4.28	16.88

[a] Theory : Ref [14]
[b] Experiment: Ref [13]

Table 5.3: Mechanical properties of lime phases in GPa units.

The calculated elastic constants of CaO_2, CaO_3, at 1atm, 65 GPa respectively are listed in Table 5.3. The above mentioned criteria are satisfied in our case, indicating that CaO_2, CaO_3 are mechanically stable at the corresponding conditions. For comparison, the values of the elastic properties of CaO are presented as well, and we notice the excellent agreement with the reported data. We may also underline that calcium oxide is more rigid and more resistant to shear deformation than calcium peroxide at the ambient conditions. Moreover, the Pugh modulus ratio [26] k=G/B is also reported in Table5.3 to show the ductile-brittle behavior of high pressure lime phases. For brittle materials, G/B is higher than 0.571, whereas, for the ductile ones, it is lower than 0.571. It follows that CaO and CaO_3 are brittle; while CaO_2 is ductile. According to the following equation of hardness [27]:

$$H= 2*(k^2G)^{0.585} - 3 \qquad (5.3)$$

The Vickers hardness H of CaO, CaO_2, and CaO_3 are 13.75, 4.28 and 16.88 GPa respectively, suggesting that the most hard phase is CaO_3 and the less hard is CaO_2.

In order to better understand the bonding behaviors, a Bader charge analysis [28] of the calculated charge densities is carried out. At ambient pressure, Bader charge analysis shows that each Ca atom gives 1.47 electrons to each O atom in CaO. In the case of CaO_2, Ca atom gives 1.56 electron/atom and O atom gets -0.78 electron/atom. At 65GPa, the charge configuration of CaO_3 is $Ca^{+1.47}$ [$O^{-0.62}O^{-0.23}O^{-0.62}$], the partial electronic charge transfer is not symmetric from the Ca to O atoms. We can also notice that the electronic charge of Ca atom is approximately the same for all phases. Besides, we have performed the total density of state for all stable phases of lime, as represented in Fig. 5.5. For comparison, we calculate the band gap value of CaO(3.65 eV), which is in perfect agreement with previous work [14]. The obtained band gap value of CaO_2, CaO_3 is 2.78 eV and 2.48 eV respectively.

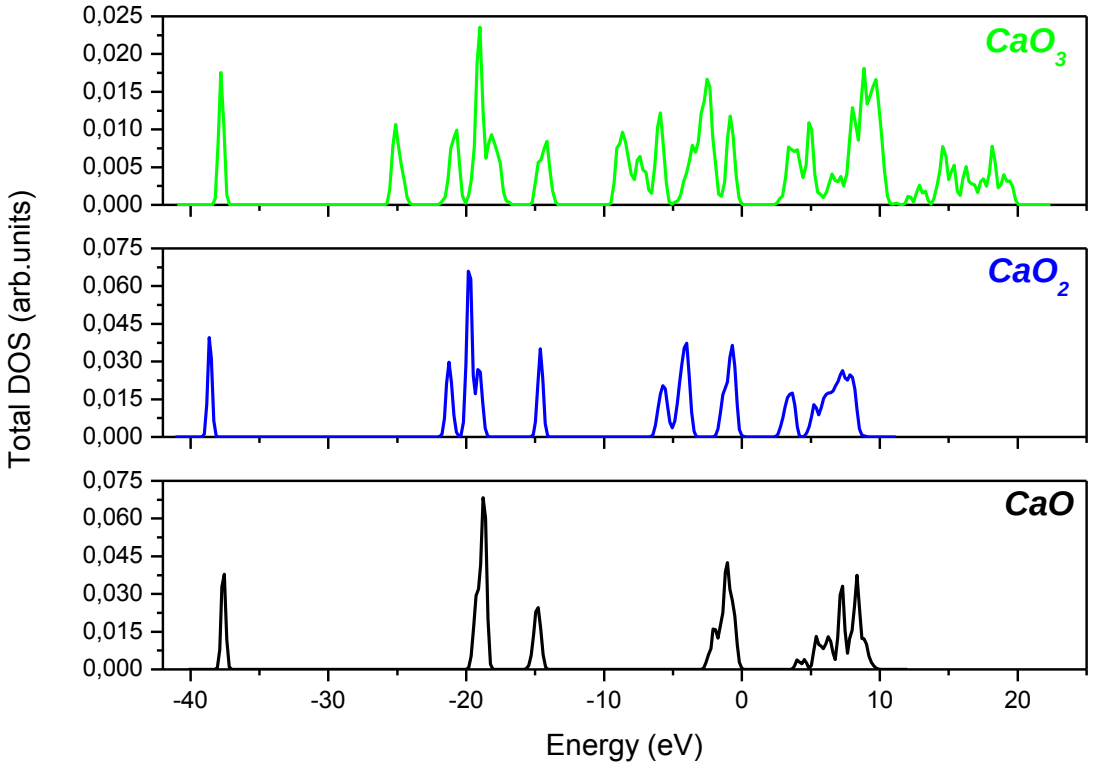

Fig. 5.5: Total DOS for each phase of Ca-O for various compositions. The Fermi level is set to zero.

In the studied pressure range, calcium peroxide knows a transition of phase at 18.5 GPa. The most stable CaO_2 at ambient conditions corresponds to the space group C2/c. Zhao et al. found that CaO_2 stabilizes in $Pna2_1$ space group structure [15]. After duplicating both structures, it follows that it is the same structure. The structures were obviously optimized in four steps with a high accuracy. The atomic positions, lattice parameters, and cell volume were fully relaxed until the force on each atom is less than 10-3 meV/Å, and stresses deviate from the desired hydrostatic pressure by less than 0.5 GPa.

In Table 5.4, we compare the atomic distances between the obtained structure and the one of Zhao. We can see that the atomic distances are quite similar. Calcium peroxide goes through a phase transition from C2/c space group structure (Fig. 5.3.a) to I4/mcm space group structure (Fig. 5.3.b) at 18.5GPa. The tetragonal structure with unit cell parameters a=5.01 Å and c= 5.92 Å is observed experimentally at a temperature of 550°C (823 K) by Mumtaz et al.[16]. The corresponding lattice parameters are very similar with our findings. In order to

understand the main reasons behind CaO_2 phase transition, let us analyze in the bonding character through the electronic charge density. Fig 5.6 represents the electronic charge density of CaO_2 compound at 1 atm and 20 GPa in the (1 1 1) plane, which contain the maximum Ca and O atoms. We can remark that the electronic structure change between 1atm and 20 GPa. Consequently, new bond between calcium and oxygen are formed at 20GPa leading to a new phase. This explain and justify the main reasons behind the transitions.

	C2/c – CaO_2	**$Pna2_1$ - CaO_2**
Ca – O (Å)	2.41 ; 2.42	2.38 ; 2.44 ; 2.42 ; 2.43 ; 2.47
O – O (Å)	1.51	1.51
Ca – Ca (Å)	3.66 ; 3.67	3.62 ; 3.64

Table 5.4: Atomic distance at ambient conditions for C2/c – CaO_2 structure and Pna21- CaO_2 structure.

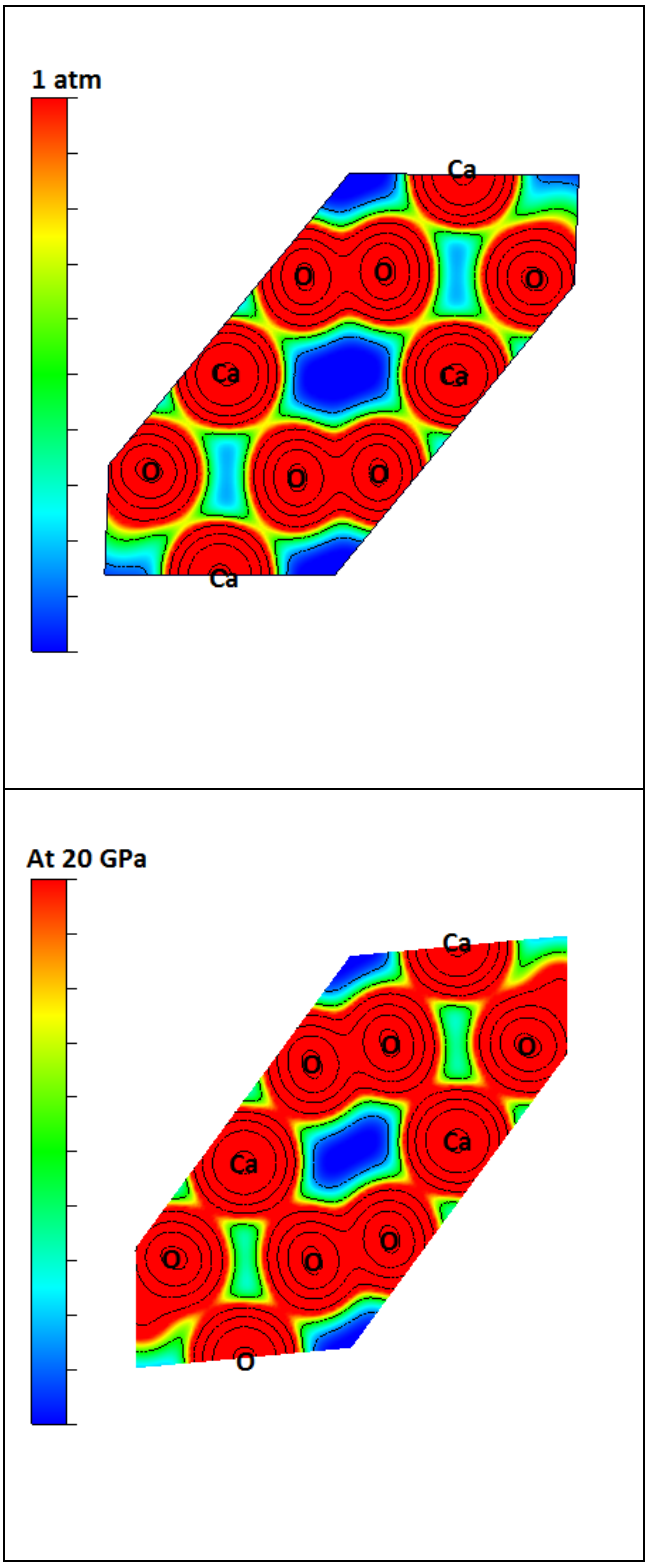

Fig. 5.6: Valence charge density of CaO_2-Phase1 along the (1 1 1) plane at 1atm and 20 GPa.

5.6 Conclusion

We have explored new phases of lime through variable-composition *ab initio* evolutionary algorithm. At ambient pressure we predicted, in addition to CaO, CaO_2 as new thermodynamically stable compound under a transition at 18.5GPa. Further compounds have been predicted such as CaO_3 above 65 GPa.

For the more complete knowledge on the new predicted compounds, we have investigated various kinds of properties including mechanical, electronic and bonding to explain the main reasons leading to the transitions giving the new class of materials from the simple lime system.

References

[1] Oganov, A.R. et al. Novel high-pressure structures of $MgCO_3$, $CaCO_3$ and CO_2 and their role in Earth's lower mantle. *Earth and Planetary Science Letters* **273**, 38-47 (2008).

[2] Ayoub, A. et al. High-pressure structural phase transitions and mechanical properties of calcite rock. Comp. Mater. Sci. **50**, 852-857 (2011).

[3] Bouibes, A. and Zaoui, A. High-pressure polymorphs of $ZnCO_3$: Evolutionary crystal structure prediction. *Nature-Scientific Reports 4,* 5172 (2014).

[4] Zaoui, A. and Shahrour, I. Molecular dynamics study of high-pressure polymorphs of $BaCO_3$. *Phil. Mag. Lett.* **90**, 689-697 (2010).

[5] Zhu, Q. ,Oganov, A. R. and Lyakhov, A. O. Novel stable compounds in the Mg –O system under high pressure. *Phys. Chem. Chem. Phys* **15**, 7796-7700 (2013).

[6] Zurek, E., et al . A little bit of lithium does a lot for hydrogen. Proc. *Natl. Acad. Sci.* **106**, 17640-17643 (2009).

[7] Baettig, P and Zurek, E. Pressure-stabilized sodium polyhydrides: NaHn (n>1). *Phys. Rev. Lett.* **106**, 237002 (2011).

[8] Zhou, D. W., et al. Ab initio study revealing a layered structure in hydrogen-rich KH_6 under high pressure. *Phys. Rev. B* **86**, 014118 (2012).

[9] Zhu, Q. et al. Stability of xenon oxides at high pressures. *Nature chemistry* **5**, 61-65 (2013)

[10] Zhang, W. W. et al. Unexpected stoichiometries of stable sodium chlorides. *Science* **342**, 1502-1505 (2013).

[11] Zeng, Q., et al. Prediction of stable hafnium carbides: Stoichiometries, mechanical properties, and electronic structure. *Phys. Rev. B* **88**. 214107 (2013).

[12] Deng, Ye, et al. Phase transition and elastic constants of CaO from first-principle calculations. *Physica B: Condens. Matter* **392**. 229-232 (2007).

[13] Richer, P., et al. Static compression and equation of state of CaO to 1.35 Mbar, *J. Geophys. Res.* **93**, 279-288 (1988)

[14] Ghebouli, B., et al. First-principles calculations of structural, elastic, electronic and optical properties of XO (X= Ca, Sr and Ba) compounds under pressure effect. *Mater. Sci. Semicond. Process.* **13**. 92-101 (2010).

[15] Zhao, X., et al. Structures and stabilities of alkaline earth metal peroxides XO_2 (X= Ca, Be, Mg) studied by a genetic algorithm. *RSC Adv.* **3**, 22135-22139 (2013).

[16] Mumtaz, M., et al. Dielectric properties of (CuO, CaO_2, and $BaO)_y$/CuTl-1223 composites. *J. Low. Temp. Phys.* **39**, 622-629 (2013).

[17] Oganov, A. R., et al. Evolutionary crystal structure prediction as a method for the discovery of minerals and materials. *Rev. Mineral Geochem.* **71**, 271-298 (2010).

[18] Oganov, A. R., Glass, C. W. Crystal prediction using ab initio evolutionary techniques: Principles and applications. *J. Chem. Phys.* **124**, 244704 (2006).

[19] Lyakhov, A. O., et al. New developments in evolutionary structure prediction algorithm USPEX. *Comp. Phys. Comm.* **184**, 1172-1182 (2013).

[20] Oganov, A. R., et al. How evolutionary crystal structure prediction works – and why. *Acc. Chem. Res*. **44**, 227-237 (2011).

[21] Perdew, J. P. et al. Generalized gradient approximation made simple. *Phys. rev lett.* **77**, 3865 (1996).

[22] Kresse, G. and Furthmüller, J. Software VASP, Vienna (1999).

[23] Kresse, G. and Furthmüller, J. Efficient iterative schemes for ab initio total-energy calculations using a plane-wave basis set. *Phys. Rev. B* **54**, 11169 (1996).

[24] Kresse, G. and Joubert, D. From ultrasoft pseudopotentials to the projector augmented-wave method. *Phys. Rev. B* **59**, 1758 (1999).

[25] Cowley, R. A. Acoustic phonon instabilities and structural phase transitions. *Phys. Rev. B* **13**, 4877 (1976).

[26] Pugh, S. F. XCII. Relations between the elastic moduli and the plastic properties of polycrystalline pure metals. *Philos. Mag.* **45**. 823-843 (1954).

[27] Chen, X., et al. Modeling hardness of polycrystalline materials and bulk metallic glasses. *Intermetallics* **19**.1275-1281(2011).

[28] Bader, R. Atoms in Molecules: A Quantum Theory. Oxford University Press, New York (1990).

Chapter 6:

New high-pressure polymorphs of Zn-O from variable composition

6.1. Abstract

The high-pressure stability of zinc oxides has been investigated here using a variable composition *ab initio* evolutionary algorithm. In addition to the well-known ZnO, we predict a new stable compound ZnO_2 with I4/mcm space group, which is thermodynamically stable only above 120 GPa. Furthermore, to shed light on the new predicted compound, we have evaluated its entire ground state properties including structural, mechanical and electronic quantities. The high-pressure investigation of Zn-O shows that ZnO knows a phase transition at around 10 GPa. It stabilizes in B4 wurtzite structure at ambient conditions up to 10 GPa. Above this pressure, ZnO stabilizes in B1 structure. This agrees well with the previous experimental and theoretical studies.

6.2 Introduction

High pressures materials happen at the centers of planets and in both natural and man-made explosions. Alkaline earth metals are abundant in planetary mantles, and understanding its high-pressure behavior is essential for construction models of the Earth's and planetary interiors. Zinc oxide is one of promising alkaline earth metals. It has various technological applications, for example, ceramics, piezoelectric, transducers, chemical sensors, varistors, thyristors, catalysis, optical coating and photovoltaic [1]. Also, it occurs naturally as a mineral and it can have several phases under high-pressure, theses phases may be geologically important as a component of the lower mantle. For these reasons, it has been the subject of several experimental and theoretical studies, in ground state and under pressures [1-4]. At ambient conditions, ZnO is thermodynamically stable in wurtzite phase. The zinc-blende ZnO structure can be stabilized only by growth on cubic substrates, and the rock-salt (NaCl) structure may be obtained at relatively high pressures [2]. Two pressures induced phase transitions were reported. The first one occurs at about 10.45 GPa and the second one at about 352 GPa [2]. As it was previously reported, the most stable ZnO at ambient condition corresponds to the B4 structure with $P6_3mc$ space group. Then, the B1 structure with Fm-3m space group becomes stable between 10.45 GPa and 352 GPa. Above 352 GPa, B2 structure with Pm3m space group becomes the most stable structure of ZnO [2]. On the other hand, zinc peroxide (ZnO_2) belongs to same system alkaline metal. ZnO_2 powder is extensively used in cosmetic, pharmaceutical, plastic, rubber, and pyrotechnic industries for making mixtures whose reaction products should not contain corrosive and hazardous components [5]. ZnO, ZnO_2 and also $ZnCO_3$ have very closer band gap energy, which indicate that they may have a same behavior as semiconductor materials [6-8]. Zinc peroxide alkaline metal was previously investigated by Chen et al. [8]. It was reported that ZnO_2 has a cubic structure with a Pa-3 space group. This structure is stable up to 504 K and 36 GPa [8]. The main goal here is to explore new possible stable phases of from the variable composition of Zn-O through ab initio evolutionary algorithm [9-10]. In Sec. II, we describe the computational methods. In sec. III, we present and discuss the obtained results. Sec. IV is the conclusion.

6.3 Computational details

Structure / Composition predictions were performed here using the USPEX code [9-13] in the variable composition mode. The first generation of structures was produced randomly and the subsequent generations were obtained by applying heredity, transmutation, softmutation, and

lattice mutation operations, with probabilities of 50%, 10%, 20%, and 10%, respectively. All structures were relaxed using density functional theory (DFT) calculations at the generalized gradient approximation level of theory, with the Perdew-Burke-Ernzerhof (PBE) [14] exchange-correlation functional, as implemented in the Vienna *Ab-initio* Simulation Package (VASP) code [15]. We used the all-electron projector-augmented wave (PAW) [16-17], the plane-wave kinetic-energy cutoff is 600 eV, and the k-point mesh resolution in reciprocal space is 2 * 0.04 A^{-1}. These settings enable excellent convergences of the energy differences, stress tensors, and structural parameters. The calculations of the elastic properties, band structure, and density of state (DOS) were calculated by the VASP code.

6.4 Results and discussion

We performed structure prediction simulations of Zn-O system at 1atm, 50 GPa, 100GPa, 150 GPa and 200GPa, all at zero Kelvin. We allowed all possible compositions in our studied system with structures containing from 8 to 16 atoms in the cell. The initial generation consisted of 100 structures, and all subsequent generations have 40 structures. The Pa-3 space group structure, which was already found experimentally [8] for ZnO_2, has seeded in the first generation of calculations. Our theoretical predictions were performed using the convex hull construction, i.e. a compound is thermodynamically stable if the Gibbs free energies of its decomposition into any other compounds are positive [18].

Fig.6.1 shows the Gibbs free energies of formation of zinc oxide system under pressure and at 0 K. One can see that between 1atm and 100 GPa, ZnO is the only one that is thermodynamically stable compound. ZnO_2 becomes stable, in addition to ZnO, at 150 GPa and 200 GPa. The thermodynamically stable structure obtained in 1atm has $P6_3mc$ space group. The structural parameters are V_0=24.79 $Å^3$ and c/a= 1.60, which is in excellent agreement with pervious experimental and theoretical studies [2,3,4]. At 50 GPa, the most stable structure of ZnO is the Fm-3m space group structure, with a lattice constant of a=4.06 Å. The same structure remains stable under pressure until 200GPa. Previous experimental and theoretical investigations confirm our prediction [2,4]. With increasing pressure, ZnO_2 becomes stable (I4/mcm space group) at 150 GPa and 200 GPa. The new obtained structure is detailed in table 6.1 and presented in Fig.6.2.

Lattice parameters			
a=4.02 Å ; c=4.66 Å			
V=75.3 Å^3			
Space group: I4/mcm			
Atoms:	X	Y	Z
Zn	0.00	0.00	0.75
O	0.38	0.12	0.00
Zn-O:	1.98Å; 2.79Å		
O-O:	1.37Å		

Table 6.1: Structural properties of the sable structure of ZnO_2.

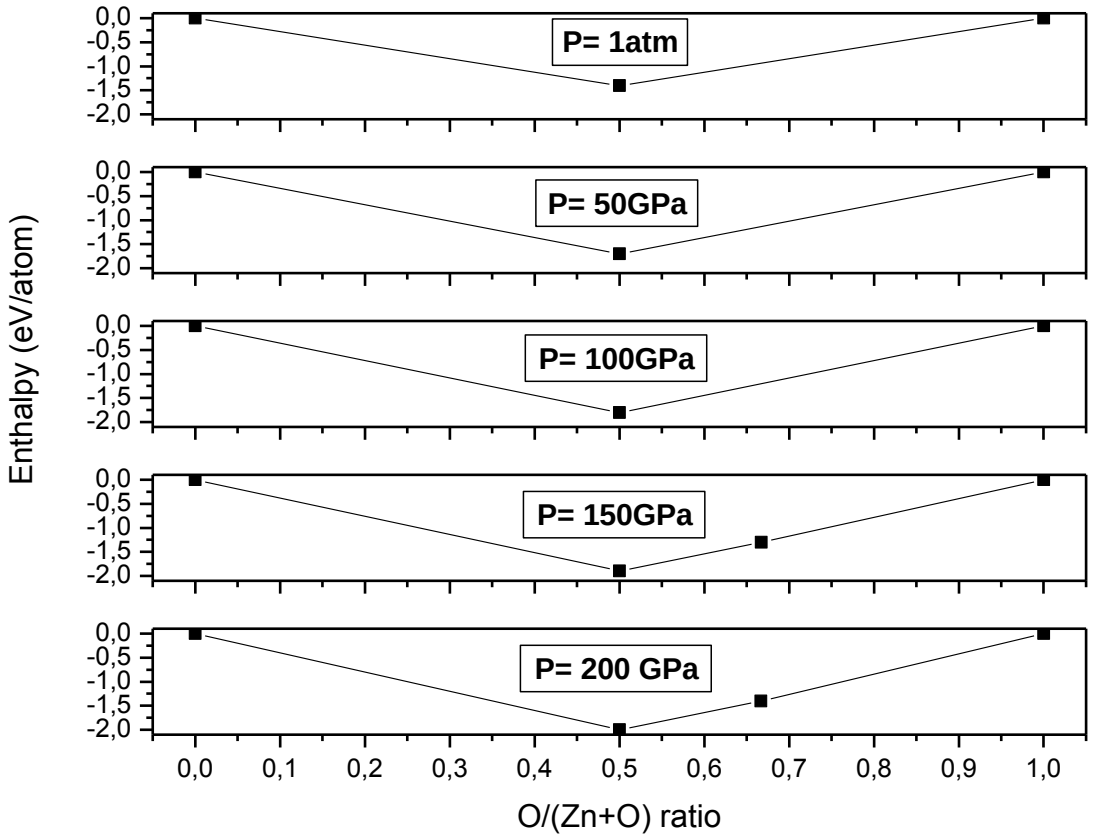

Fig. 6.1: Convex hull diagrams for the Zn – O system at different pressures.

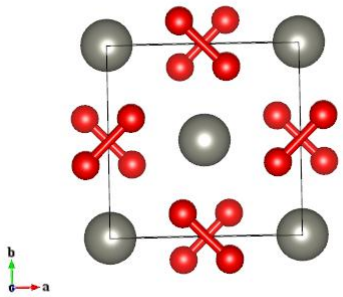

Fig. 6.2: Crystal structure I4/mcm-ZnO_2. Large gray spheres –Ca atoms, small red spheres – O atoms.

All obtained zinc oxides have been optimized with very strict computational conditions at pressures ranging from 0 GPa to 200 GPa. Fig.6.3 shows the enthalpy as a function of pressure. ZnO compound is thermodynamically stable between 1atm and 120 GPa. Above the latter pressure, ZnO_2 and ZnO are both thermodynamically stable. The most stable structure of ZnO at ambient conditions is wurtzite with $P6_3mc$ space group. The phase transition occurs around 10GPa. Between 10 GPa and 200 GPa , B1 structure (Fm-3m space group) becomes the most stable ZnO structure. In addition to ZnO compounds, ZnO_2 (I4/mcm space group) becomes thermodynamically stable above 120GPa. This new structure has never been reported before. Moreover the P-3a space group structure, reported by Chen et al. for ZnO_2, is energetically higher than ZnO. Therefore P-3a – ZnO_2 structure is theoretically unstable as shown in Fig.6.3.

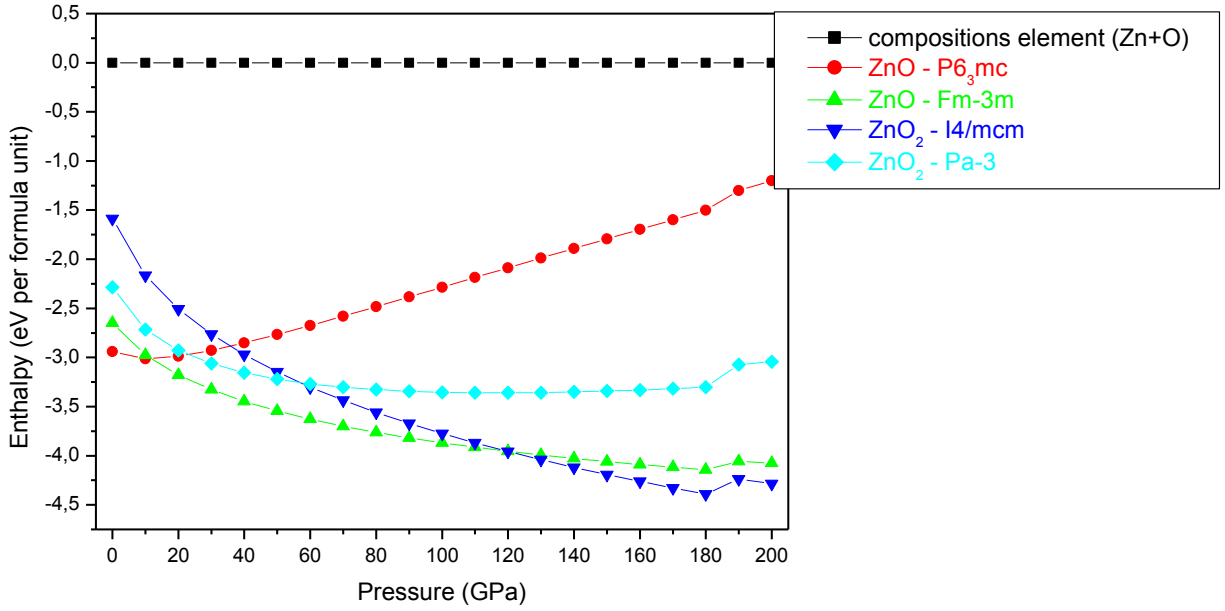

Fig. 6.3: Enthalpies of formation of stable zinc oxides as function of pressures.

For a deeper knowledge of ZnO_2, let us determine, first, its mechanical properties. The set calculated data at 120 GPa are listed in Table 6.2. The corresponding quantities are directly related to the mechanical stability. The criteria of the mechanical stability of a tetragonal crystal are as follows [19]:

$$C_{44} > 0,\ C_{66} > 0,\ C_{11}-C_{12} > 0,\ (C_{11}+C_{12})C_{33}-2C_{13}^2 > 0 \qquad (6.1)$$

These criteria are satisfied here, what indicates that ZnO_2 is mechanically stable at 120 GPa and 0K. The Pugh modulus ratio [20] *k* (*k*=G/B) is also reported in Table 6.3 in order to show the ductile-brittle behaviors of the obtained phases. For brittle materials, G/B is higher than 0.571; whereas, for the ductile ones, it is lower than 0.571. We may notice, from Table 6.2, that the Zn-O systems have ductile behaviors.

Thereafter, we have performed the total density of state for ZnO_2, as reported in Fig.6.4. The latter figure shows that the valance band of ZnO_2 consists of three regions. The first one has peaks, which lies between -26.65 eV and -23.32eV, the main one comes from oxygen atoms. The region has peaks between -19.08 eV and -16.96 eV, which comes principally from oxygen atoms. The third region lies between -12.26 eV and 0 eV, which is

marked by a wide dominant contribution of zinc atoms from -8.30 eV to -3.26 eV, with almost the same contribution of both atoms. The conduction band is located between 1.7 eV and 15.3 eV and it is constituted by both zinc and oxygen atomic contributions. The main electronic band gap corresponds to 1.7 eV. We may underline here that the band gap of ZnO_2 is much closer to some semiconductors such as CdSe (Eg =1.84 eV [21]).

On the other hand, we have also carried out a Bader charge analysis [22] of the calculated charge densities. At 120 GPa, the charge configuration of ZnO_2 is $Zn^{+1.34}$ $[O^{-0.62}O^{-0.72}]$, the partial electronic charge transfer is not equal from the Zn to O atoms. Each O has almost 7 valence electrons (6.72 *e* for O1 and 6.62 *e* for O2); thus with the formation of singly bonded dumbbell the octet rule is fulfilled. Each O-O dumbbell can be viewed as a peroxide-ion $(O\text{-}O)^{2-}$ with a closed-shell electronic configuration.

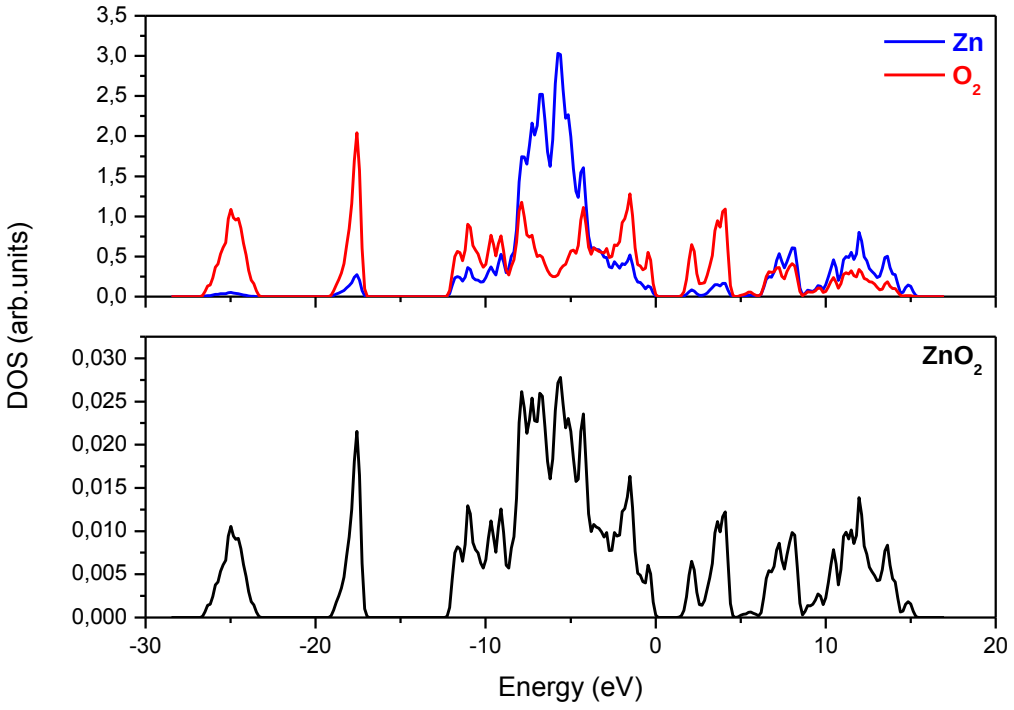

Fig. 6.4: Total DOS of ZnO_2at 120 GPa, with contribution for each atom.

C_{ij} (GPa)	**ZnO_2-I4/mcm**
C_{11}	725.27
C_{22}	731.68
C_{33}	735.08
C_{44}	352.90
C_{55}	145.87
C_{66}	142.22
C_{12}	499.77
C_{13}	323.94
C_{23}	326.88
B	497.88
G	242.73
H=G/B	0.49

Table 6.2: Mechanical properties of ZnO_2 at 120 GPa.

6.5 Conclusion

In summary, we have performed a theoretical prediction for possible stoichiometries in the Zn-O system at pressures up to 200GPa. We have found that ZnO_2 becomes thermodynamically stable at pressure above 120GPa. Our predictions give a phase transition around 10 GPa for ZnO compound. The latter stabilizes in B4 wurtzite structure at ambient conditions up to 10GPa. Above 10 GPa, ZnO stabilize in B1 structure. These results fit perfectly with available experimental and theoretical studies. At 120 GPa, ZnO_2 becomes the most stable. It stabilizes in I4/mcm space group structure. For more a complete knowledge of the new structure, we have calculated and discussed its structural, mechanical and electronic properties.

References

[1] Ahuja, R., et al. Elastic and high pressure properties of ZnO. *J. Appl. Phys.* **83**, 8065-8067 (1998).

[2] Zaoui, A., and W. Sekkal. Pressure-induced softening of shear modes in wurtzite ZnO: A theoretical study. *Phys. Rev.B* **66**, 174106 (2002).

[3] Zaoui, A., Energetic stabilities and the bonding mechanism of ZnO {0001}/Pd (111) interfaces. *Phys. Rev.B* **69**, 115403 (2004).

[4] Desgreniers, S. High-density phases of ZnO: Structural and compressive parameters. *Phys. Rev. B* **58**, 14102 (1998).

[5] Escobedo-Morales, A., et al. Structural and vibrational properties of hydrothermally grown ZnO_2 nanoparticles. *J. Cryst. Growth* 316, 37-41 (2011).

[6] Bouibes, A., et al. Bonds, bands and elasticity of smithsonite rock. *Solid State Commun*. **166**, 76–82 (2013).

[7] Bouibes, A. and Zaoui, A. High-pressure polymorphs of $ZnCO_3$: Evolutionary crystal structure prediction. *Sci. Rep.* **4**. (2014).

[8] Chen, W., et al. Synthesis, thermal stability and properties of ZnO_2 nanoparticles. *J. Phys. Chem. C*. **113**, 1320-1324 (2009).

[9] Lyakhov, Andriy O., et al. Crystal structure prediction using evolutionary approach. *Modern Methods of Crystal Structure Prediction* 147-180 (2010).

[10] Oganov, A. R., et al. Evolutionary crystal structure prediction as a method for the discovery of minerals and materials. *Rev. Mineral Geochem.* **71**, 271-298 (2010).

[11] Oganov, A. R., Glass, C. W. Crystal prediction using ab initio evolutionary techniques: Principles and applications. *J. Chem. Phys.* **124**, 244704 (2006).

[12] Lyakhov, A. O., et al. New developments in evolutionary structure prediction algorithm USPEX. *Comp. Phys. Comm.* **184**, 1172-1182 (2013).

[13] Oganov, A. R., et al. How evolutionary crystal structure prediction works – and why. *Acc. Chem. Res*. **44**, 227-237 (2011).

[14] Perdew, J. P. et al. Generalized gradient approximation made simple. *Phys. rev lett.* **77**, 3865 (1996).

[15] Kresse, G. and Furthmüller, J. Software VASP, Vienna (1999).

[16] Kresse, G. and Furthmüller, J. Efficient iterative schemes for ab initio total-energy calculations using a plane-wave basis set. *Phys. Rev. B* **54**, 11169 (1996).

[17] Kresse, G. and Joubert, D. From ultrasoft pseudopotentials to the projector augmented-wave method. *Phys. Rev. B* **59**, 1758 (1999).

[18] Zeng, Q., et al. Prediction of stable hafnium carbides: Stoichiometries, mechanical properties, and electronic structure. *Phys. Rev. B* **88**. 214107 (2013).

[19] Cowley, R. A. Acoustic phonon instabilities and structural phase transitions. *Phys. Rev. B* **13**, 4877 (1976).

[20] Pugh, S. F. XCII. Relations between the elastic moduli and the plastic properties of polycrystalline pure metals. *Philos. Mag.* **45**. 823-843 (1954).

[21] Solanki, R., et al. Atomic layer deposition of ZnSe/CdSe superlattice nanowires. *Appl. Phys. Lett.* **81**. 3864-3866 (2002).

[22] Bader, R. Atoms in Molecules: A Quantum Theory. Oxford University Press, New York (1990).

General conclusion

In this thesis, we have performed a theoretical prediction of new civil engineering materials from existing compounds such as smithsonite, lime and zinc oxide. To this end, we have employed universal structure prediction method for both fixed and variable compositions, based on *ab initio* approach. We have employed pseudopotential method as well as several as various functional for the exchange-correlation. Remarkable results have been obtained regarding the new predicted systems.

From smithsonite, which was still an unknown carbonate, we started the work by studying its ground state properties. A number of mechanical properties such as bulk modulus, elastic constants, Young and shear moduli, transversal and longitudinal sound velocities were evaluated. Obtained results showed that the zinc carbonate harder and more rigid than the other carbonates like calcite. Electronic properties were also determined such as the band gap energy that is close enough to some semiconductors rather than insulators.

Then, we have predicted smithsonite ($ZnCO_3$) behaviors at high pressures. Two phase transitions have been found: the first one at 78 GPa; while the second one occurs at 121 GPa. Below 78GPa, $ZnCO_3$ stable structure has R-3c space group (calcite structure); and between 78GPa and 121 GPa, $ZnCO_3$ takes up a more complex structure (magnesite phase II) with C2/m space group. Above 121 GPa, the new smithsonite structure with $P2_12_12_1$ space group becomes more stable.

Furthermore, using variable composition *ab initio* evolutionary algorithm, we have obtained surprisingly new stable compounds from Ca-O. At ambient pressure we have predicted, in addition to lime phase, CaO_2 as a new thermodynamically stable compound. The latter goes from C2/c to I4/mcm space group structure at 18.5GPa. Under increasing pressure, further compounds such as CaO_3 become the most stable and stabilize in P-42_1m space group structure above 65 GPa.

The last material that we have studied in this thesis is zinc oxide. We have performed a theoretical prediction for possible stoichiometries in the Zn-O system at pressures up to 200 GPa. We have found that ZnO_2 becomes thermodynamically stable at pressure above 120GPa. It stabilizes in I4/mcm space group structure. Our predictions give a phase transition around 10 GPa for ZnO compound. The latter is stable in B4 wurtzite structure at ambient conditions up to 10GPa. Above 10 GPa, ZnO became more stable in B1 structure. These results strongly support our predictions since they agree perfectly with available experiment and previous theoretical studies.

To sum up, the new predicted materials should create a new vision for further civil engineering applications. This could create a remarkable impact in improving various properties and behaviors of this kind of materials. At last, we hope that the present contribution and the obtained results will stimulate further studies in civil engineering.

Abstract:

The civil engineering progress would not been possible without new materials development. In fact, new materials with efficient properties allowed the construction of modern structures, taller building, longer bridges,…etc. Furthermore, it is essential for the progress continuity of this field in the future. Especially, in the smart construction approach we will need new materials with the very efficient properties. The study of the properties of materials at the molecular level, allow a better understanding of how those materials will function and react on a macro level. It is through such studies that we are able to understand their behaviors under a large number of conditions.

In this thesis, we focus our efforts on three types of materials. The first one is zinc carbonate. The second one is Lime, which is widely used in building and public works; and the last one is zinc oxide, which is an important material for steel construction. The purpose here is to investigate in details the three different materials at various pressures and variable compositions by means of the universal structure prediction method based on *ab initio* tool.

For smithsonite, a number of mechanical properties were evaluated. We mainly show that this system is harder and more rigid than the other carbonates. Besides, the investigation of its electronic properties reveals that the energy band-gap is close enough to some semiconductors. Moreover, two high-pressure phase transitions have been found: the first one at 78 GPa and second one at 121 GPa. Below 78 GPa, $ZnCO_3$ is found to be the most stable structure with R-3c space group (calcite structure); and between 78 GPa and 121 GPa, $ZnCO_3$ has another structure (magnesite phase II) with C2/m space group. Above 121 GPa, we show that new structure with $P2_12_12_1$ space group becomes more stable.

In addition, by means of variable composition *ab initio* evolutionary algorithm, we show surprisingly new stable compounds from Ca-O. At ambient pressure CaO_2 is predicted as a thermodynamically stable system. This new compound goes from C2/c to I4/mcm space group structure at 18.5GPa. Under increasing pressure, further compounds become stable such as CaO_3 which stabilize in P-42_1m space group structure above 65 GPa.

Finally, our studies on ZnO show that ZnO_2 becomes thermodynamically stable at pressure above 120 GPa. A phase transition is obtained at 10 GPa for ZnO, which is stable in B4 wurtzite structure at ambient conditions up to 10GPa. Above 10 GPa, ZnO becomes more stable in B1 structure. These results strongly support our predictions since they agree perfectly with available experiment and previous theoretical studies.

Résumé:

Le progrès dans le domaine du génie civil n'aurait pas été possible sans le développement de nouveaux matériaux. En fait, les nouveaux matériaux avec des propriétés performantes ont permis la construction de structures modernes, de plus grands bâtiments, de plus grands ponts…etc. En outre, il est important de continuer le progrès et le développement des matériaux dans le futur. En particulier, dans l'approche des constructions intelligentes, nous aurons besoin de nouveaux matériaux aux propriétés très performantes. L'étude des propriétés des matériaux, à l'échelle moléculaire, permet une meilleure compréhension de la façon dont ces matériaux fonctionnent et réagissent à un niveau macro. C'est grâce à de tells études que nous sommes en mesure de comprendre leurs comportements sous des conditions variables.

Dans cette thèse, nous focalisons nos efforts sur trois types de matériaux. Le premier est le carbonate de zinc. Le second est la chaux, qui est largement utilisée dans le domaine de la construction et les travaux publics; et le dernier est l'oxyde de zinc, qui est un matériau important pour les constructions en acier. Notre but est d'étudier en détail ces trois différents matériaux à diverses pressions et à compositions variables par la méthode de prédiction de structures basée sur l'approche *ab initio*.

Pour la smithsonite, un bon nombre de propriétés mécaniques a été évalué. Nous montrons notamment que ce système est plus dur et plus rigide que les autres carbonates. En outre, l'étude de ses propriétés électroniques révèle que l'énergie de la bande interdite est assez proche de certains semi-conducteurs. Par ailleurs, deux transitions de phase à haute pression ont été trouvées: la première à 78 GPa et la seconde à 121 GPa. En dessous de 78 GPa, $ZnCO_3$ est stable sous la structure de groupe d'espace R-3c (structure de calcite); et entre 78 GPa et 121 GPa, $ZnCO_3$ se stabilise sous une autre structure dont le groupe d'espace est C2/m (structure de magnésite phase II). Au-delà de 121 GPa, nous montrons que la nouvelle structure de groupe d'espace $P2_12_12_1$ devient la plus stable.

Par ailleurs, en utilisant la méthode de prédiction de structure –composition variable- basée sur l'approche *ab initio*, nous montrons que le système Ca-O pourraient se stabiliser sous de nouvelles compositions chimiques autres que le CaO. À pression ambiante, CaO_2 est prédit comme étant un système thermodynamiquement stable. Ce nouveau composé passe de la structure de groupe d'espace C2/c à celle de groupe d'espace I4/mcm à 18.5GPa. En augmentant la pression, d'autres composés deviennent plus stables tels que CaO_3 qui se stabilise dans la structure de groupe d'espace P-42_1m à partir de 65 GPa.

Enfin, nos études sur ZnO montrent que ZnO_2 devient thermodynamiquement stable à une pression supérieure à 120 GPa. Une transition de phase est obtenue à 10 GPa pour ZnO, qui est stable dans la structure wurtzite B4 dans des conditions ambiantes et jusqu'à 10GPa. Au-delà de 10 GPa, ZnO devient plus stable dans une structure de type B1. Ces résultats confortent nos prédictions puisqu'ils s'accordent parfaitement avec les travaux expérimentaux et théoriques précédents.